Aston University

Some pages of this thesis may have been removed for copyright restrictions.

If you have discovered material in AURA which is unlawful e.g. breaches copyright, (either yours or that of a third party) or any other law, including but not limited to those relating to patent, trademark, confidentiality, data protection, obscenity, defamation, libel, then please read our Takedown Policy and contact the service immediately

Dispersion aspects of periodically amplified soliton transmission systems

Finlay M. Knox

Doctor of Philosophy

The University of Aston in Birmingham

October 1995

This copy of the thesis has been supplied on condition that anyone who consults it is understood to recognise that its copyright rests with its author and that no quotation from the thesis and no information derived from it may be published without proper acknowledgement.

The University of Aston in Birmingham

Dispersion aspects of periodically amplified soliton transmission systems

Finlay M. Knox

Doctor of Philosophy

1995

This thesis presents improvements to optical transmission systems through the use of optical solitons as a digital transmission format, both theoretically and experimentally. An introduction to the main concepts and impairments of optical fibre on pulse transmission is included before introducing the concept of solitons in optically amplified communications and the problems of soliton system design.

The theoretical work studies two fibre dispersion profiling schemes and a soliton launch improvement. The first provides superior pulse transmission by optimally tailoring the fibre dispersion to better follow the power, and hence nonlinearity, decay and thus allow soliton transmission for longer amplifier spacings and shorter pulse widths than normally possible. The second profiling scheme examines the use of dispersion compensating fibre in the context of soliton transmission over existing, standard fibre systems. The limits for solitons in uncompensated standard fibre are assessed, before the potential benefits of dispersion compensating fibre included as part of each amplifier are shown. The third theoretical investigation provides a simple improvement to the propagation of solitons in a highly perturbed system. By introducing a section of fibre of the correct length prior to the first system amplifier span, the soliton shape can be better coupled into the system thus providing an improved "average soliton" propagation model.

The experimental work covers two areas. An important issue for soliton systems is pulse sources. Three potential lasers are studied, two ring laser configurations and one semiconductor device with external pulse shaping. The second area studies soliton transmission using a recirculating loop, reviewing the advantages and draw-backs of such an experiment in system testing and design. One particular example of employing the recirculating loop is also examined, using a novel method of pulse shape stabilisation over long distances with low jitter. The future for nonlinear optical communications is considered with the thesis conclusions.

Additional key words and phrases

Nonlinear optics, optical pulse dynamics.

To mum and dad. Thanks.

Contents

List of Figures

Chapter 1

Introduction to soliton communication systems

Since the telephone was invented by Alexander Graham Bell in 1876, the proliferation of telephone and communication systems has steadily increased, as has the traffic these systems carry. This continual increase in demand has driven research into systems that will carry the load more efficiently, more clearly, over longer distances and most importantly at a higher number of calls per line. Electronic systems using coaxial cables coped with the demands for many years, but eventually progress in laser engineering and the development of a suitable transmission medium in optical fibre in 1970 began the shift to optically based systems. The first undersea optical systems initially carried the same 280 Mbit/s traffic as the best electronic systems but at a much reduced cost [1]. It was not long however before the optical data rate outstripped that possible using coaxial cable.

From that time an enormous amount of research has been directed towards making the best use of the potential capacity of optical fibres. The data rates in use have increased rapidly over the years, with the next transatlantic link being installed during 1995 raising the long distance data rate to 5 Gbit/s on a single optical fibre. There have been many advances in technology required to achieve this capacity, with probably the most significant that of the erbium-doped fibre amplifier [2]. However, the pressure to increase the available data rate continues, more so now that inter-site computer communications are becoming more prevalent, the best example of which is the "Internet" international computer network of

computer networks which desire fast, error-free communication of large amounts of data around the world. As the growth of computer networks and the Internet continues unabated, so the communication systems they rely on are required to increase in capacity and accuracy.

The subject of this thesis is a study of one potential method of reaching the next generation of optical communication systems beyond 5 Gbit/s, making use of fibre nonlinearity and the optical soliton [3]. The reasons solitons are of interest is outlined in the first two chapters. Later chapters study some novel methods of making optical transmission systems more suitable for solitons to allow an increase in the data rate and some of the requirements of the systems components.

1.1 Optical fibre and transmission limitations

Before considering the place of solitons in optical communications an understanding of the problems associated with high speed optical fibre communications is required. In this section we introduce the main features of optical fibres and discuss briefly their implications for linear and nonlinear optical transmissions.

Throughout this thesis we shall only be considering propagation in single-mode fibres. In optical fibres the signal is guided through the glass medium by encasing a slightly higher refractive index core within a lower refractive index cladding region. Naturally the electric field traverses this boundary but the containment of the electric field by the core-cladding boundary is sufficient to guide the signal through the fibre. The difference between the single mode fibres and the alternative multi-mode fibres used in the early days of optical fibre work is the size of the core radius. Now that the technology exists to manufacture small central cores it is possible to restrict the light to a single mode of the fibre, the HE_{11} fundamental mode, whereas with larger cores several propagation modes of the fibre can be supported. The core radius required to restrict the light to a single mode is found from the normalised frequency [4],pp.3

$$V = k_0 a (n_1^2 - n_2^2)^{1/2} \tag{1.1}$$

where $k_0 = 2\pi/\lambda$ is the propagation constant of wavelength λ, a is the radius of the

core region with a refractive index n_1 and n_2 is the cladding refractive index. For the fibre to be single mode this normalised frequency must be $V < 2.405$. Typically multi-mode fibres have a core radius 25–30 μm. Single mode fibres generally have a relative core-cladding index difference $\Delta = \frac{n_1 - n_2}{n_1}$ of around 3×10^{-3} which results in a core radius of 2–7 μm for 1550 nm wavelengths. The only restriction on the cladding radius is that it be large enough to entirely contain the electric field, such that the cladding–air (or cladding–protective coating) boundary does not guide other unwanted modes. A radius of 50 μm is generally sufficient, with the industry standard now 62.5 μm. Although these equations were developed for step index fibres (SIFs), sometimes called standard fibres, they also apply in general to other fibre cross-sectional index profiles such as graded-index fibres where the index decreases gradually from the fibre centre. Different fibre core sizes and profiles allow for tailoring of the fibre dispersion and birefringence, as discussed below.

1.1.1 Optical fibre characteristics

There are four main fibre characteristics to be taken into account. The first is that of the optical fibre attenuation. Using the fibre pulling techniques now available [4],pp.4, the loss has been minimised to the point where only three loss mechanisms are important. The first two loss mechanisms are the intrinsic losses of the silica medium, due to Rayleigh scattering and the electronic infra-red absorption. Rayleigh scattering is a fundamental loss mechanism which depends on the constituents of the fibre core. It is caused by random density fluctuations of the silica and varies as λ^{-4} making it dominant for shorter wavelengths. Electronic absorption dominates over Rayleigh scattering beyond around 1.6 μm in silica. The third important loss mechanism is that of OH-absorption. Whilst care is taken in the manufacturing process to minimise both these effects the technological limits restrict this to the approximate loss profile as given in figure 1.1.

This loss profile is the deciding factor in the operating windows for long distance optical transmission systems. The first so-called transmission window at ~ 850 nm is not shown in figure 1.1 as it is not applicable to long distance transmissions as it has a high intrinsic loss. Its role is mainly for short transmissions (eg. metres to a few kilometres) due to the high loss but it is useful due to the

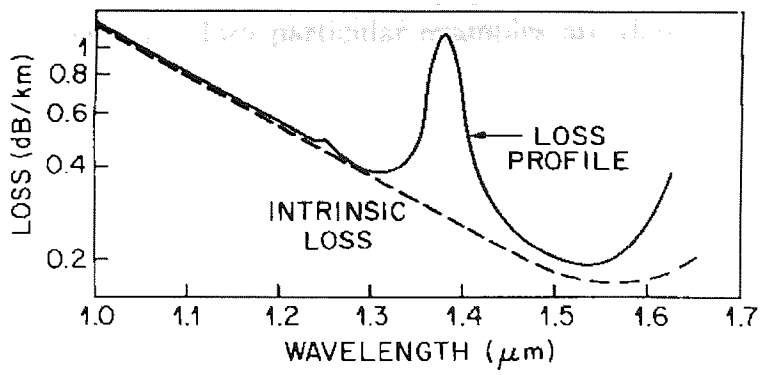

Figure 1.1: Measured loss profile of a single mode optical fibre, from [4],pp.6. The dashed curve is the intrinsic loss from Rayleigh scattering and infrared absorption of pure silica, the solid line the measured profile clearly showing a peak in the loss from the OH-absorption at 1.4 μm and a smaller peak at 1.25 μm

availability of cheap, simple silicon electronics for the transmitter and receivers. The second transmission window is at 1.3 μm which has been the main one used in fibre systems installed to date due to the low dispersion of the step-index fibres in this window, as discussed below. The third transmission window which is now coming to the fore is at the loss minimum of 1.55 μm. This thesis concentrates on the third transmission window at 1.55 μm which has been opened up to systems design through two developments, dispersion shifted fibres and the erbium doped fibre amplifier.

The second fibre characteristic is that of chromatic dispersion. The interaction of the electro-magnetic wave with the bound electrons of the medium results in a frequency dependence of the refractive index, $n(\omega)$. As discussed in more detail in section 2.3, this dependence affects the propagation of optical pulses as the propagation speed of their constituent frequency components is given by $c/n(\omega)$. This results in the components arriving at different times producing a temporal dispersion of the pulse. This can be a serious limitation to optical transmission. The rate of this dispersion is described by the dispersion parameter D_2, essentially the second derivative of the refractive index with respective to wavelength. Figure 1.2 shows a typical dispersion profile for a "standard" step-index fibre. In standard fibres the dispersion is mainly due to the chromatic dispersion of the optical fibre although there is a small contribution from the waveguiding effect of the fibre, known as waveguide dispersion. The dispersion zero wavelength can be

deliberately varied by tailoring the fibre core and cross-section profile to increase the waveguide dispersion. Two particular examples are that of moving the dispersion zero into the third transmission window to give "dispersion shifted fibres" (DSFs), permitting long distance transmission here, and of moving the dispersion zero beyond $1.6\mu m$ to produce "dispersion compensating fibres" (DCFs) which are of great interest currently [5]–[12].

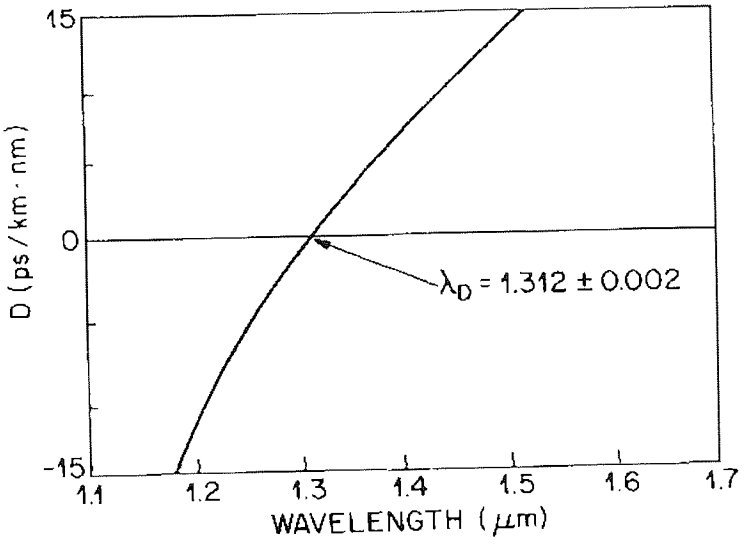

Figure 1.2: Variation of the dispersion parameter D_2 with wavelength for a step-index single-mode fibre, taken from ref. [4],pp.11

The third fibre characteristic is that of the fibre nonlinearity. Due to the symmetries of the silica there is essentially no second order susceptibility $\chi^{(2)}$ term. The nonlinearity of optical fibre comes from the third order susceptibility, $\chi^{(3)}$, of the silica and can result in effects such as four-wave mixing and nonlinear refraction. Four-wave mixing occurs between co-propagating waves of different frequencies resulting in the generation of new frequencies. Here we are concerned mainly with single wavelength propagation and shall concentrate on nonlinear refraction. This occurs both through the self-action of wave on itself as well as between different waves and polarisations. It results in a nonlinear variation of the net refractive index $\bar{n}(\omega, |E|^2)$ of the fibre with intensity $|E|^2$ [4],pp.16. Although optical fibres have a very small nonlinear index coefficient, over long transmission distances this intensity dependence of the refractive index leads to a number of effects, including the important effects of self-phase modulation and cross-phase modulation, which

are discussed below.

The final fibre characteristic of interest is that of the fibre birefringence. In a perfectly cylindrical fibre core there would be no coupling between the two polarisation modes of a single-mode fibre. However manufacturing defects lead to deviations from cylindrical symmetry and result in a birefringence. For a constant difference in the refractive indices of the two modes there is a fast and a slow axis with the fast axis having the lower refractive index. Generally however local fluctuations in the core and hence in the local birefringence are introduced by imperfections in the manufacturing process. Light launched into a single mode fibre with linear polarisation will quickly reach some arbitrary polarisation due to the resultant mixing of the polarisation modes. The implication for optical transmission systems is that ordinary fibres will not be able to support one potential method of increasing the data transmission capacity, polarisation division multiplexing, as the signals will mix on propagation and the data will be corrupted, although some success has been found [13, 14]. Again, tailoring of the fibre core cross-sectional profile can induce a stronger and essentially constant birefringence to create polarisation maintaining fibres which should allow polarisation multiplexing. The birefringence is also responsible for polarisation mode dispersion (PMD), discussed below, which is currently presenting limitations for upgrading existing standard fibre systems [15] as low birefringence and hence low PMD was not specified when the fibre was commissioned.

1.1.2 NRZ, solitons and the EDFA

The above fibre characteristics can lead to signal degradation in an optical transmission system. To date all optical transmission systems have relied on a linear transmission format, where nonlinear effects are avoided through the use of square pulses filling the bit period, known as non-return-to-zero (NRZ) transmission [8, 12, 16]–[22]. These systems are designed such that the detrimental effects the pulses experience are not significant over a single amplifier span. At the end of each transmission span of 30–50 km, the pulses are electronically detected, re-timed and retransmitted amplified and reshaped. High speed electronics are required after each fibre span adding unwanted expense and complexity at each amplifier node.

The system is also restricted in operations to a single data rate by the electronics as in order to upgrade the system by increasing the data rate each regenerator must be replaced. Obviously this will be expensive and for trans-oceanic links is not generally practical. However, linear transmission systems have been designed and installed for transmissions at data rates of 2.5 Gbit/s for oceanic distances.

The original interest in soliton transmission systems stemmed from the fact that soliton pulses balance the main effect of the fibre nonlinearity, self-phase modulation against that of the fibre dispersion, dispersive broadening. This nonlinear transmission, return-to-zero (RZ) format was originally seen as a possible answer to the signal degradation from both dispersive and nonlinear effects allowing transmission for longer lengths between regenerators. However, the fibre attenuation leads to a reduction in the optical power and hence the effect of the nonlinearity removing the required nonlinearity–dispersion balance. It was shown that the pulses could be maintained if the optical power was not varied too much [23]–[26] but this necessitates even more frequent amplification than for NRZ systems. However, the periodic reshaping required for NRZ systems to remove dispersive broadening is not necessary for soliton transmission systems. This led to the search for a suitable, simple power amplifier that might be used with soliton systems. The first step in this direction was the use of Raman amplification to provide the necessary gain [27] which showed that very long distance soliton transmission was feasible.

A major advance in the development of solitons for optical transmission systems was the erbium-doped fibre amplifier (EDFA) [28]–[40]. These amplifiers use the rare earth element erbium as a dopant within a fibre to provide optical gain in the 1.55 μm transmission window. The gain medium is optically pumped, usually at 980 or 1480 nm, with the pump coupled in through a fibre wavelength division multiplexer (WDM) providing an all-fibre power amplifier. While these amplifiers can be used with NRZ signals, there is no re-timing or reshaping so the unwanted propagation effects are allowed to build up. However they do provide a purely optical, all-fibre gain function suitable for solitons. In addition, as the EDFA gain is linear with intensity (at a fixed average power) the pulse shape is maintained through the amplifier. EDFAs also remove the complexity of the regenerators as they are purely passive and contain no high speed electronics.

Naturally, these amplifiers are not without their problems. As well as providing gain from $\sim 1520 - 1570nm$ they also introduce amplified spontaneous emission (ASE) noise [41]–[48]. The amount of noise depends on the quality of the amplifier but has a theoretical minimum which depends on the pumping regime [49]–[52]. The absolute minimum is for a co-propagating pump beam (ie. in the same direction as the signal) which is quantum limited for the high gain amplifiers required to a noise figure value of 3 dB. This translates into a doubling of the noise content propagating with the signal at each amplifier [47]. Unchecked, this can destroy the signal within a few amplifications (found to be generally less than 10 amplifications using the recirculating loop of chapter 7). The noise can be filtered out with a bandpass filter with a bandwidth of several times the soliton bandwidth (the choice of such a wide filter is so as not to remove too much energy from the spectral wings of the pulse and thus destroy its shape). Even if a perfect filter could be designed, some ASE noise would get through within the bandwidth required for the signal. Despite filtering, ASE causes problems, in particular a random timing jitter for long distance soliton transmissions [53]. However, the passive, data rate transparent nature of the amplifiers means that provided a systems upgrade is designed to maintain the original amplifier output power and gain levels there is no need to replace them allowing a very simple upgrade path. Also, the very wide bandwidth of the amplifiers, and in particular the relatively flat gain region from $\sim 1550 - 1565nm$ allows the possibility of multiple wavelength signals being transmitted through a single optical fibre (wavelength division multiplexing, WDM) [54] without any need to separate the different wavelengths along the length of the transmission link. These advantages have made the EDFA itself a very attractive prospect for future transmission systems, and their use with solitons a very strong possibility.

1.2 Thesis overview

Thus far we have discussed in general terms the limitations to pulse transmission in fibre optic communications and the place of solitons in such systems. In chapter 2 we expand on these ideas and discuss some of the limitations to soliton propagation in more detail. With this as our background, we wish to find ways to alleviate some

of the problems in order that solitons can be used in real transmission systems. This thesis considers methods of improving soliton propagation in optical fibres using a variety of novel techniques, mainly concerning the dispersion profile of the fibre transmission line.

The first three chapters of new work were performed theoretically and computationally. In chapter 3 we consider an improved fibre dispersion profile for soliton transmission, by developing an optimised stepwise approximation to the exponential decay in the dispersion which would balance the power loss and hence the decay in the nonlinear effect due to fibre loss. By exactly following the power decay with the equivalent dispersion decay, the soliton power–dispersion relationship (discussed in chapter 2) can be maintained to produce a fundamental soliton in lossy fibre. By approximating the decay, improved propagation was found. Chapter 4 assesses the limits to solitons in standard fibre systems with a view to upgrading existing systems. After finding the transmission distance limit somewhat prohibitive we consider the use of dispersion compensating fibre and show the resulting improvements to soliton propagation possible. Chapter 5 studies an improvement to the average soliton model derived from moving the launch point to average over the pulse shape changes as well as power in highly perturbed systems.

The experimental work is contained in chapters 6 and 7. Chapter 6 looks at suitable sources for soliton propagation including one novel laser, the actively mode-locked figure-eight laser. In chapter 7 we introduce the experimental model for soliton propagation, the recirculating loop, and with it investigate a novel RZ pulse propagation regime where pulses can be transmitted jitter-free and with no shape changes for more than global distances. Finally, chapter 8 summarises the conclusions of this work and considers the current and future position of solitons in the world of fibre optic communications.

Chapter 2

The nonlinear Schrödinger equation

2.1 Introduction

In order to study soliton propagation we need an accurate mathematical model which describes the features of the transmission of light pulses through the optical fibre medium. This section studies in more detail the most important features for soliton propagation, namely group velocity dispersion (GVD) and self-phase modulation (SPM), the two effects responsible for the existence and nature of solitons. These two effects are considered first in isolation from each other before their combined effect is studied. Other important effects are also outlined later. All of the following equations can be arrived at from Maxwell's equations with the appropriate substitutions, reductions and approximations. A rigorous derivation is not particularly helpful to the understanding of the results we wish to consider and can be found in a good textbook on the subject, for example ref. [4] from which much of what follows is taken. Here we shall include only an overview of the derivation.

2.2 Wave equation derivation of the NLSE

The starting point for the derivation is the wave equation in the standard form [4],pp.34

$$\nabla^2\mathbf{E} - \frac{1}{c^2}\frac{\partial^2\mathbf{E}}{\partial t^2} = -\mu_0\frac{\partial^2\mathbf{P}_L}{\partial t^2} - \mu_0\frac{\partial^2\mathbf{P}_{NL}}{\partial t^2} \tag{2.1}$$

where $\mathbf{E}(\mathbf{r},t)$ is the electric field, c is the speed of light in free space, μ_0 is the vacuum permeability. $\mathbf{P}_L$ is the linear and $\mathbf{P}_{NL}$ the nonlinear part of the polarisation field $\mathbf{P}(\mathbf{r},t) = \mathbf{P}_L(\mathbf{r},t) + \mathbf{P}_{NL}(\mathbf{r},t)$ which are related to the electric field through the dielectric tensor, $\chi^{(1)}$ for the linear part and $\chi^{(3)}$ for the nonlinear polarisation field parts [4],pp.28.

Several assumptions are required in order to proceed. The first is that $\mathbf{P}_{NL}$ is treated as a small perturbation to $\mathbf{P}_L$, the second that the optical field maintains a linear input polarisation along the fibre allowing a scalar approximation. The third is that the slowly varying wave approximation is valid allowing us to write the electric field in the form

$$\mathbf{E}(\mathbf{r},t) = \frac{1}{2}\hat{x}[\bar{E}(\mathbf{r},t)exp(-i\omega_0 t) + c.c.] \tag{2.2}$$

where $\hat{x}$ the unit vector of the linearly polarised light, $\bar{E}(\mathbf{r},t)$ is a slowly varying field relative to the period associated with the optical frequency ω_0 and $c.c.$ denotes the complex conjugate. The polarisation components $\mathbf{P}_L$ and $\mathbf{P}_{NL}$ can be expressed similarly. Another simplification is used in obtaining the nonlinear polarisation from the electric field in that the nonlinearity is taken to be instantaneous, which is generally valid for optical fibres for pulse widths greater than 0.1 ps [4],pp.36.

The wave equation for the slowly varying amplitude $\bar{E}(\mathbf{r},t)$ is found through the use of the Fourier domain, which is valid when $\mathbf{P}_{NL}$ is taken as a small perturbation. This wave equation is given by

$$\nabla^2\tilde{E} + \epsilon(\omega)k_0^2\tilde{E} = 0 \tag{2.3}$$

where $k_0 = 2\pi/\lambda$ is the propagation constant at wavelength λ and $\epsilon(\omega)$ is the dielectric constant which is related to dielectric tensor and allows us to find the

coefficient of nonlinearity n_2 as [4],pp.37

$$n_2 = \frac{3}{8n}\chi^{(3)}_{xxxx}. \tag{2.4}$$

through the use of the definition

$$\bar{n}(\omega, |E|^2) = n(\omega) + n_2|E|^2. \tag{2.5}$$

From equation (2.5) we see that the nature of the nonlinearity is as a modification to the linear refractive index, $n(\omega)$, depending on the square of the electric field, the intensity. It is this intensity dependent refractive index change, known as nonlinear refraction, which gives rise to the effect of self phase modulation, discussed below.

Equation (2.3) has the solution of the form

$$\tilde{E}(\mathbf{r}, \omega - \omega_0) = \int_{-\infty}^{\infty} \bar{E}(\mathbf{r}, t) exp([i(\omega - \omega_0)t]dt. \tag{2.6}$$

Further solution is obtained by separating the variables for the electric field using

$$\tilde{E}(\mathbf{r}, \omega - \omega_0) = F(x, y)\tilde{A}(Z, \omega - \omega_0)exp(i\beta_0 z) \tag{2.7}$$

where $\tilde{A}(Z, \omega - \omega_0)$ varies slowly with Z and $F(x, y)$ contains the lateral fibre mode dependence, approximately Gaussian for a single mode fibre and unaffected by changes in the refractive index hence ignored below, and β_0 is the propagation constant. Using this substitution the propagation equation (2.3) becomes

$$\frac{\partial \tilde{A}}{\partial Z} = i[\beta(\omega) + \Delta\beta - \beta_0]\tilde{A} \tag{2.8}$$

where $\Delta\beta$ is found from the modal distribution through $F(x, y)$. To obtain the temporal solution of the slowly varying amplitude $A(Z, t)$ we take the inverse transform of equation (2.8), for which it is useful to expand $\beta(\omega)$ as a Taylor series about the carrier frequency ω_0 as

$$\beta(\omega) = \beta_0 + (\omega - \omega_0)\beta_1 + \frac{1}{2}(\omega - \omega_0)^2\beta_2 + \frac{1}{6}(\omega - \omega_0)^3\beta_3 + \cdots \tag{2.9}$$

where

$$\beta_n = \frac{\partial^n \beta}{\partial \omega^n} \tag{2.10}$$

with β_0, β_1, β_2 and β_3 the propagation constant, inverse group velocity, group velocity dispersion and the third order dispersion respectively. The cubic and higher order terms are generally negligible if the spectral width is much less than the carrier frequency ($\Delta\omega \ll \omega_0$). The cubic term can become significant if $\beta_2 \simeq 0$.

Performing this substitution and Fourier transform on equation (2.8) and evaluating $\Delta\beta$, which includes the effects of fibre loss and nonlinearity, we obtain [4],pp.40

$$\frac{\partial A}{\partial Z} + \beta_1 \frac{\partial A}{\partial t} + \frac{i}{2}\beta_2 \frac{\partial^2 A}{\partial t^2} + \frac{\alpha}{2} A = i\gamma |A|^2 A \tag{2.11}$$

where the nonlinear coefficient γ is defined as

$$\gamma = \frac{n_2 \omega_0}{c A_{eff}} \tag{2.12}$$

with A_{eff} the effective core area of the fibre, the area of the core and cladding the signal propagates within. Although there is still some discussion, the value of n_2 is known to be around $2.5 \times 10^{-20} m^2 W^{-1}$. Typically the effective core area at 1.55 μm is 50 - 80 μm^2, depending on the fibre type.

One further simplification is to move to a frame of reference moving with the pulse we wish to study at the group velocity $v_g = 1/\beta_1$ by making the transformation

$$T = t - \frac{Z}{v_g} = t - \beta_1 Z. \tag{2.13}$$

This gives equation (2.11) as

$$i\frac{\partial A}{\partial Z} = -\frac{i}{2}\alpha A + \frac{1}{2}\beta_2 \frac{\partial^2 A}{\partial T^2} - \gamma |A|^2 A \tag{2.14}$$

This is our desired propagation equation, often known as the generalised nonlinear Schrödinger equation. If the loss is taken as $\alpha = 0$ it is known simply as the nonlinear Schrödinger equation (NLSE).

Loss aside, equation (2.14) gives four regimes of operation to consider when studying optical pulse propagation. These can be loosely defined through the use

of two length scales, the dispersion length L_D and the nonlinear length L_{NL}:

$$L_D = \frac{\tau_0^2}{|\beta_2|} \tag{2.15}$$

$$L_{NL} = \frac{1}{\gamma P_0} \tag{2.16}$$

where P_0 is the peak power of the pulse of width τ_0 and γ is the nonlinear coefficient. The four regimes of operation are found from the relative magnitudes of these two length scales compared with the transmission distance L. If $L \ll L_D, L_{NL}$ the pulse will not experience significant linear or nonlinear effects, but this regime requires long pulses (>100 ps) at low peak powers (<0.1 mW) which are not of interest for high speed communications. The remaining operating regimes, where dispersion dominates ($L \gtrsim L_D$, $L \ll L_{NL}$), nonlinearity dominates ($L \gtrsim L_{NL}$, $L \ll L_D$) and where both nonlinearity and dispersion are significant ($L \gtrsim L_D, L_{NL}$), are outlined below.

2.3 Group velocity dispersion

The first operating regime we consider is where dispersion has a significant effect on the optical pulse, characterised by $L \gtrsim L_D$ and $L \ll L_{NL}$. In any medium, different optical wavelengths will travel at a slightly different velocity due to the variation in the refractive index with wavelength. This means that the constituent wavelengths of a pulse will arrive at slightly different times, giving a temporal dispersion known as group velocity dispersion (GVD). The usual comparison made for GVD is the refraction of a white light source through a prism splitting the light into its constituent colours and revealing the optical spectrum. This well known effect is likewise the result of the difference in refraction experienced by the colours of the light due to the refractive index variation.

Mathematically, we start from the NLSE with loss as defined by eqn. (2.14). Assuming the effects due to nonlinearity are negligible, n_2 and hence γ are set equal to zero removing this term. It is not necessary to exclude the effect of loss as it has no effect on pure dispersion and can be removed through the use of a normalised

pulse envelope $U(Z,T)$ with,

$$A(Z,T) = \sqrt{P_0} exp\,(-\alpha Z/2)\, U(Z,T). \tag{2.17}$$

This gives the normalised version of equation (2.14) in the dispersive regime as

$$i\frac{\partial U}{\partial Z} = \frac{1}{2}\beta_2 \frac{\partial^2 U}{\partial T^2} \tag{2.18}$$

which can easily be solved through the Fourier method. If $\tilde{U}(Z,\omega)$ is the Fourier transform of $U(Z,T)$ such that,

$$U(Z,T) = \frac{1}{2\pi}\int_{-\infty}^{\infty} \tilde{U}(Z,\omega) exp(-i\omega T) d\omega \tag{2.19}$$

then it will satisfy the ordinary differential equation

$$i\frac{\partial \tilde{U}}{\partial Z} = -\frac{1}{2}\beta_2 \omega^2 \tilde{U} \tag{2.20}$$

with the solution

$$\tilde{U}(Z,\omega) = \tilde{U}(0,\omega) exp\left(\frac{i}{2}\beta_2 \omega^2 Z\right) \tag{2.21}$$

where $\tilde{U}(0,\omega)$ is the Fourier transform of the input pulse at $Z = 0$ given by

$$\tilde{U}(0,\omega) = \int_{-\infty}^{\infty} U(0,T) exp(i\omega T) dT. \tag{2.22}$$

Equation (2.21) shows that the relative phase of the pulse spectral components change as a function of propagation distance and the square of the frequency of that component. These phase changes do not alter the spectral content of the pulse but will change the shape of the pulse. The general solution of equation (2.18) is obtained by substitution of equation (2.21) into equation (2.19) to give

$$U(Z,T) = \frac{1}{2\pi}\int_{-\infty}^{\infty} \tilde{U}(0,\omega) exp\left[\frac{i}{2}\beta_2 \omega^2 Z\right] dT. \tag{2.23}$$

In order to assess the impact of GVD on a pulse, let us consider an example

of an input transform-limited Gaussian pulse of the form

$$U(0,T) = exp\left(-\frac{T^2}{2\tau_0^2}\right) \tag{2.24}$$

where τ_0 is the input $1/e$ half width of the pulse, related to the full width at half maximum (FWHM) pulse width through $\tau_f = 2\sqrt{ln2}\tau_0 \simeq 1.665\tau_0$. By performing the substitutions and integrations in equations (2.22) and (2.23) we obtain the solution for a pulse after a given propagation distance as

$$U(Z,T) = \left(\frac{\tau_0^2}{\tau_0^2 - i\beta_2 Z}\right)^{1/2} exp\left(-\frac{T^2}{2(\tau_0^2 - i\beta_2 Z)}\right). \tag{2.25}$$

The Gaussian temporal pulse profile is preserved on propagation, but the peak intensity drops and the pulse becomes broader such that after some distance Z the pulse width τ_1 is

$$\tau_1 = \tau_0\sqrt{1 + \left(\frac{Z}{L_D}\right)^2}. \tag{2.26}$$

Evidence for this is shown in the simulation of figure 2.1(a) which shows the input pulse and profiles after propagation through fibre. The diagram shows the intensity against time, in a frame moving with the pulse at the group velocity, with increasing distance. We see from equation (2.26) that the extent of the temporal broadening varies as β_2 and is inversely dependent on the input pulse width τ_0. This results in short pulses broadening more quickly and is due to the broader spectral range required to support a shorter transform limited pulse.

A chirp is accumulated across the pulse as it broadens. Mathematically this can be found by separating the pulse envelope into the amplitude and phase parts

$$U(Z,T) = |U(Z,T)|exp(i\phi(Z,T)) \tag{2.27}$$

which gives the phase $\phi(Z,T)$ as

$$\phi(Z,T) = -\frac{sgn(\beta_2)(Z/L_D)}{1 + (Z/L_D)^2}\frac{T^2}{\tau_0^2} + tan^{-1}\left(\frac{Z}{L_D}\right) \tag{2.28}$$

with $sgn(\beta_2)$ signifying the sign of β_2. The instantaneous frequency difference

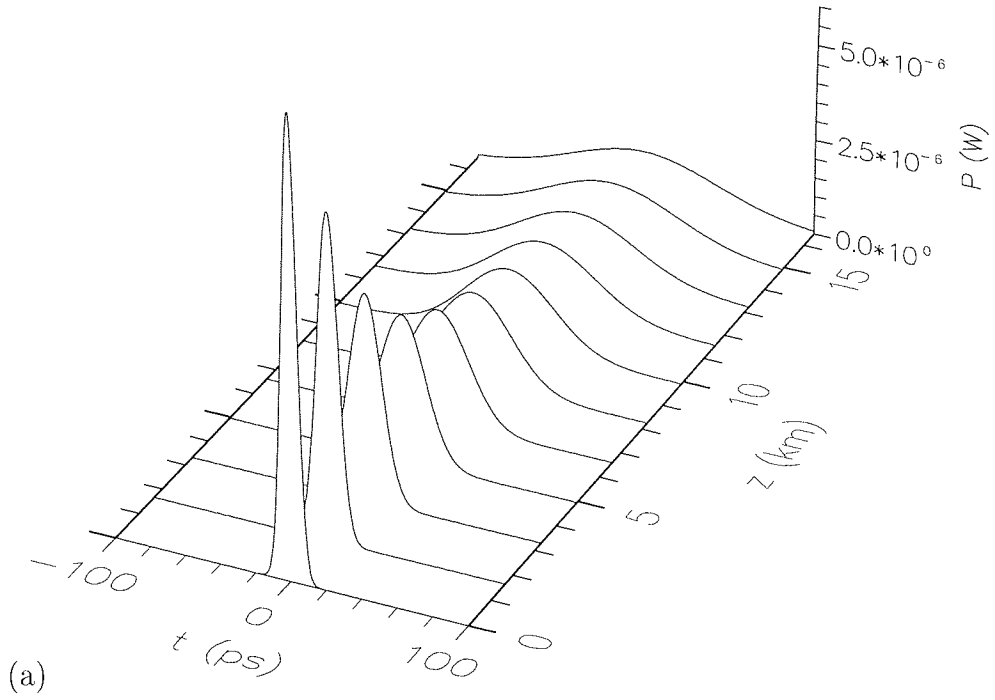

(a)

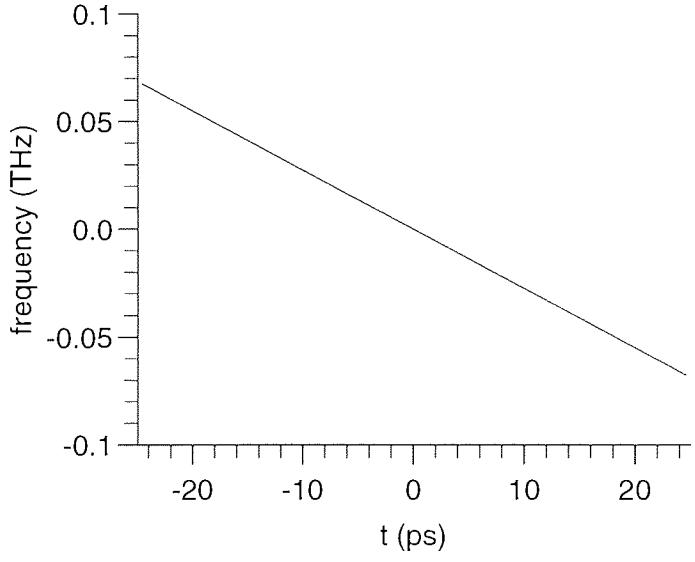

(b)

Figure 2.1: Effect of GVD on an input $10ps$ Gaussian pulse (Z=0) with propagation over 10 L_D in optical fibre with a GVD of $\beta_2 = 21.8ps^2/km$ (or $D_2 = 17ps/nm/km$), and loss $\alpha = 0$. (a) Temporal shape after each $L_D = 1.651km$. (b) chirp (instantaneous frequency against time) after 10 L_D.

across the pulse $\delta\omega$ is then given by

$$\delta\omega = -\frac{\partial\phi}{\partial T} \tag{2.29}$$

$$= 2\frac{sgn(\beta_2)(Z/L_D)}{1+(Z/L_D)^2}\frac{T}{\tau_0^2} \tag{2.30}$$

which shows a linear frequency change across the pulse, a linear frequency chirp, as shown in figure 2.1(b). The sign of the chirp is dependent on the sign of the GVD parameter β_2, through the definition of L_D. In the anomalous dispersion regime ($\beta_2 < 0$) this results in the "blue" components of the pulse travelling faster than the "red" and vice versa for the normal dispersion regime ($\beta_2 > 0$).

The effect of GVD becomes more complex when the input pulse is not transform limited and thus has an initial chirp. Whilst the dispersive effect is the same, the degree of temporal broadening experienced by a given pulse will depend on its initial chirp as compared to the dispersive chirp accumulated on propagation. An up-chirped pulse, one whose frequency increases from leading to trailing edge, in a normal dispersion fibre will broaden more quickly than an unchirped pulse as the frequencies continue to spread away in the same temporal direction as the initial chirp. The same will be true for a down-chirped pulse in the anomalous dispersion regime. The reverse of these two cases is more interesting however, as the initial chirp of the pulse will effectively have to be "undone" before pulse broadening occurs, leading to pulse compression. This useful result is exploited later in compressing down-chirped DFB pulses through in normal dispersion fibre (see section 6.3). Pulse profile also plays an important role in the dispersion characteristics of a pulse. Smooth pulse profiles, such as the Gaussians, tend to maintain a smooth shape under dispersive broadening. More sharply defined pulses such as super-Gaussians can develop oscillations in the trailing edges of the pulse as the more complex spectrum required to support such a pulse shape disperses [4],pp.67.

In deriving the NLSE the higher order terms in the Taylor expansion of equation (2.9) were ignored, as in general they are insignificant compared with the second derivative, the group velocity term β_2. However the third order dispersion term β_3 can become significant when the second order term is small ($\beta_2 \simeq 0$). Defining another length scale $L'_D = \tau_0^3/|\beta_3|$, third order effects will be noticeable

when $L'_D \lesssim L_D$ or equivalently $\tau_0|\beta_2/\beta_3| \lesssim 1$ which, using typical values, requires a very low dispersion of $\beta_2 \lesssim 0.01 ps/nm/km$ [4],pp.65. Mathematically the effect of β_3 is to introduce an additional term to equation (2.18)

$$i\frac{\partial U}{\partial Z} = \frac{1}{2}\beta_2\frac{\partial^2 U}{\partial T^2} + \frac{1}{6}\beta_3\frac{\partial^3 U}{\partial T^3} \tag{2.31}$$

which can again be solved through the Fourier technique. The effect of this extra term is to introduce asymmetric pulse shaping and an oscillatory temporal structure [4],pp.66. However, as the GVD must be so low this is not generally a problem.

Finally, a comment on the notation used for GVD. Throughout the derivation above the group velocity dispersion parameter β_2 was used. However, there is a second notation used through much of the rest of this thesis, that of the group delay dispersion D_2 which tends to be a more useful quantity in practical terms. The difference between them is that group delay dispersion (GDD) is the second derivative of the refractive index with respect to wavelength rather than frequency. The simple relation between group delay and group velocity dispersion is

$$D_2 = \frac{-2\pi c}{\lambda^2}\beta_2. \tag{2.32}$$

2.4 Self-phase modulation

Next we consider the most relevant nonlinear effect in optical fibres as far as soliton formation is concerned, self-phase modulation (SPM). Nonlinear effects are the most significant effects experienced by pulses being transmitted along an optical fibre when the length scales are $L \gtrsim L_{NL}$ and $L \ll L_D$. In order to concentrate on the effect of SPM in this section we assume that the group velocity dispersion is negligible and take $\beta_2 = 0$. Again starting from the NLSE with loss (equation (2.14)) and using the normalisation for the amplitude (equation (2.17)) we arrive at the partial differential equation

$$\frac{\partial U}{\partial Z} = \frac{i}{L_{NL}} exp(-\alpha Z)|U^2|U \tag{2.33}$$

Note that despite the amplitude normalisation, the loss coefficient α is still contained in this equation since, as the nonlinearity is intensity dependent, loss will reduce its effect. This equation is easily solved with the solution

$$U(Z,T) = U(0,T)exp\left(i\phi_{NL}(Z,T)\right) \tag{2.34}$$

with $U(0,T)$ again the input pulse amplitude and the nonlinear phase term ϕ_{NL} given by

$$\phi_{NL}(Z,T) = |U(0,T)|^2 \frac{Z_{eff}}{L_{NL}} \tag{2.35}$$

where the effective length Z_{eff} is

$$Z_{eff} = \frac{1}{\alpha}\left(1 - exp(-\alpha Z)\right) \tag{2.36}$$

and gives a reduced length that effectively rescales the nonlinearity for the presence of fibre loss.

Equation (2.34) shows that the effect of self-phase modulation is to induce an intensity dependent phase change across the pulse, through the dependence on $|U(Z,T)|^2$, increasing with propagation distance. As in equation (2.29) the frequency chirp this phase shift induces across the pulse is

$$\delta\omega = -\frac{\partial\phi_{NL}}{\partial T} = -\frac{\partial|U(0,T)|^2}{\partial T}\frac{Z_{eff}}{L_{NL}}. \tag{2.37}$$

This frequency chirp, through the $\frac{\partial|U(0,T)|^2}{\partial T}$ differential is dependent on the shape of the input pulse and in particular the rate of change of the pulse shape.

The effect of this chirp is to generate new frequencies at the edges of the pulse spectrum, redistributing the pulse energy to these frequencies. As the chirp increases in magnitude with propagation distance it will exceed the bandwidth of the original pulse and new frequencies will be self generated by the pulse. Note the contrast here with GVD which does not introduce additional frequencies but merely realigns their relationship to each other as they propagate at different velocities. Thus the effect of self-phase modulation is a spectral broadening of the pulse.

By way of example, taking the Gaussian input pulse of equation (2.24) and this time considering its propagation in the presence of nonlinearity we find the

spectral broadening shown in figure 2.2(a). In the absence of loss ($\alpha = 0$, $Z_{eff} = Z$), the peak nonlinear phase shift experienced by the pulse centre is given by

$$\phi_{max}(Z, 0) = \frac{Z}{L_{NL}} = \gamma P_0 Z \tag{2.38}$$

which increases linearly with distance and with peak power P_0. The most striking feature of the spectral changes induced by SPM is the oscillatory nature of the spectrum. This can be explained if we consider the temporal variation of the frequency chirp across the pulse as shown in figure 2.2(b), which shows the chirp after a distance of 10 L_{NL} corresponding to the last trace in figure 2.2(a). From this we see that the pulse has the same instantaneous frequencies occurring at two points in its temporal profile. This can be thought of as two waves of equal frequency but different phase and as such these waves can either constructively or destructively interfere, depending on the phase difference. It is this interference which results in the multiple peaks in the spectrum.

If the input pulse used is chirped, there is a change to the nature of the SPM induced. This change depends on the sign of the chirp, as an up-chirped pulse will add with the SPM induced chirp increasing the oscillatory nature of the spectrum, while the opposite will be true for a down-chirped pulse [4],pp.84. Another important point to note is that, as mentioned above, the degree of self phase modulation depends on the rate of change of the pulse intensity. For a squarer, super-Gaussian pulse, there would be little variation in the pulse shape over the central part of the pulse and very fast changes in the edges of the pulse. The effect of this that while the pulse still develops the same number of peaks in its spectral structure, the majority of the pulse energy experiences little SPM and this energy remains in the central peak of the spectrum [4],pp.83. Only the wings of the pulse contribute to the generation of new frequencies leading to far lower peaks in the spectrum in contrast to that of the Gaussian where the outer spectral peaks contain the most energy. It is this dependence on pulse shape that leads to the use of squarer pulses in NRZ transmission systems, as most of the pulse energy remains within the input spectral width.

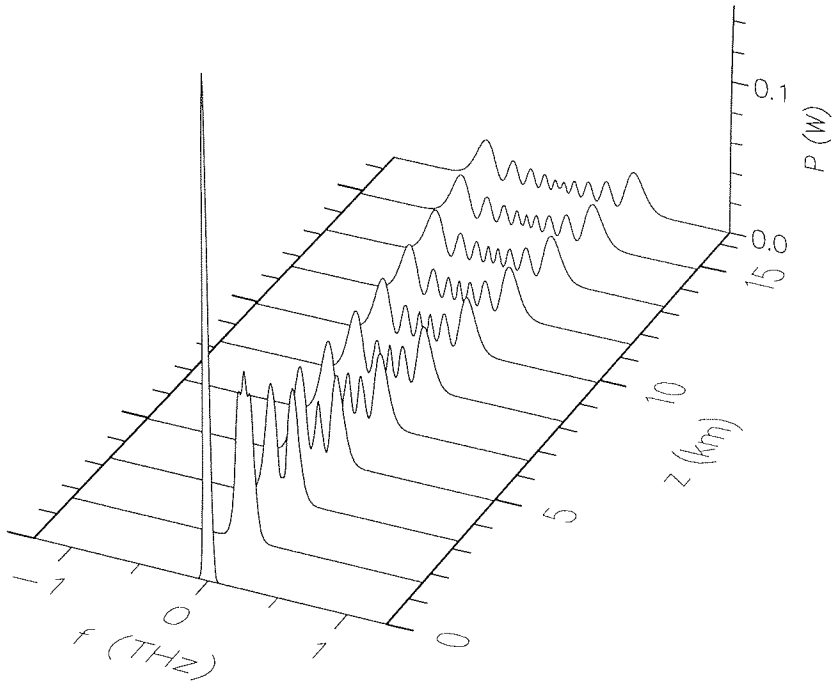

(a)

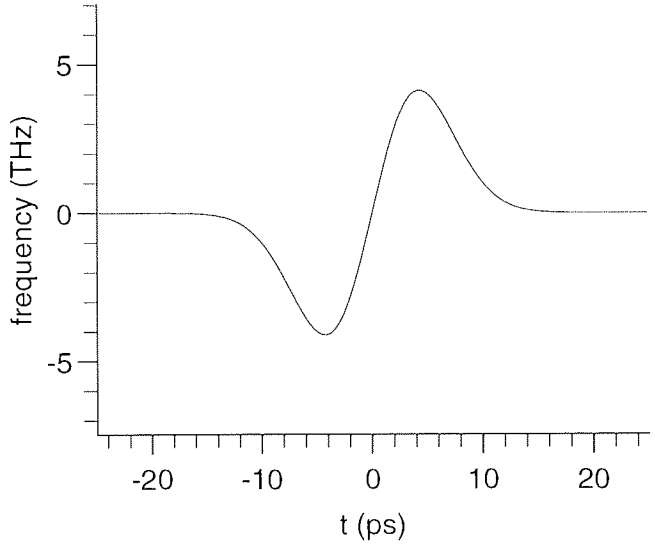

(b)

Figure 2.2: Effect of SPM on a 10 ps Gaussian input pulse in the presence of nonlinearity but no dispersion or loss for $10L_{NL}$. (a) Spectral output after each $L_{NL} = 1.651km$. (b) Chirp (instantaneous frequency) against time after $10L_{NL}$.

2.5 The NLSE and the soliton solution

The final regime to consider, in terms of the length scales, is that where both the linear and nonlinear transmission effects are significant, $L \gtrsim L_D, L_{NL}$. Here the combined effects of GVD and SPM lead to a significantly different variation in the pulse dynamics from either case separately. Initially we shall look at the lossless case for which the governing equation is the nonlinear Schrödinger equation (NLSE) of equation (2.14) with the loss coefficient $\alpha = 0$ giving

$$i\frac{\partial A}{\partial Z} = \frac{1}{2}\beta_2\frac{\partial^2 A}{\partial t^2} - \gamma|A|^2 A. \tag{2.39}$$

The dynamics of this equation depend on the sign of the GVD parameter β_2. There is a c.w. solution to this equation which is stable for the normal dispersion regime ($\beta_2 > 0$) but in the anomalous dispersion regime ($\beta_2 < 0$) it leads to modulational instability, a modulation to the temporal profile which will start spontaneously from noise [4],pp.105. Here we are more concerned with pulsed solutions to the NLSE.

To simplify equation (2.39) we introduce

$$u = N\frac{A}{\sqrt{P_0}},\ z = \frac{Z}{L_D},\ \tau = \frac{T}{\tau_0} \tag{2.40}$$

where the parameter N is defined as

$$N^2 = \frac{L_D}{L_{NL}} = \frac{\gamma P_0 \tau_0^2}{|\beta_2|}. \tag{2.41}$$

and hence obtain the standard form of the nonlinear Schrödinger equation,

$$i\frac{\partial u}{\partial z} + \frac{1}{2}\frac{\partial^2 u}{\partial \tau^2} + |u|^2 u = 0 \tag{2.42}$$

where we have taken the case for the anomalous dispersion regime ($sgn(\beta_2) = -1$). For the normal dispersion regime the dispersion term, the second derivative with respect to time, is preceded by a minus sign.

This equation can be solved exactly using the inverse scattering transform method in terms of eigenvalues. The method was first proposed by Gardner *et al.*

[55] and was used by Zakharov and Shabat [56] to solve the NLSE in 1973. We shall not go into this method here, other than to say it is similar in style to the Fourier transform method of solving linear partial differential equations. Whilst higher order solutions exist ($N > 1$), the solution of most interest to us here is the single eigenvalue solution which corresponds to $N = 1$ [4],pp.114 and which has the form

$$u(z,\tau) = 2\zeta sech(2\zeta\tau)exp(2i\zeta^2 z) \tag{2.43}$$

where ζ is the single eigenvalue. We can obtain a simplified, canonical form for the soliton if we make use of the normalisation to set $u(0,0) = 1$ by setting $2\zeta = 1$ resulting in the fundamental soliton solution

$$u(z,\tau) = sech(\tau)exp(iz/2). \tag{2.44}$$

From equations (2.40) and (2.41) we see that this relates in the context of optical fibres to choosing the input peak power P_0 and pulse width τ_0 such that $N = 1$, ie. we set the peak power for a given pulse width and fibre parameters to be

$$P_0 = \frac{|\beta_2|}{\gamma\tau_0^2}. \tag{2.45}$$

This choice of parameters gives the fundamental soliton which will be supported without change upon transmission, the stable soliton solution. This is more obvious by studying the various dependencies of the soliton solution. We see from equation (2.43) that the effect of the eigenvalue ζ is to link the power, pulse width and phase relationship of the fundamental soliton. However, there is no dependence of this solution with distance for the pulse width, only for the phase. On propagation the soliton will remain the same hyperbolic secant shape and width but will accumulate a phase across the entire pulse linearly with distance. This phase accumulation however has no temporal dependence thus the pulse does not acquire a chirp. To illustrate these effects, figure 2.3 shows the temporal evolution of a fundamental soliton with distance and the phase of the pulse. Also shown is the evolution of the soliton spectrum which as there is no chirp accumulated also remains invariant.

An alternative way to consider the formation of solitons as found from the

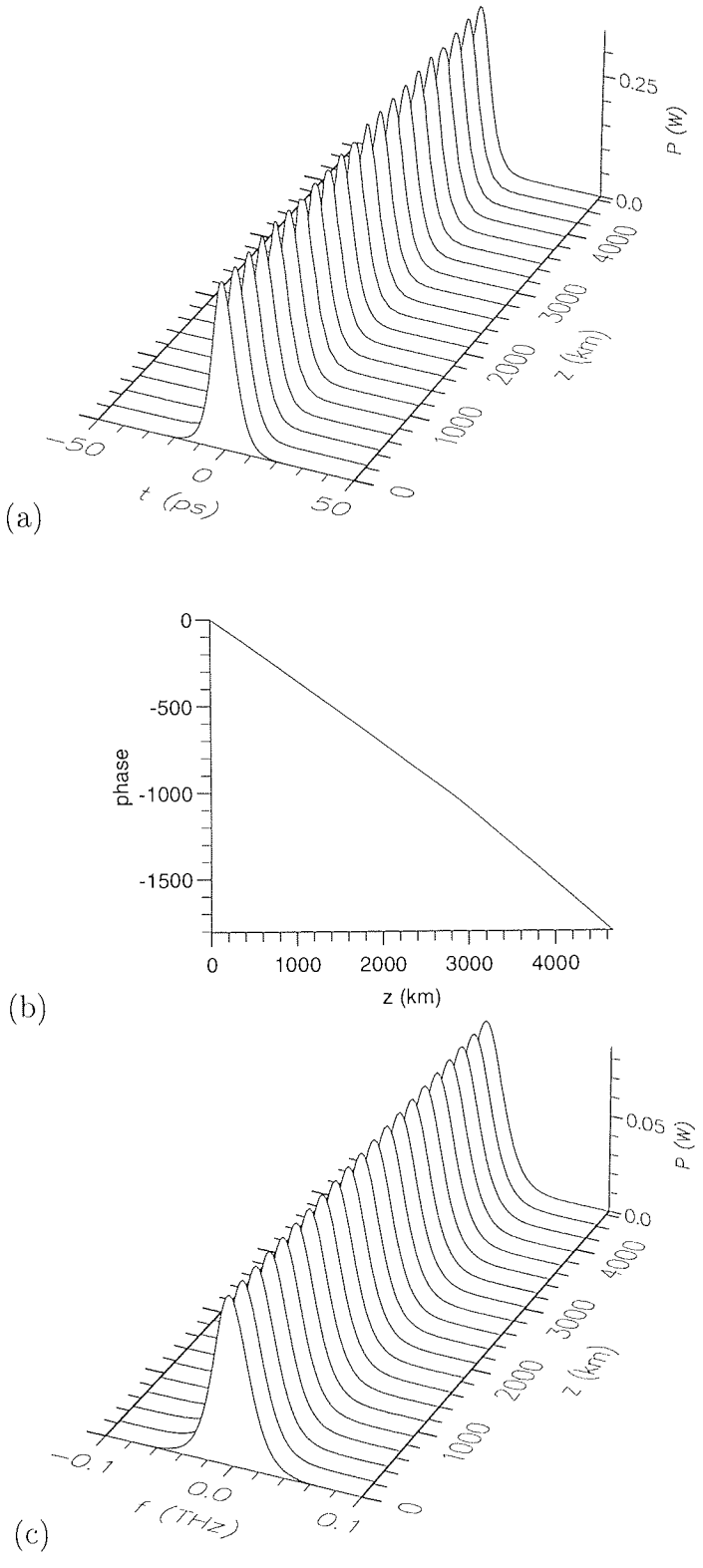

Figure 2.3: Evolution of a 10 ps fundamental solitons (a) temporal shape (b) phase and (c) spectrum with distance, in fibre with loss $\alpha = 0$ and $D_2 = 17ps/nm/km$.

NLSE is to consider the chirps imposed on a pulse by GVD and SPM. We saw above that the sign of the chirp for GVD depends on the sign of the dispersion parameter β_2, whilst that from the SPM is always of the same sign. In the normal dispersion regime this leads to a combined and detrimental effect, but in the anomalous dispersion regime the signs of these two chirps oppose each other. The formation of a soliton can thus be thought of as the pulse shape which gives the correct frequency chirp balance between GVD and SPM, with the power and pulse width chosen such that the SPM chirp contribution exactly balances the GVD chirp. As such there is no build up of any temporal chirp across the pulse and hence no temporal or spectral broadening.

The linear increase in the phase of a soliton allows us to define the soliton period Z_0 which is defined as the distance required for a $\pi/2$ phase rotation, and in normalised units is $z_0 = \pi/2$, or in physical units as

$$Z_0 = \frac{\pi}{2} L_D = \frac{\pi}{2} \frac{|\beta_2|}{\tau_0^2}. \tag{2.46}$$

This soliton period is frequently used as a length scale for describing the evolution of a soliton under various effects and perturbations. The choice of $z_0 = \pi/2$ was chosen originally as this is the period of the shape evolution of higher order solitons [4],pp.115.

Another important feature of solitons is their resilience to perturbations. As the soliton solution of the NLSE is a stable solution if a perturbation such as a small change in the pulse's temporal or spectral profile is applied to the soliton it will attempt to regain the soliton solution. This can be shown mathematically using linear stability analysis and similar techniques. The resilience of solitons does give rise to unusual and undesirable effects, such as Gordon-Haus timing jitter discussed below, but does provide an additional advantage in general over other transmission formats. The fact that the soliton is a stable solution of the NLSE also results in non-soliton pulses evolving toward the soliton solution from any reasonably close input chirps and shapes [57]–[60].

It is this temporal and spectral invariance that make solitons so attractive for optical communication systems. Unlike NRZ transmission systems where GVD and SPM will work to destroy the pulse, fundamental solitons remain stable for the

length of the system, in an ideal world. However in the above we have made several omissions including one particularly important one, the effect of fibre attenuation, which we consider next.

2.6 The NLSE with loss - the average soliton

Although we have seen the effect of loss for GVD and SPM individually, their combined effect leads to a different dependence on loss than for either individual case. The major problem for solitons in an optical fibre resulting from the loss is that the decrease in the power of the pulse results in a decay in the nonlinear effect it experiences, removing the balance between dispersive and nonlinear chirps. If an $N = 1$ soliton is launched into an optical fibre this decay in the nonlinear effect results in pulse broadening as the GVD chirp gradually becomes dominant over that from the SPM. In order to balance out the effect of loss, the power must be re-amplified periodically before the signal is lost to the noise propagating with it [61]. For soliton systems this can be done all optically with the EDFA as pulse shape changes should not be significant, provided the dispersion does not destroy the pulse [23]–[26, 62]. This has led to the concept of the *average soliton*, which has a major impact on the propagation of solitons in real optical fibres. In discussing the average soliton we shall see that the EDFA has been instrumental in the elevation of solitons to a practical transmission format for optical communications. However, the use of EDFAs is not without its own problems, mainly due to the noise that these amplifiers introduce to the optical signal. These problems are addressed later.

We consider the effect of distributed loss and periodic discrete gain has on soliton propagation. The EDFA can be taken as a discrete amplifier as its length (typically a few metres) is short compared to the fibre transmission length between amplifiers (a few 10's of kilometres). We return to the NLSE with loss and normalise as before (equation (2.40)) to obtain

$$i\frac{\partial u}{\partial z} + \frac{1}{2}\frac{\partial^2 u}{\partial \tau^2} + |u|^2 u = -i\Gamma u \tag{2.47}$$

where we have used the normalised loss Γ

$$\Gamma = \frac{\alpha}{2} L_D. \tag{2.48}$$

To exactly compensate for the distributed loss along each fibre section, the discrete gain from the amplifiers must be such that the fields, u_1 and u_2, before and after each (j^{th}) amplifier respectively, are related by

$$u_2(jz_a) = G^{1/2} u_1(jz_a) \tag{2.49}$$

where $G = e^{2\Gamma z_a}$ is the power amplification factor required to restore the signal after the exponential loss and $z_a = L_a/L_D$ is the amplifier spacing L_a normalised to the dispersion length. Introducing the transformation $u(z,t) = \Lambda(z)R(z,t)$, eqn.(2.47) becomes

$$i\frac{\partial R}{\partial z} + \frac{1}{2}\frac{\partial^2 R}{\partial \tau^2} + \Lambda^2(z)|R|^2 R = 0 \tag{2.50}$$

where

$$\Lambda^2(z) = \Lambda^2(0) e^{-\Gamma(z - jz_a)}. \tag{2.51}$$

Thus, the exponential energy variation in the periodically forced NLSE is equivalent to an exponential variation, $\Lambda^2(z)$, in the nonlinear coefficient of the lossless NLSE (cf. equation (2.42) with $\gamma = \Lambda^2(z)$ and $u = R$). If the period of $\Lambda^2(z)$ is short on the characteristic length scale of the soliton evolution ($L_a \ll Z_0$, or equivalently $z_a \ll \pi/2$), its average is a good approximation in eqn.(2.50) and the so called *average soliton model* is obtained [23]–[25]. By averaging the variation of $\Lambda^2(z)$ over the first amplifier span ($j = 0$) and equating it to the desired normalised average value of 1

$$< \Lambda^2(z) >= \frac{1}{z_a} \int_0^{z_a} \Lambda^2(z) dz = 1 \tag{2.52}$$

gives

$$\Lambda^2(0) = \Lambda_0^2 = \frac{2\Gamma z_a}{1 - e^{-2\Gamma z_a}}, \tag{2.53}$$

where Λ_0^2 is the peak amplitude of the input average soliton.

Figure 2.4 shows the variation in the soliton energy on propagation along a few amplification periods of such a system. Essentially, the average soliton model

balances the excess nonlinear chirp of the initial section of propagation between amplifiers with the excess dispersive chirp of the second part so that on average the dispersion and nonlinearity balance. Diagrammatically, this is equivalent to the areas above and below the $\Lambda^2(z) = 1$ line being equal.

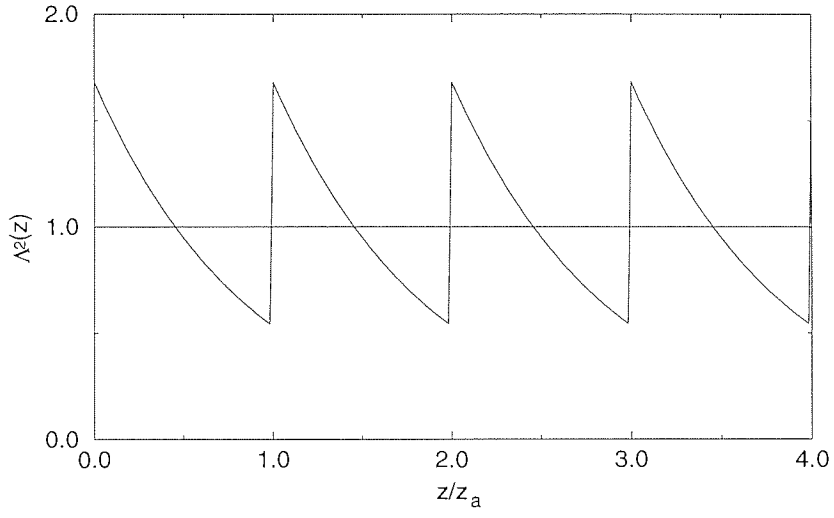

Figure 2.4: Variation of the soliton energy with propagation distance over 4 amplification spans, each with a net loss of 5 dB. $\Lambda^2(z) = 1$ is the energy of an N=1 soliton in a lossless fibre to which the soliton is averaging.

Although this discussion has focused on the most important perturbation to the soliton transmission, loss, it is also applicable to other perturbations. The prescription can be applied to other periodic variations of the fibre, which means their period must also be short compared to the soliton period. Defects from the manufacturing process for example must meet this criteria, but as these defects are generally short compared with any realistic amplification period, designing the system for the average soliton will also remove their effect.

2.7 Cross-phase modulation and birefringence

There are several other effects that can occur in an optical fibre. These effects are often not particularly significant and can be designed around but can be a problem given appropriate conditions. Here we summarise some of these effects, namely polarisation mode dispersion, polarisation dependent loss and gain and cross-phase modulation.

Beginning again with the linear effect and ignoring nonlinearity, the birefringence of the optical fibre can cause problems. As mentioned above, the random variation in the local birefringence due to imperfections in the manufacturing process breaks the degeneracy of the polarisation modes in a nominally cylindrical fibre. This results in mixing between the modes and hence any light launched into the fibre will quickly reach some arbitrary polarisation. Whilst this is not generally a problem for single polarisation transmissions, the net difference in the group velocities of the fast and slow axes of the two orthogonal polarisation states can, if large enough, result in a pulse splitting for a randomly orientated input polarisation pulse. As for the spectral components with GVD, the different propagation rates lead to a temporal dispersion of the polarisation components. This effect, known as polarisation mode dispersion (PMD), is not often a significant problem with new optical fibres due to the improvements in the manufacturing process, but older fibres including a majority of the installed fibre base can have very significant PMD and make upgrading to higher data rates with NRZ formats difficult [63]. The effect of PMD on solitons is discussed below once the nonlinear effects have been introduced. PMD can also be significant in other devices used in optical communications, such as the optical isolators used to restrict propagation to one direction and eliminate reverse travelling ASE noise from one amplifier interfering with a previous one.

Likewise, less of a problem for fibres now but still important when considering older fibres and other devices are the effects of polarisation dependent loss (PDL) and polarisation dependent gain (PDG) [64]–[67]. PDL is not really a serious problem in optical fibres due to the birefringent polarisation mixing, but can be more of a problem with other devices used in optical communications. In particular, lithium-niobate modulators, used to impose data on a pulse stream, tend to be highly polarisation sensitive due to the waveguiding used for these slab devices, with PDL values around 10 dB common. Generally such high polarisation dependent losses must be avoided, with polarisation controllers used to set the appropriate state for minimum loss for a single polarisation signal. With polarisation division multiplexed systems more involved solutions would be necessary. In a similar way, polarisation dependent gain, due to preferential alignment of the erbium

ions to one polarisation state during the manufacture of erbium fibre, can become a serious problem. Again, this problem has generally been overcome for erbium fibre at the manufacturing process, although just as for PDL, other devices can have stronger PDG, such as the semiconductor laser amplifiers discussed in section 6.3.

Cross-phase modulation (XPM) is another nonlinear effect which describes the phase modulation of one pulse at frequency ω_1 on co-propagation with another at ω_2. The NLSE with XPM can be found in a similar way to that of the original NLSE formulation from the wave equation by replacing the slowly varying electric field of equation (2.2) by that describing the combined fields [4],pp.173

$$\mathbf{E}(\mathbf{r},t) = \frac{1}{2}\hat{x}[E_1 exp(-i\omega_1 t) + E_2 exp(-i\omega_2 t)] + c.c. \tag{2.54}$$

It is then possible to solve for the resultant change Δn in the refractive index $n(\omega) = \bar{n} + \Delta n$ which is found as [4],pp.175

$$\Delta n_j = n_2(|E_j|^2 + 2|E_{3-j}|^2) \tag{2.55}$$

where $j = 1, 2$ for the two wavelengths. The first term in E_j is the self-phase modulation term described above. The second term in E_{3-j} shows that the nonlinear refractive index change when two waves are co-propagating depends not only on their own intensity for SPM but also on the intensity of the other wave. This refractive index change leads to a phase modulation by one pulse on another given by

$$\phi_j^{NL} = \frac{\omega_j z}{c}\Delta n_j = \frac{\omega_j z n_2}{c}\left[|E_j|^2 + 2|E_{3-j}|^2\right]. \tag{2.56}$$

The phase modulation due to the XPM term is seen from these equations to be twice that of the SPM term for the same intensity. This comes through the mathematics from the squaring of the electric field (equation (2.54)) for the nonlinear polarisation field giving twice the number of terms for different frequencies than for one.

The difference between v_{g1} and v_{g2}, the group velocities of the two pulses, is important when considering XPM. Whilst two pulses may initially be co-propagating, the difference in their group velocities will lead to a walk-off. Once the pulses no longer overlap there will be no cross-phase modulation. This limits the extent of the XPM for any given two wavelengths in an optical fibre. Whilst detrimental for

optical transmission lines, XPM can be useful as we shall show below (section 6.4).

The nonlinear effect of birefringence is also an XPM process between two waves of the same frequency but different polarisations. As such it can be studied by using as the input the field for an elliptically polarised optical wave [4],pp.177

$$\mathbf{E}(\mathbf{r},t) = \frac{1}{2}(\hat{x}E_x + \hat{y}E_y)exp(-i\omega_0 t) + c.c. \tag{2.57}$$

for the amplitudes E_x and E_y in each polarisation state. Again the result is a modulation of the refractive index for each polarisation component by the other known as nonlinear birefringence and is given by

$$\Delta n_x = n_2\left(|E_x|^2 + \frac{2}{3}|E_y|^2\right) \tag{2.58}$$

$$\Delta n_y = n_2\left(|E_y|^2 + \frac{2}{3}|E_x|^2\right). \tag{2.59}$$

We see that the XPM between polarisations is less significant than that for different frequencies as the dependence on the other wave is a factor of 2/3 rather than 2. Other than this, the qualitative behaviour is the same. This change in the refractive index produces a rotation of the polarisation ellipse of the input elliptical wave.

One consequence of this variation in the polarisation is the effect known as nonlinear polarisation rotation (NPR). As the nonlinearity is essentially instantaneous, the high power central peak of a nonlinear pulse will self-induce a greater index change and hence polarisation rotation than the low power wings. This effect can be used as a pulse shaping mechanism when used in conjunction with a polarisation element. If a pulse is input to the fibre at some angle to the polariser and there is sufficient nonlinear polarisation rotation to align the peak of the pulse with the polariser this part of the pulse will be transmitted whilst the lower power and hence less polarisation-rotated wings of the pulse will be rejected. This effect has been used in laser cavities [68, 69] and is investigated below in the context of pulse transmission (section 7.3).

For solitons, once again the dispersive and nonlinear effects must be considered together. While work continues to understand their effect in the random birefringence of ordinary fibres, consideration of more strongly birefringent fibres gives a qualitative indication of the effect [4],pp.190. Essentially, if the birefringence

is below $\sim 0.3D_2$ [70] the lower power polarisation component of an elliptically polarised pulse will be "trapped" by the higher power component, preventing the pulse from splitting as expected for linear pulses, although it may lead to a timing jitter [71]. At higher levels of birefringence the nonlinear index change is insufficient to balance out the dispersive effect and the pulse will split as before. However, this resilience to PMD pulse splitting is currently creating further interest in solitons for upgrading older systems [15].

2.8 Soliton system design considerations

Now that the properties and effects of optical fibre transmission and solitons have been introduced, we can consider the requirements for designing an optical soliton transmission system. Various trade-offs are necessary to design any given system for its competing requirements. In general, soliton system design falls into two main areas namely short and long haul. Short haul systems are taken here to mean distances of hundreds of kilometres and long haul to be trans-oceanic system lengths (thousands of kilometres). The length of system changes the emphasis of the design constraints as discussed below. One very important consideration for any length of soliton system is that of the average soliton limit to the amplifier spacing, $L_a \ll Z_0$. Typically systems designers take a factor of 10 for safety to mean "much less than" but use the full soliton period ($8z_0 = 2\pi$), giving this limit as $L_a < 8/10Z_0$ [72]. The other problems considered here are those of soliton interactions, random timing jitter, the signal-to-noise ratio (SNR) requirements, acoustic interactions and the average power requirement.

2.8.1 Soliton–soliton interactions

For a high speed transmission system it is desirable that solitons be placed as close together as possible in order to maximise the possible data rate (R) achievable. It is therefore important to assess how closely two solitons can be placed without detrimental effects. Unfortunately the nonlinearity of the optical fibre that leads to the existence of solitons also provides the mechanism for interaction between the solitons. This topic has attracted a great deal of interest over the last few years

[73]–[80], as have potential methods of dealing with the problems [81]–[83].

There are two main cases to consider when studying soliton interactions. The first applies to solitons in optical time-division multiplexed (OTDM) systems, that of the interactions of solitons of equal frequency [4, 84]. A pair of solitons at the input to a transmission fibre can be described as

$$u(0,\tau) = sech(\tau - \frac{T_R/2}{\tau_0}) + rsech\left(r(\tau\frac{T_R/2}{\tau_0})\right)e^{i\theta} \tag{2.60}$$

where $T_R = 1/R$ is the initial separation, r is the relative amplitude and θ is the relative phase of the two input pulses. The solutions for this input to the NLSE has been calculated by both the inverse scattering method and perturbation theory, as well as by numerical simulations [84]. It has been shown that two solitons in phase ($\theta = 0$) and of equal amplitude ($r = 1$) will periodically be attracted and collapse upon propagation, as shown in figure 2.5. If the separation is comparatively large compared with the pulse width ($T_R \gg 2\tau_0$) the pulses will collapse and separate with a period [4],pp.132

$$Z_p = Z_0 exp\left(\frac{1}{2R\tau_0}\right) \tag{2.61}$$

with the collapse occurring $Z_p/2$, in a perfect lossless system. As this distance is related to the soliton period, Z_0, this has implications for a soliton system as, even though this behaviour is predictable this is for a perfect pair of solitons in a lossless system. Systems designers wish to avoid any potential failure mechanism however and so any system is designed to ensure that it is shorter than the collapse length. As the behaviour is predictable, it is usually sufficient to make the system length up to half the collapse length. Alternatively, and more frequently used, if the solitons are separated by a sufficient mark-to-space ratio the exponential of equation (2.61) will be large enough to avoid interactions over global distances. Generally the mark-to-space ratio taken is between 1:6 and 1:10.

If the pulses are out of phase ($\theta = \pi$), a different evolution occurs in that the pulses do not attract but instead repel, as shown in figure 2.6. While repulsion may initially seem to be more desirable for soliton system design as it avoids the pulse collapse of in phase solitons, it is not as the pulses continue to separate for the entire system length at the same rate, regardless of how far apart they become.

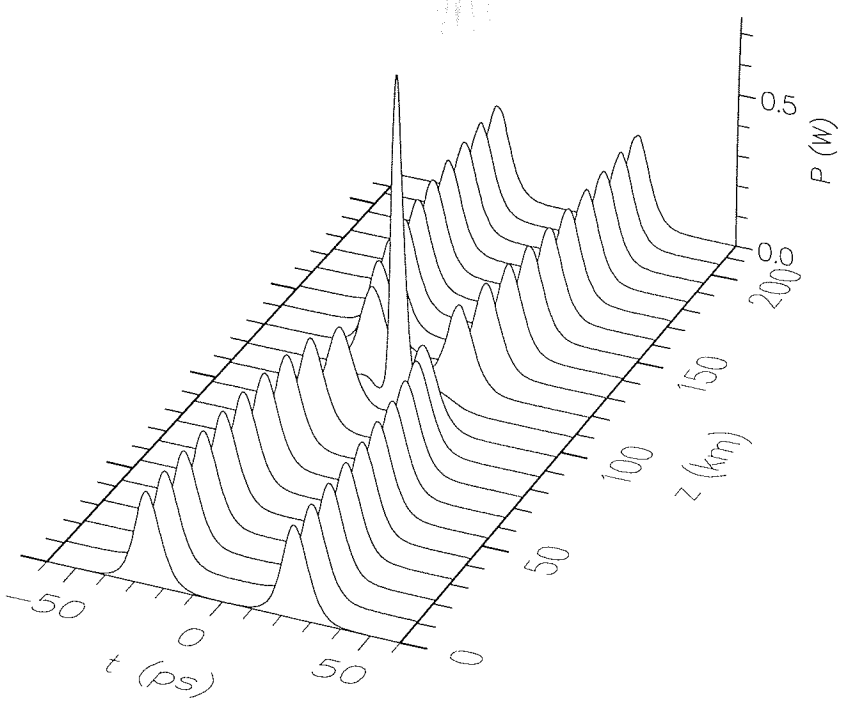

Figure 2.5: Evolution of two in-phase, equal amplitude solitons along a transmission line. The fibre dispersion of 15 ps/nm/km and pulse width of 10 ps give a collapse distance of 108 km ($Z_P = 216.7km$) at the data rate of 20 Gbit/s.

This can result in out of phase pulses walking into adjacent bit slots producing errors. It has been suggested that in the context of a pulse stream the mutual repulsion from out of phase pulses on either side will give a stable operating point with no pulse movement [85]. However in the usual amplitude modulation format of a soliton data stream there cannot be pulses either side of every pulse and thus this method fails. This result is borne out in section 4.2.3. Another possibility is that midway between in and out of phase there is a point at which the pulses neither attract or repel ($\theta = \pi/2, 3\pi/2$), but this point is unstable and any perturbation will cause the phases to shift to one of the two extremes outlined above.

So far we have only considered pulses of equal amplitude (r=1). The case where the amplitudes are unequal has attracted a certain amount of interest recently [86]–[88]. Unequal amplitude solitons introduce an interesting behaviour to a transmission line, in that they essentially eliminate the problem of soliton interactions. Figure 2.7 shows the evolution of two such solitons, with an amplitude difference of 10%. Although there is an interplay between the pulses, unnoticable on this figure, their actual position in time does not change and they remain in

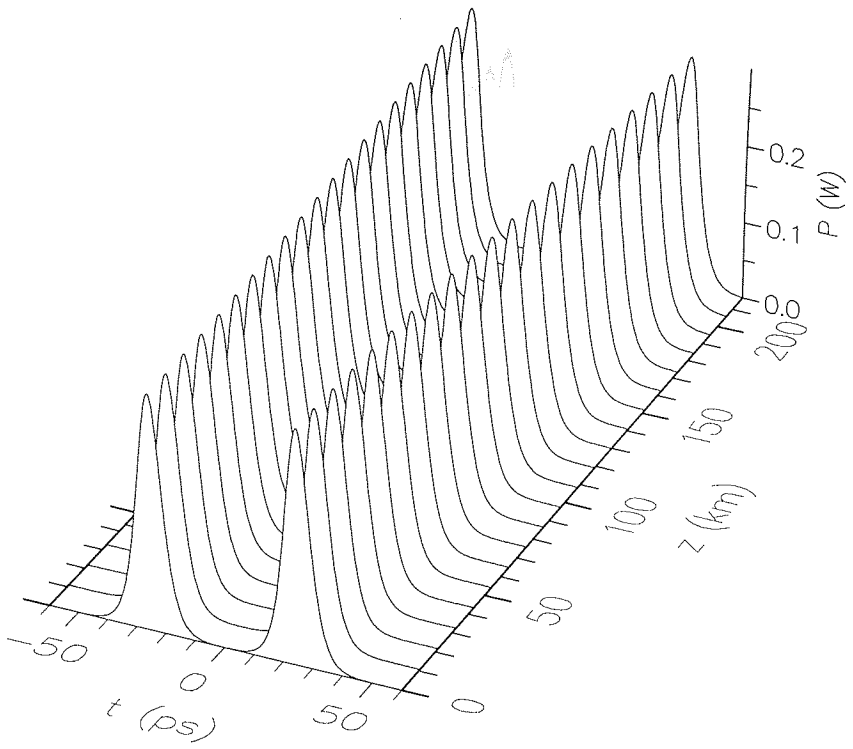

Figure 2.6: Two 10 ps pulses at 20 Gbit/s in standard fibre, as in figure 2.5, but with a π phase difference between them.

their given bit slots. This behaviour arises from the difference in the evolution rates of the phases of the two pulses. As described above (equation (2.44)) the rate of evolution of phase is related to the pulse amplitude. Thus the phases of unequal amplitude pulses will vary at different rates, constantly going in and out of phase, hence the pulses periodically attract and repel and both effects cancel out. This effect has been used successfully to propagate solitons for 11500 km at 20 Gbit/s [87] and 500 km at 80 Gbit/s [88].

The other distinct soliton interaction case is that of solitons of different frequencies, as used in a wavelength-division multiplexed (WDM) communication system [84, 89]–[91]. Trains of pulses of different frequency will travel at different rates due to the difference in the group velocity and will hence collide and interfere periodically when they are in conjunction. After interfering the pulses emerge unperturbed from the encounter, as illustrated in figure 2.8.

Even though the pulses do emerge unscathed by their encounter, there is a small modification to the pulse position, seen in the figure, resulting from the modification to the refractive index. The manifestation of the refractive index change is

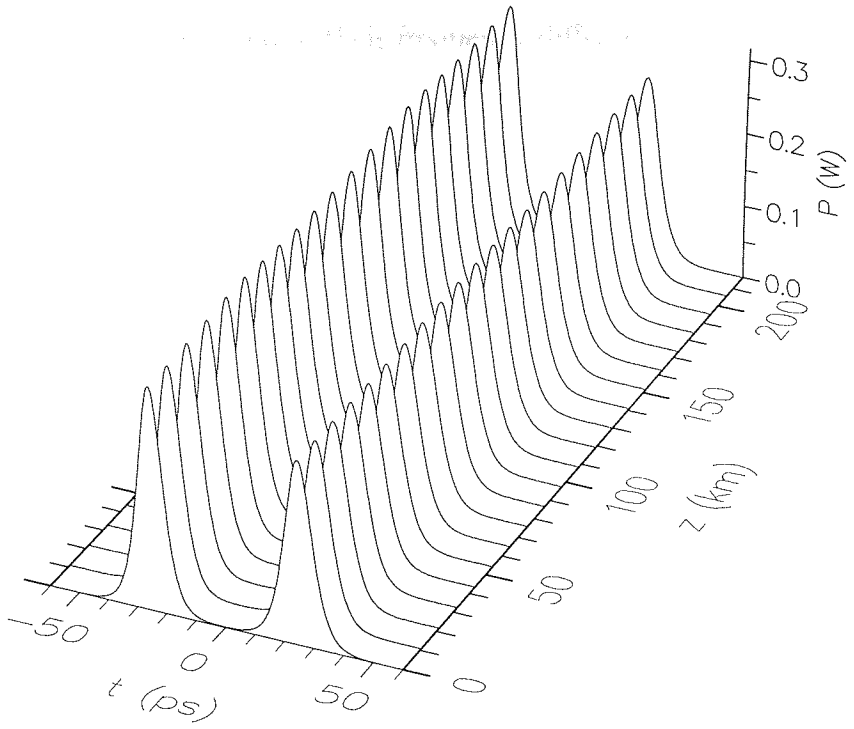

Figure 2.7: Interaction of two in-phase solitons at 20 Gbit/s in standard fibre with an amplitude difference of 10%

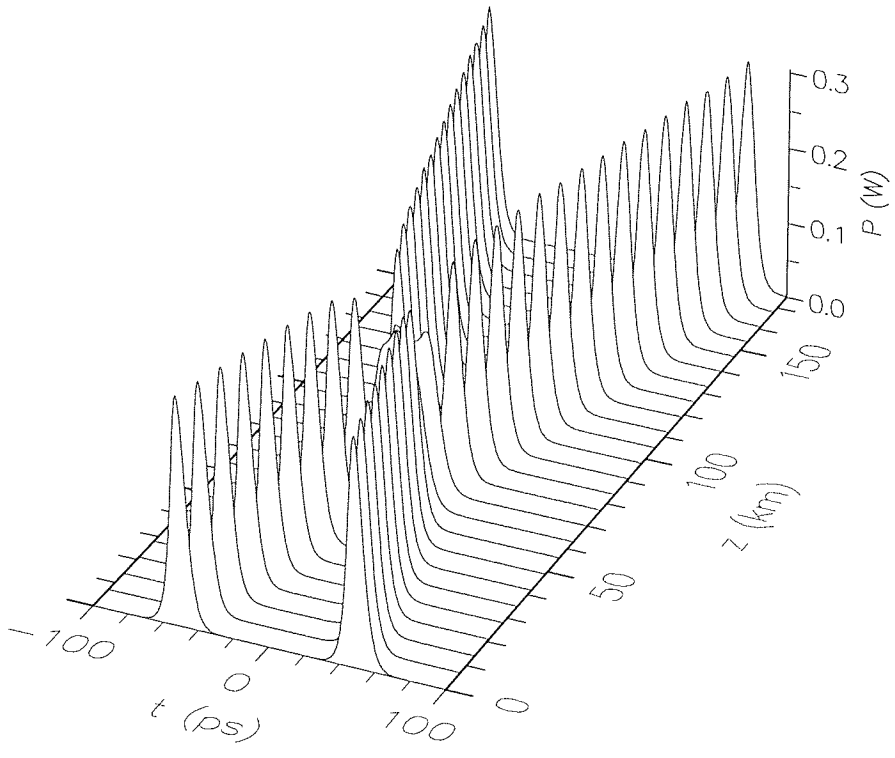

Figure 2.8: Interaction of two 10 ps pulses of different frequency (40 GHz frequency separation) on propagation along an optical fibre.

that while the pulses interfere, the slower pulse is retarded and the faster pulse advanced, by a time proportional to their frequency difference [72, 89]. Although both pulses return to their original velocity once the interaction is complete, there is an implication for data in a WDM transmission system. Due to the random data imposed on the communication data stream, the pulses of one stream will not always encounter a pulse from the other. This results in a random number of temporal shifts any given pulse encounters. Over a long-haul communication system, the temporal shifts can become significant and thus limit how closely WDM channels can be placed. This thesis considers only single wavelength channel propagation so this effect shall be left out of the systems design considered below.

2.8.2 The Gordon-Haus effect

It was mentioned above that solitons are resilient to perturbations, as they try to re-attain the stable soliton solution if perturbed. This can lead to somewhat unusual consequences, such as the random timing jitter solitons experience in long transmission systems, know as the Gordon-Haus effect [53, 92]. This resilience also leads directly to one method of dealing with this timing jitter problem.

The Gordon-Haus effect is a result of the ASE noise introduced by the EDFAs to the propagating signal. This noise affects all four of the parameters required to define a soliton, namely the temporal position, the spectrum, the pulse width and the phase, but the most important perturbation is found to be that experienced by the soliton spectrum [93],pp.130. The resilience of the soliton to perturbations means that the pulse will try to absorb this noise component. This absorption results in a small change in the soliton spectrum as its average central frequency will be shifted by the new noise induced component of the spectrum, toward or away from the new noise component frequency, depending on the relative phases. This frequency shift can have a profound effect. The problem encountered is not however in the frequency domain but in the temporal domain. The slight change in frequency gives a small change in the group velocity of the pulse. Over a long propagation distance, this will result in a difference in the arrival time of the pulse from the centre of its nominal bit slot, the random timing jitter.

Briefly, the Gordon-Haus effect comes from the change in the group delay

of a pulse over one amplifier span L_a of $\Delta t_g = \beta_2 L_a \Delta\omega$ for a frequency change $\Delta\omega$. By considering an ensemble of pulses and summing their variation over the full system length an estimate of the standard deviation of the pulse arrival time $< t_N^2 >^{1/2}$ can be derived as [92]

$$\left\langle t_N^2 \right\rangle = \frac{2\pi n_2 N_{SP} |\beta_2| hc(G-1)L^3}{9\tau_0 \lambda^2 A_{eff} \Lambda_0^2} \tag{2.62}$$

where N_{SP} is the spontaneous emission factor of the amplifiers, h is Planck's constant, G is the amplifier gain and τ_0 is the pulse width. This equation shows that the deviation of the pulse position and hence jitter experienced is dependent on the system length by $L^{3/2}$. For short systems this will mean that the jitter is low (depending on the other parameters) and not a significant problem, but for longer system lengths the jitter may become significant and can be the limiting factor in long distance systems design.

In order for the detector at the end of a system not to receive an error the pulse must arrive within a time window $\pm t_w$ around its input position. Assuming Gaussian statistics, obtaining a typically acceptable bit-error ratio (BER) of less than 10^{-9} requires that the variance allowable is [72, 92]

$$\left\langle t_N^2 \right\rangle = \left(\frac{t_w}{6.1} \right)^2. \tag{2.63}$$

Through equations (2.62) and (2.63) we can find the maximum transmission distance allowed for a given set of parameters and this error ratio as

$$L_{max}^3 \leq 0.1372 \frac{\tau_f t_w^2 A_{eff} L_a \Lambda_0^2}{N_{SP} n_2 D_2 h (G-1)} \tag{2.64}$$

where we have used the experimentally useful units D_2 and $\tau_f = 2ln(1+\sqrt{2})\tau_0 = 1.763\tau_0$, the full-width at half-maximum width for a soliton. Thus we see that there is a limit to the length of any soliton transmission system due to the ASE noise shifting the frequency of the signal and hence the arrival time of the pulse through the interaction of the pulse with dispersion. This is illustrated in figure 2.9 for a typical system of 10,000 km. The jitter is clearly seen as the pulses have moved away from their input position at the zero point of the time axis. The system

simulated is too jittered for use if the data rate were 10 Gbit/s and a typical arrival window of one third of the bit interval $t_w = 33$ ps is used.

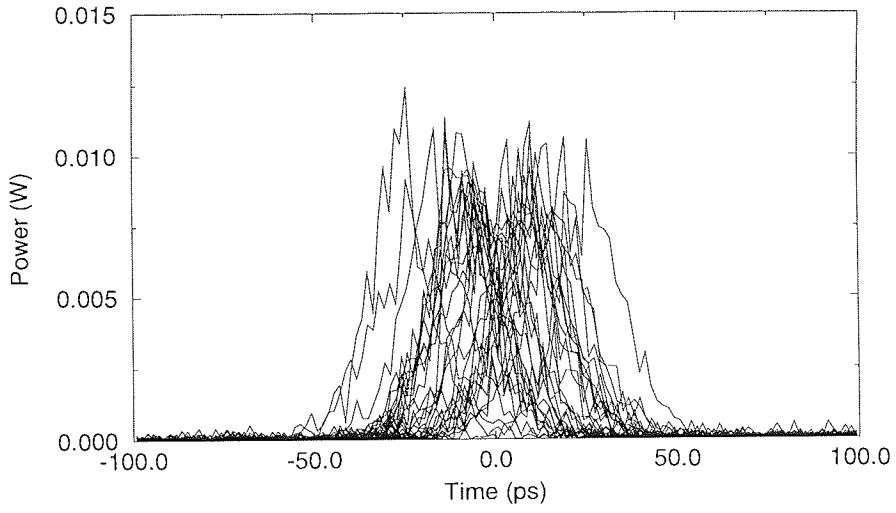

Figure 2.9: Example of the Gordon-Haus effect on 32 pulses, 20 ps wide after transmission through 400 amplifiers spaced every 25 km, giving a system length of 10,000 km. The amplifiers were assumed to be perfect ($N_{SP} = 1$) and the fibre dispersion was 1 ps/nm/km, giving a deviation in the pulse arrival time at this point of $< t_N^2 >^{1/2} = 49$ ps.

We mentioned earlier the use of filters to reduce ASE noise introduced to an optical signal by EDFAs. However, filtering the noise away from the solitons is a somewhat double-edged sword in that whilst filtering reduces the bandwidth of the noise and hence the shift in frequency experienced, it also introduces an additional loss to the wings of the soliton. In practice filters also have a finite insertion loss across the whole bandwidth. In order to compensate these losses, the gain of the amplifier must be increased. This again leads to an increase in the jitter. As the ASE noise introduced to the signal increases linearly with gain [92] the noise at the centre of the soliton spectrum which cannot be filtered will increase degrading the signal-to-noise ratio discussed below. Thus a balance must be struck as to the bandwidth of the filtering and gain that is acceptable [94].

One other possible way to reduce the Gordon-Haus jitter would appear from equation (2.62) to be that of reducing the dispersion of the fibre link. Whilst this method does give some benefit, reducing the dispersion reduces the power required to support a fundamental soliton. If the dispersion is taken too low the energy in per pulse will be insufficient for the detector to distinguish the signal from the

noise resulting in errors at the receiver. There are other problems that can be encountered by solitons in low dispersion systems, particularly the effects of higher order dispersion and polarisation mode dispersion (PMD) which limit how low the dispersion can be taken. Optimisation must be performed to find the exact dispersion required.

As this timing jitter appears to limit the possibility of long distance soliton transmission and the data rates of such systems, a great deal of work has been directed to reducing or eliminating its effects [95]–[102]. There is an overlap here to other soliton work towards an optical fibre "soliton storage ring" where pulses can be maintained for long times (and hence long distances) in order to provide an optical buffer or memory [103]–[106] which obviously suffers similar problems to soliton transmission. One novel result has returned solitons to the fore again. It has been shown that this resilience could lead to a substantial reduction in the ASE noise build-up and the accumulation of timing jitter, by forcing the solitons to follow a change in their central wavelength [107]–[111]. By gradually changing the central wavelength of the filters in a transmission line away from the input wavelength, the solitons are forced to slide to the new central wavelength. However as the noise is linear it cannot follow the shifting wavelength and will eventually be attenuated by the filters. This "sliding-guiding" filter technique has been used to great effect to propagate solitons of 20 Gbit/s over 14,000 km error-free [111]. The advantages found from this form of filtering by far outweigh the disadvantages of the extra gain requirement. There are still concerns however over this filtering technique regarding its implementation in a real system where supervisory systems are required, such as its compatibility with optical time-domain reflectometry (OTDR).

2.8.3 The required signal-to-noise ratio

Another consequence of noise for optical communication systems is the requirement that the signal-to-noise ratio (SNR) be maintained at a level which is acceptable at the detector. The SNR from signal-spontaneous beat noise is given by [14]

$$SNR = \frac{< i_{sig}^2 >}{< i_{sig-spon}^2 >} = \frac{(eP_{out}/(h\nu))^2}{(2e/(h\nu))^2 P_{out} F_{out}} \tag{2.65}$$

where $F_{out} = N(G-1)\mu h\nu B$ is the total ASE power at the output of amplifier N in a bandwidth B and P_{out} is the average optical power in a signal pulse. As the power required to support a fundamental soliton is a function of the dispersion of the optical fibre, this requirement can limit how low the dispersion can be taken in trying to eliminate effects such as Gordon-Haus jitter. Frequently the minimum SNR requirement is taken as 23 dB within a bandwidth of half that required for the data rate, $B = 1/2T_R$ [72].

2.8.4 Average power considerations

At the other end of the power scale from the required SNR, there are other power aspects of soliton system design. For a soliton data stream, the average power requirement is found by averaging over a single bit period,

$$P_{av} = \frac{1}{2T_R}\int_{-T_R/2}^{T_R/2} P_0 sech^2(t/\tau_0)dt \tag{2.66}$$

$$= \frac{P_0\tau_0}{2T_R} \tag{2.67}$$

where the factor of 1/2 assumes 50% data ones in the data stream. Substituting from equations (2.41) and (2.32) we obtain the average output power required from an amplifier as

$$P_{av} = \frac{N^2|D_2|\lambda^2}{\pi c\gamma\tau_0 T_R}. \tag{2.68}$$

The first power aspect to consider is that of the maximum safe average power in the fibre. As equation (2.68) shows, the power requirements for solitons goes up linearly with the data rate and the dispersion, and inversely with pulse width. As the drive to ever higher data rates continues, so the average powers required will increase to the point that they may approach the limits set for the average powers by safety standards. Current UK safety limits allow up to 50 mW of optical power. Whilst this is generally not a problem as yet, it may become one in the not too distant future. The problem is more acute for upgrading the existing standard fibre base to higher data capacity, due to the large dispersion at $1.55\mu m$ of around 17 ps/nm/km.

Another power consideration that causes concern amongst those in favour of NRZ transmissions is that of the average power required to support solitons.

Systems designers wish to keep powers low partly because for laser diodes higher operating output powers generally mean lower device lifetimes hence lower reliability and additional replacement costs. The argument against solitons is that as solitons are nonlinear pulses, the power required to support them must necessarily be greater than that for NRZ systems. On the face of it this is a valid argument but neglects the mark-to-space ratios of the two formats. NRZ systems essentially have a mark-to-space ratio of one, with an NRZ data one essentially filling its data slot. As discussed above though, in order to avoid unwanted soliton-soliton interactions (assuming in-phase, equal amplitude pulses, as usually preferred for soliton system designs), solitons require a mark-to-space ratio of 1:6 – 1:10. Thus although the peak power of the solitons may well be higher than that of NRZ pulses, the average power per bit interval can in fact be significantly lower. The NRZ average power requirement stems from the need to maintain a given signal to power ratio, given by

$$P_{out} = 2SNR(G-1)N_{SP}h\mu B\frac{L}{L_a}. \tag{2.69}$$

By way of example, for a given fibre dispersion of 0.5 ps/nm/km and loss 0.2 dB/km over amplifier spacings of 25 km at a data rate of 10 Gbit/s, the average power required to support a data stream of 10 ps solitons at 1.55 μm will be 0.93 mW at the output of any amplifier in the system. Taking the requirements of $SNR = 23dB$ and $B = 1/2T_R$ as above, $N_{SP} = 2.0$ and a total system length of 10,000 km for an NRZ system the average power will be a minimum of 0.44 mW. Hence this example soliton system would require approximately twice the minimum power of an equivalent NRZ system. However, this is the actual soliton power required fixed by the average soliton prescription as opposed to the minimum for the NRZ system. Such a factor of 2 may well be absorbed by further safety margins in the NRZ system and so giving similar average powers for both types of system.

2.8.5 Acoustic interactions

Solitons propagating along a transmission fibre send an acoustic shock wave transverse to the fibre axis into the fibre cladding through electrostriction [112]–[114]. This results in a self-frequency shift in the pulse again giving a temporal shift with

propagation. In addition, there is an interaction with pulses arriving later, as the wave reflects from the cladding boundary $\sim 20ns$ later. These shifts in the carrier frequency, as for the Gordon-Haus effect, give a change in the GVD the pulse experiences giving a shift in the arrival time of a pulse. The main concern for optical communications is not the self-action, which will be the same for each pulse, but the pulse-pulse interaction as, if data is imposed on the optical signal, whether or not a pulse experiences this interaction will depend on whether a data one is the correct distance ahead or not. This random timing jitter increases as the square of the distance transmitted, or linearly with distance when using filters [115].

As the strength of the acoustic interaction varies with the square of the dispersion [112]–[114], this mechanism can become very significant in high dispersion systems, such as in the first experimental observation of this jitter [116]. As long distance systems generally require lower dispersions, Gordon-Haus jitter will tend to dominate in these systems. However as shorter systems can use higher dispersion, acoustic interactions can be the dominant jitter mechanism for solitons. This may present a limit particularly with regard to the upgrading standard fibre systems over 1,000 km as even if dispersion compensation is used to remove the other unwanted effects of high dispersion this jitter mechanism will not be compensated and will continue to build up in the standard fibre sections.

2.8.6 Soliton system design diagrams

Now that the main limits to soliton systems have been discussed we need some way of assessing their combined impact, to find the possible set of parameters under which a system can be operated. This is generally done through the use of a soliton systems design diagram, where the above limitations are plotted as a function of pulse widths against amplifier spacing. Here we consider the design diagrams for long distance high data rate transmission, namely trans-Atlantic ($> 6,000km$) and trans-Pacific ($> 10,000km$) systems.

Figures 2.10 and 2.11 are the design diagrams found, using the above limitations, at data rates of 5 and 10 Gbit/s respectively for (a) trans-Atlantic and (b) trans-Pacific system lengths. As can be seen, there is a wide range of allowable pulse widths and amplifier spacings for 5 Gbit/s even for 10,000 km. However, for

10 Gbit/s while the system can be operated over 6,000 km, there is no region of operation for 10,000 km. In this case the major limitation is the Gordon-Haus jitter which requires such long pulse widths to suppress its effects (see equation (2.64)). Thus, as stated above Gordon-Haus jitter is generally the main limitation to soliton propagation over long distances. Given the small region of operation for 10 Gbit/s over 6,000 km is seems unlikely that data rates above this, the next two being 20 and 40 Gbit/s, will even make transatlantic distances.

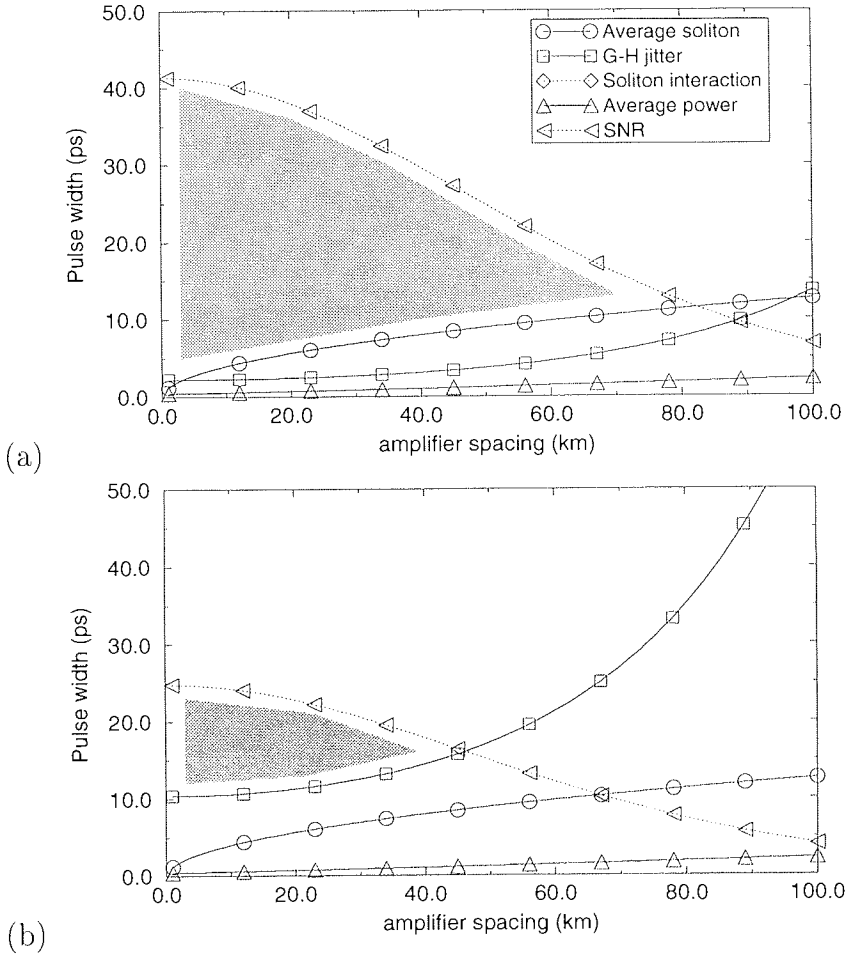

(a)

(b)

Figure 2.10: Design diagrams for a 5 Gbit/s transmission system for distances of (a) 6,000 km and (b) 10,000 km. Limits are above solid lines and below dotted lines, shaded area shows acceptable region of operation. Other parameters used were $\lambda = 1.555\mu m, D_2 = 0.5ps/nm/km, \alpha = 0.22dB/km, N_{SP} = 1.4, A_{eff} = 40\mu m^2, SNR = 23dB$ within a bandwidth $B = 1/2T_R$, Gordon-Haus jitter $BER = 10^{-9}$ in a window $T_R/2$. Note that the soliton interaction limit is unimportant for this system configuration and length and is above the maximum pulse width shown.

It must be noted that the rules outlined above used for such design diagrams are necessarily conservative, although this is counterbalanced by their over-

simplicity in ignoring other effects such as PMD. Actual systems design will take these design diagrams only as a starting point, with the eventual choice of system parameters found by extensive numerical simulation and experimental testing. Obviously they do not include some of the more advanced techniques to extend the transmission distance such as sliding-guiding filtering. As such, although these diagrams can form a basis for further work, their main function can be to set the direction of the work required to improve the transmission. An example of this will be seen for shorter system lengths in chapter 4.

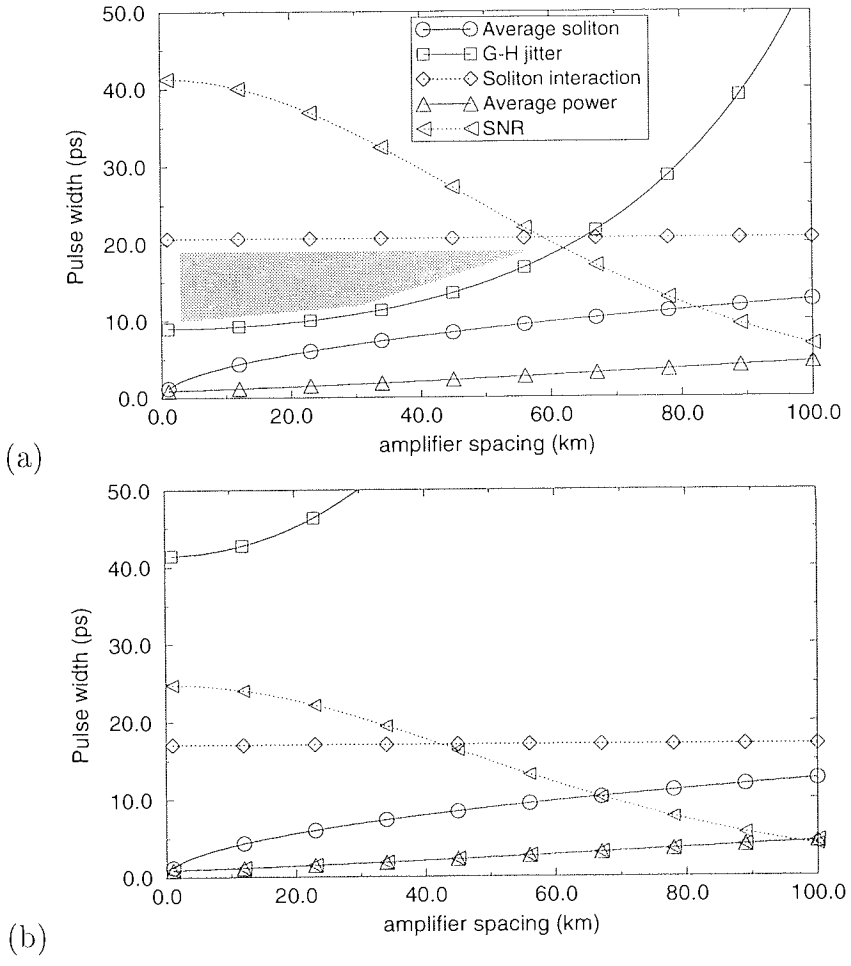

(a)

(b)

Figure 2.11: Design diagrams for 10 Gbit/s as in figure 2.10.for distances of (a) 6,000 km and (b) 10,000 km. Limits are above solid lines and below dotted lines, shaded area shows acceptable region of operation. Again, other parameters used were $\lambda = 1.555\mu m, D_2 = 0.5ps/nm/km, \alpha = 0.22dB/km, N_{SP} = 1.4, A_{eff} = 40\mu m^2, SNR = 23dB$ within a bandwidth $B = 1/2T_R$, Gordon-Haus jitter $BER = 10^{-9}$ in a window $T_R/2$.

Chapter 3

Stepwise dispersion profiling optical transmission systems

3.1 Introduction

The perturbations to solitons from the loss-gain cycle of a periodically amplified communications system are essentially negligible if the system is designed such that amplifier spacing condition of the average soliton prescription is satisfied ($L_a \ll Z_0$ or $z_a \ll z_0$), . However, as $L_a \to Z_0$ the perturbations to the pulses can become so great that the solitons can no longer recover and the pulse may be destroyed within a few L_a. Since the period of a soliton Z_0 is proportional to τ_0^2/D_2 as we move to ever higher data rates and hence shorter pulses so the soliton period and allowable amplifier spacing decreases and the problem becomes exacerbated. For an average soliton of width τ_0 in a system of fixed amplifier spacing L_a, the soliton period may be increased by reducing the fibre dispersion, D_2, hence reducing the perturbations. However, since the soliton power is also proportional to D_2, this has a detrimental effect of simultaneously reducing the pulse power and therefore the signal-to-noise ratio (section 2.8.3). Alternatively, the distortions may be reduced by improving the balance between dispersion and nonlinearity. One possible method is to replace the erbium-doped fibre amplifiers with distributed amplification provided by low doped erbium fibre throughout the transmission line [117, 118], thereby smoothing the variations in the soliton power. However, distributed amplification presents practical difficulties because of the long amplification distances and criticality of the

pumping scheme. A second possibility is to tailor the fibre dispersion to match the variation of the soliton power and hence improve the GVD–SPM balance [119, 120]. Tailoring is entirely passive, may be implemented with no reduction in the average system dispersion, and therefore no reduction in the signal to noise ratio, but does require careful design of the dispersion profile for optimum results. It is this scheme and in particular its design problem which is the subject of this chapter.

A number of studies of soliton propagation in fibres with periodically varying fibre parameters have already been reported. One particular application is the generation of high repetition rate solitons by propagation of the beat signal from two c.w. waves separated in frequency by the required repetition rate through a suitable dispersion decreasing fibre [121]. For soliton communication systems, it has been shown that average soliton concepts also apply to soliton propagation in such fibres [25]. Thus, the average soliton is robust to the perturbations resulting from fluctuations in the fibre parameters, arising during the manufacturing process provided, as above, the period of these variations is short compared with the soliton period. Indeed, under this condition, soliton robustness to large scale changes in the fibre dispersion has been studied and verified numerically [26]. Deliberate profiling of the fibre dispersion to improve propagation results was first suggested by Tajima in 1987 [119]. It was noted that an exponentially varying fibre dispersion which matched the exponential variation of the pulse energy could in principle facilitate distortionless transmission. However, such careful profiling of fibre dispersion is difficult to achieve over long fibre lengths at present. Therefore, it was suggested subsequently that the exponential variation could be approximated by a stepwise linear decrease [122], using many fibre sections of equal length and the dispersion required at the section midpoint. The results were studied using a variational approach over a single unamplified span and improvements in transmission fidelity were obtained. This chapter considers in further detail the potential advantages of stepwise dispersion profiling to periodically amplified systems. Using an intuitively appealing perturbation function, a simple scheme for optimal profiling is derived which is shown to allow average soliton propagation beyond the usually accepted limits. While soliton communication systems are the focus of this discussion, the results apply equally to unidirectional erbium fibre ring lasers.

3.2 Mathematical model description

In section 2.6 the concept of the average soliton was introduced, wherein a pulse can propagate as if in a lossless medium. However, although the soliton appears to propagate with the nonlinearity and dispersion in balance over many amplifications, over one amplifier span there is a local mismatch. Figure 3.1 shows the nonlinear coefficient of the NLSE, $\Lambda^2(z)$, defined in equation (2.51) and therefore the mismatch between dispersion and nonlinearity over an amplification period, for an example soliton communication system. The above average intensity level in the first part of the period results in an initial surplus of self phase modulation chirp over group velocity dispersion chirp, which is then compensated during the latter part of the period, where the group velocity dispersion dominates over self phase modulation. (In a fibre laser, the presence of distributed gain and lumped loss, as opposed to lumped gain and distributed loss, reverses the order of these dominating influences.) This spatial mismatch results in a perturbation to the average soliton which depends on the depth and period of the modulation and has been shown to be $O(z_a^2)$ [23, 24] where as before $z_a = L_a/L_D$. Detailed expressions for its magnitude can be obtained as a function of the distance variable, z, via a perturbation approach [23] or per amplifier spacing, z_a, via an operator approach [62]. In this work a simple integrated measure of the perturbation per amplifier spacing is considered to be the *mismatch area*, $A_1(\Gamma, z_a)$, between the function $\Lambda^2(z)$ and its average, given by,

$$A_1 = \int_0^{z_a} |\Lambda^2(z) - 1| dz = \frac{1}{\Gamma}\left[\Lambda_0^2 - 1 - ln\Lambda_0^2\right] \tag{3.1}$$

with $\Gamma = \frac{\alpha}{2} L_D$ the normalised loss as before (equation (2.48)) and

$$\Lambda_0^2 = \frac{2\Gamma z_a}{1 - e^{2\Gamma z_a}} \tag{3.2}$$

as in section 2.6. This function is $O(z_a^2)$ for small z_a and is directly related to the first order perturbation function ($\tilde{A}_1(z)$) derived in [23] which is itself $O(z_a)$ and perturbs the nonlinear Schrödinger equation with nonlinear terms of $O(z_a^2)$. Thus A_1 is a lowest order and intuitively appealing measure of the net periodic perturbation. This takes no account of any evolution in the soliton parameter but,

as confirmed below, provides an accurate basis for predicting improved propagation characteristics.

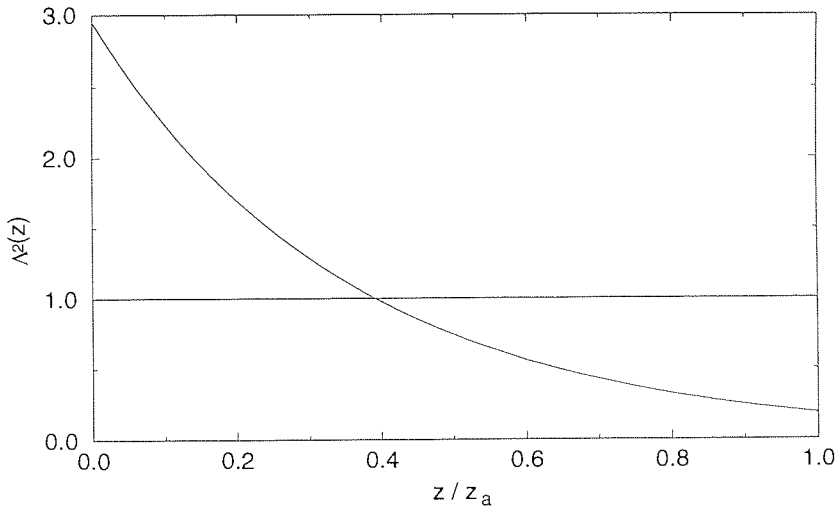

Figure 3.1: Variation of the perturbation function $\Lambda^2(z)$ against distance (normalised to the amplifier spacing) in a periodically amplified soliton communication system (pulse energy, peak intensity and amplitude have similar variations). Here the total span loss is $\Gamma z_a = 12$ dB

In the remainder of this chapter we shall adopt a slightly different notation for the dispersion from that of chapter 2. The group delay dispersion of a given fibre will be D, as opposed to D_2 throughout the rest of the thesis, as we wish to use the dispersions of the various profile sections to be $D_1, D_2, \ldots, D_j$. Now consider a stepwise variation in the fibre dispersion D with average value D_a and periodicity z_a, as shown for example in figure 3.2(a). The period z_a is divided into n sections each with dispersion D_j, start point z_{j-1} and end point z_j ($z_{00} = 0, z_n = z_a$, with z_{00} the zero point to avoid confusion with the soliton period z_0). The relevant renormalised quantities are then given by

$$\Lambda' = \frac{D_a}{D_j}\Lambda, \quad \Gamma' = \frac{D_a}{D_j}\Gamma, \quad (z' - z'_{j-1}) = \frac{D_j}{D_a}(z - z_{j-1}), \tag{3.3}$$

where

$$\sum_{j=1}^{n} D_j(z_j - z_{j-1}) = D_a z_a. \tag{3.4}$$

It was mentioned above that if it were possible to taper the dispersion exponentially

[119], in our notation according to,

$$D(z) = D_a \Lambda_0^2 e^{-2\Gamma z} \tag{3.5}$$

the GVD would balance the SPM continuously over the entire period. It follows that a stepwise approximation of equation (3.5), such as that in figure 3.2(a), would improve the balance. Alternatively, one can think of each dispersion step acting as an *effective amplification* [121] to rescale the soliton amplitude, keeping the function $\Lambda^{2'}(z')$ closer to its optimum value of unity, as shown in figure 3.2(b). Clearly, the greater the number of steps, the better the approximation and so the reduction in the perturbation. Therefore, the optimal dispersion profile, for any given number of profile steps, is defined as that which minimises the total mismatch area per amplifier spacing.

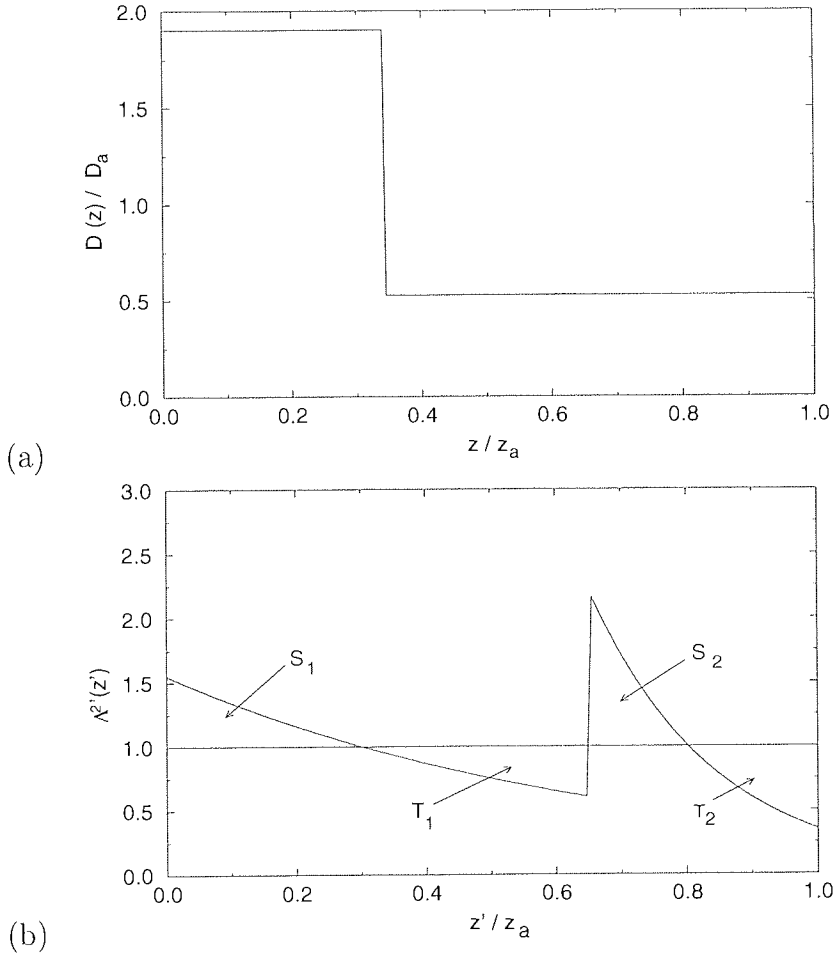

Figure 3.2: (a) Stepwise 2-fold periodic variation of the fibre group delay dispersion $D(z)$ with normalised distance to follow the soliton energy variation. (b) $\Lambda^{2'}(z')$ in the profile of (a). Note the reduction of the total mismatch area compared with figure 3.1

Under the above renormalisation, the total areas above and below the line $\Lambda^{2'}(z') = 1$ remain equal as befits an average soliton, but the total mismatch area,

$$A_n = \sum_{j=1}^{n} \int_{z'_{j-1}}^{z'_j} |\Lambda^{2'}(z') - 1| dz', \tag{3.6}$$

varies according to the specific profile in question. For example, figure 3.3 illustrates the variation of $\Lambda^{2'}(z')$ under a 2-fold rising dispersion profile, similar to the one studied in ref. [26], which actually opposes the variation in the soliton power. The average soliton condition is still satisfied over the period z_a, but not within each profile subsection. Here, in comparison to the unprofiled case of figure 3.1, the average soliton experiences greater excess self phase modulation in the first fibre, followed by even more dominant dispersion in the second fibre. Consequently, A_n increases in line with the increased perturbation.

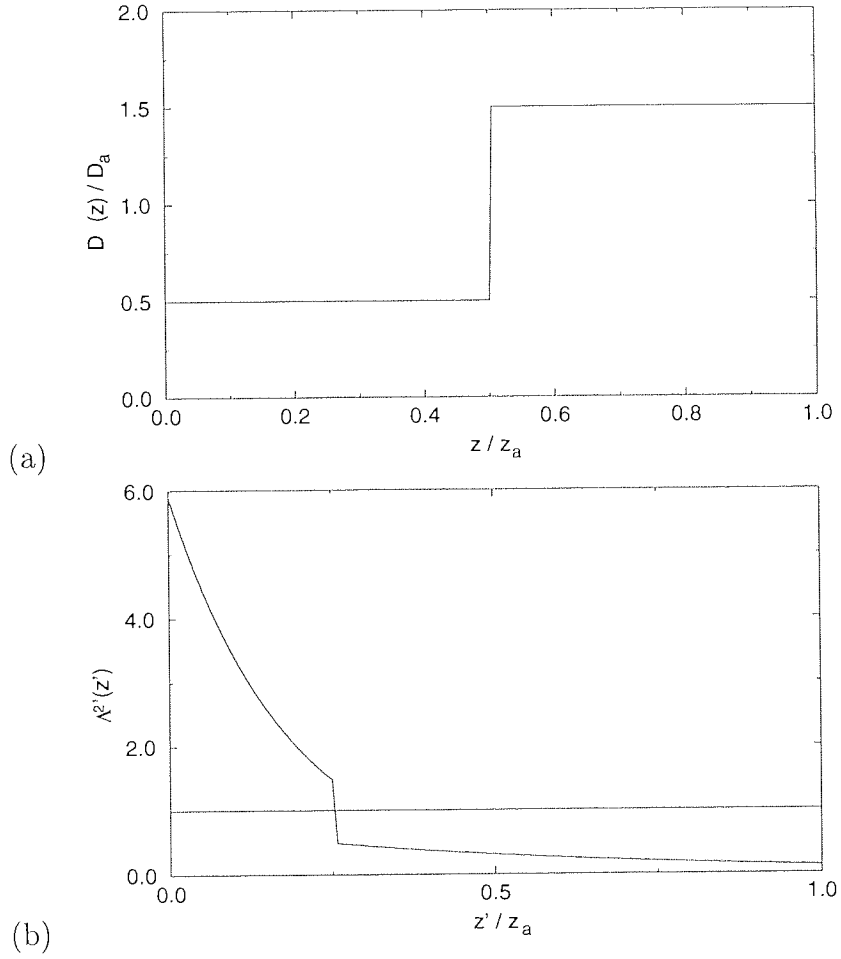

Figure 3.3: (a) Stepwise 2-fold periodic variation of $D(z)$ with normalised distance to oppose the soliton energy variation, for $\Gamma z_a = 12$ dB ($z_1 = z_a/2$, $D_1 = D_a/2$ and $D_2 = 3D_a/2$). (b) $\Lambda^{2'}(z')$ in the profile of (a). Note the increase in the total mismatch area compared to figure 3.1

To optimise the whole profile by minimising A_n, the average soliton condition if first applied to each profile section, i.e.,

$$\int_{z'_{j-1}}^{z'_j} \Lambda^{2'}(z')dz' = (z'_j - z'_{j-1}), \tag{3.7}$$

which minimises each individual mismatch areas. The dispersive profile of the fibre is then slaved to the decaying exponential of eqn. (3.5), and given by,

$$D_j = D_a \Lambda_0^2 \left[\frac{e^{-2\Gamma z_{j-1}} - e^{-2\Gamma z_j}}{2\Gamma(z_j - z_{j-1})} \right]. \tag{3.8}$$

In the simplest case of a 2-fold profile, this gives a set of solutions dependent on the single dispersion step z_1. For example, figure 3.4(a) shows the dependence of D_1 and D_2 on z_1 for $\Gamma z_a = 12dB$. Figure 3.4(b) shows the corresponding variation of the total mismatch area A_2, which is minimised for $z_1 = 0.344 z_a$, when it is approximately 48% of A_1. Therefore, if $D_a = 1ps/nm/km, \Gamma = 0.24dB/km$ and $L_a = 50km$, the optimal profile consists of 17.2 km of fibre with $D_1 = 1.90ps/nm/km$, followed by 32.8 km of fibre with $D_2 = 0.53ps/nm/km$ (figure 3.2). Although the minimum of A_2 is close to the point at which the contributions to A_2 of each section are equal, i.e. $S_1 + T_1 = S_2 + T_2$ in figure 3.4, they do not quite coincide.

In general, the n-fold optimal profile is found similarly, by applying the average soliton condition to each profile section and then minimising A_n. In a concise form the solution is obtained as follows: defining,

$$\Lambda_j^2 = \frac{2\Gamma(z_j - z_{j-1})}{1 - e^{-2\Gamma(z_j - z_{j-1})}} \tag{3.9}$$

eqn. (3.6) becomes,

$$A_n = \frac{\Lambda_0^2}{\Gamma} \sum_{j=1}^{n} \frac{e^{-2\Gamma z_{j-1}}}{\Lambda_j^2} \left(\Lambda_j^2 - 1 - ln\Lambda_j^2 \right) \tag{3.10}$$

which is minimised numerically with respect to the (n-1) free parameters z_1 to z_{n-1}. The dispersion profile is then given by eqn. (3.8), or equivalently by,

$$D_j = D_a \frac{\Lambda_0^2}{\Lambda_j^2} e^{-2\Gamma z_{j-1}}. \tag{3.11}$$

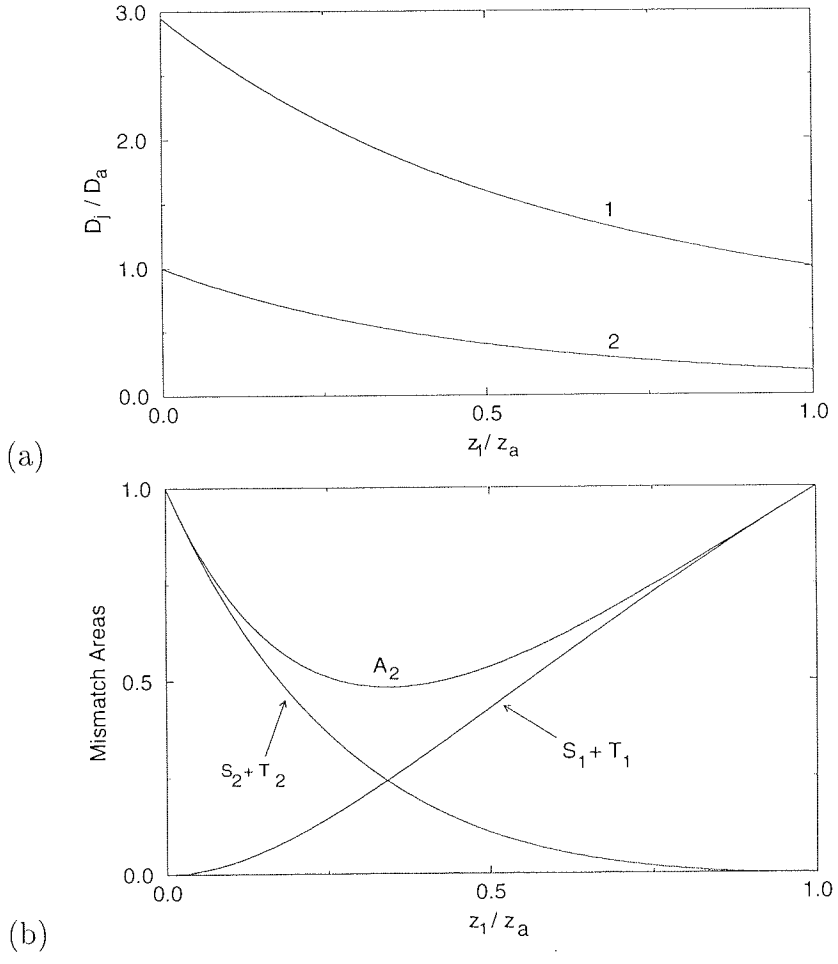

Figure 3.4: (a) D_1 and D_2 versus z_1 for 2-fold profiling and $\Gamma z_a = 12$ dB. (b) Corresponding variations in the mismatch areas $S_1 + T_1$, $S_2 + T_2$ (see figure 3.2 and the total mismatch area A_2.

3.3 Results and discussion

The results above can be summarised in a pair of optimal system design diagrams for each number of profiling steps, n. For example, figures 3.5 and 3.6 show sample optimal design diagrams for two-fold and four-fold profiling. The required dispersion values and lengths only depend on the product Γz_a and can be determined for any given average dispersion and net periodic loss. In each case, the n pairs of values $(D_j,\ z_j - z_{j-1})$, which describe the profile, fan out from $(D_a,\ z_a/n)$ as $\Gamma z_a \to 0$, to give profile sections of gradually decreasing dispersion and increasing length. In renormalised units, this corresponds to modulations of $\Lambda^{2\prime}(z')$ of decreasing length and gradually increasing amplitude, as in figure 3.2(b). In general, as in the two-fold profiling case detailed above, the optimal dispersion profile distributes the total mismatch area and therefore the perturbation near-evenly, but not exactly, across the period. For instance, in the four-fold optimal profile for $\Gamma z_a = 10dB$, the mismatch area per section varies by less than 1%. In long haul communication systems, the periodic fibre loss is likely to be less than 10 dB in order to minimise the effects of noise [123]. Thus, optimal stepwise profiling would require fibres with dispersions varying from about twice D_a to a few tenths of D_a. On the other hand, systems which could accommodate greater periodic losses would require a set of fibres with a greater range of D. For a large profiling parameter n, the required range of D extends over a maximum range from $\Lambda_0^2 D_a$ to $\Lambda_0^2 D_a e^{-2\Gamma z_a}$ (see equation (3.5)).

The reductions in the relative mismatch areas, A_n/A_1, for optimal dispersion profiles are given in figure 3.7, showing a near $1/n$ behaviour and a very weak dependence on Γz_a. It is instructive to compare these improvements in A_n with those obtained by reducing the amplifier spacing from z_a to (z_a/n). In the latter case, the total mismatch area for n sections is given by $nA_1(\Gamma, z - a/n)$ (eqn.(3.1)). These functions have similar $1/n$ dependencies to those of figure 3.7, differing only in that their slight curvature is upward rather than downward. Taking for example, $\Gamma z_a = 10dB$ and n=4, the optimal profile ratio $A_n(\Gamma, z_a)/A_1(\Gamma, z_a)$ is 0.242, whereas the reduced amplifier spacings ratio $nA_1(\Gamma, z_a/n)/A_1(\Gamma, z_a)$ is 0.266. Therefore, according to our simple analysis and confirmed by numerical simulations described below, perturbations to average solitons in a system with n-piece optimally disper-

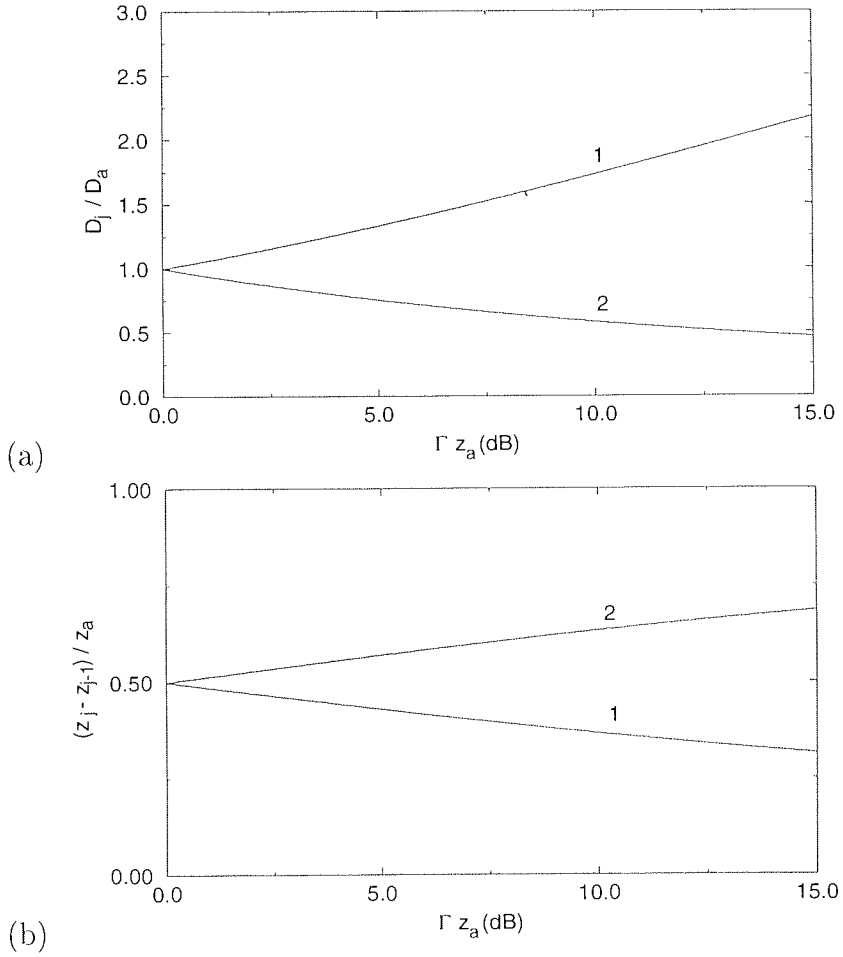

Figure 3.5: Optimal design diagrams for periodically amplified soliton systems with 2-fold profiling (a) dispersion values (normalised to the average dispersion), (b) fibre lengths (normalised to the amplifier spacing), both against total span loss ΓZ_a. $D_1 - -D_2$ from top to bottom and $(z_1 - z_{00})$ to $(z_2 - z_1)$ from bottom to top.

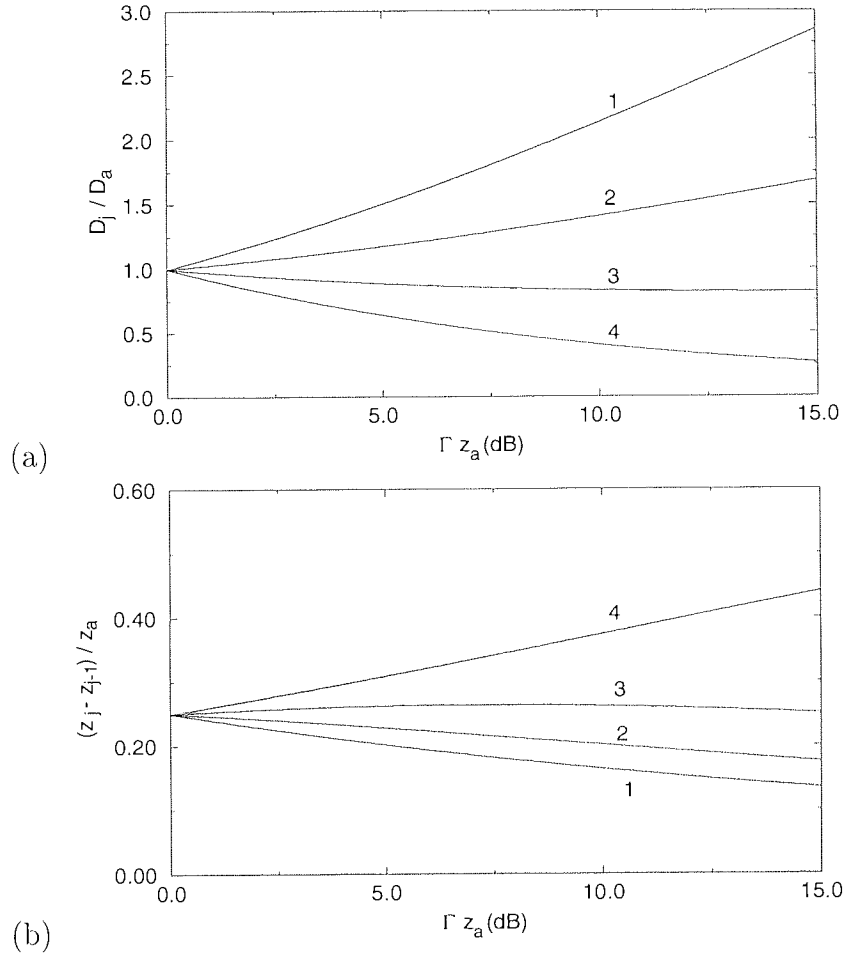

Figure 3.6: Optimal design diagrams for periodically amplified soliton systems with 4-fold profiling (a) dispersion values (normalised to the average dispersion), (b) fibre lengths (normalised to the amplifier spacing), both against total span loss ΓZ_a. $D_1 - D_n$ from top to bottom and $(z_1 - z_{00})$ to $(z_n - z_{n-1})$ from bottom to top.

sion profiled fibre spans are marginally less than those same solitons in a system where the amplifier spacing is z_a/n. This implies that the increase in perturbations caused by doubling the amplifier spacing could be readily compensated by doubling the dispersion profiling parameter n. Alternatively, since the increase in perturbations caused by halving the soliton period (ie. by reducing the pulse width by $\sqrt{2}$) is equivalent to doubling z_a (see the NLSE scalings), it could also be compensated by doubling n.

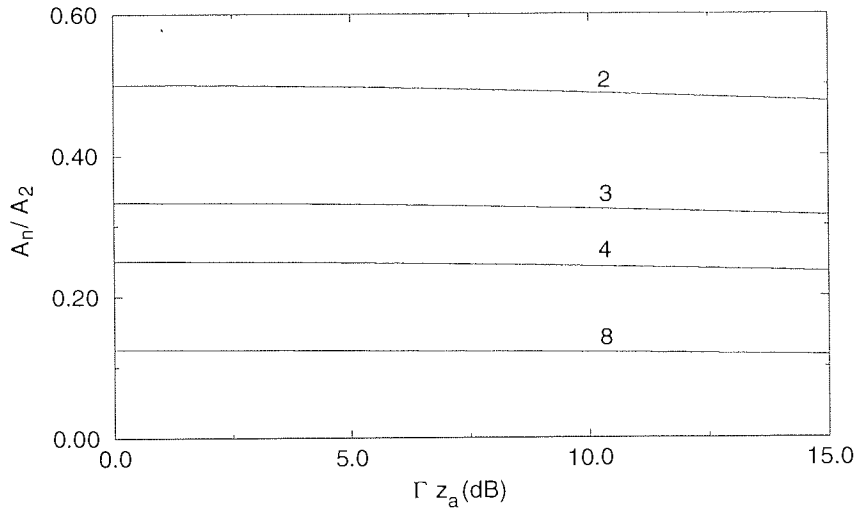

Figure 3.7: Variation of the normalised total mismatch area A_n/A_1 with Γz_a for n=2, 3, 4 and 8

In the above, the potential application of stepwise dispersion profiling to allow either an increase of L_a and therefore decrease of the number of amplifier stations, or a decrease of τ_0 and therefore increase of the data rate R ($R \propto 1/\tau_0$ at a fixed mark-to-space ratio) was considered. However, the potential gains of increasing R or L_a may be mitigated by associated increases in the detrimental effects of amplified spontaneous emission (ASE) noise. ASE noise increases with both R and L_a, and is particularly important in long-haul systems where it degrades the signal to noise ratio (SNR) and gives rise to the Gordon-Haus effect [53]. Moreover, since the RMS Gordon-Haus jitter is inversely proportional to $\sqrt{\tau_0}$ and the amount of tolerable jitter decreases linearly with τ_0, its relative importance increases strongly with the data rate R [53, 92]. On the other hand, increase of L_a also increases the Gordon-Haus jitter, due to higher gain amplifiers required to overcome the greater periodic losses. As a function of G, the associated penalty is

given by [123],

$$F(G) = \frac{[(G-1)/lnG]^2}{G} \tag{3.12}$$

also rising significantly with G and therefore L_a. Thus, in long-haul systems the potential gains are limited by noise considerations. If, however, the ASE noise and in particular the Gordon-Haus effect can be controlled using one of the techniques proposed recently [94, 95, 97, 107], then this dispersion profiling technique could be used effectively. Moreover, in shorter span systems where the effects of concatenated ASE noise are not so critical (the RMS Gordon-Haus jitter varies as $L^{3/2}$, where L is the total system length), the cost and maintenance benefits of increasing data capacity and/or using a greater amplifier spacing could be attractive to system designers.

3.4 Numerical Examples

To demonstrate the effects of stepwise dispersion profiling, figures 3.8 – 3.10 compare numerical simulations of pulse propagation along potentially realistic unprofiled and optimally profiled fibre systems. The chosen parameter values correspond to a path average dispersion $D_a = 1ps/nm/km$, a fibre loss of $0.24dB/km$ and an amplifier spacing of $L_a = 25km$, giving a periodic amplification of 6 dB. With these parameters, the usual design constraints allow operation of long-haul systems, in unprofiled fibre, say 6000 km in length, at 5 Gbit/s using 20ps (FWHM) solitons. Here, a conservative bit interval $(1/R)$ of 10 times the soliton FWHM has been taken to avoid soliton-soliton interactions (in principle the solitons could be closer, giving higher R for a given τ_0). At this data rate, the average soliton period of 158.5 km is six times the amplifier spacing and the perturbations due to the dispersion-nonlinearity mismatch are almost negligible. The length of the system is then chiefly limited by the Gordon-Haus effect. However, as mentioned above, if the Gordon-Haus effect can be overcome, or if the total system length is only a few tens of amplifier periods, in which case the Gordon-Haus effect is relatively small, then the dispersion-nonlinearity mismatch perturbations become increasingly important as the data rate is increased. For operation at 10 Gbit/s, the 10 ps pulses have soliton periods of just under 40 km and these perturbations

are significant; beyond 10 Gbit/s, they are a dominant constraint. Therefore, to further enhance these effects and investigate their reduction using dispersion profiling, the numerical simulations summarised in figures 3.8 – 3.10 were initiated with 5.62 ps pulses ($Z_0 = L_a/2 = 12.5km$), well within the normally disallowed parameter region, thereby modelling systems with potential for operation at data rates of 20 Gbit/s (and beyond, depending on the soliton-soliton spacing). Propagation distances of a few hundred kilometres were considered and to concentrate on average soliton effects ASE noise due to the amplifiers was not included.

Figure 3.8 shows a comparison between pulse shape evolutions in an unprofiled communication system and in a four-fold optimally dispersion profiled system. The difference in their stability is clearly evident in the time domain. In the unprofiled fibre, the initial pulse is immediately broadened and diminished during its early phase of propagation, shedding significant amounts of radiation. Such behaviour is typical of this operation regime. Propagation of the initial soliton cannot be supported by the periodically amplified system so it sheds dispersive wave radiation, losing energy and broadening (note the amplitude–pulse width relationship for solitons) until its pulse width corresponds to a soliton period which is sufficiently long to satisfy the average soliton condition . In contrast, in the optimally profiled fibre, the initial pulse is virtually unperturbed. These observations are confirmed in the corresponding and dramatically different frequency spectra shown in figure 3.9. The spectra of the unprofiled system show significant amounts of energy lost to dispersive radiation, large modulation of the central maximum and rapid growth of the first sideband resonance peak. The higher order resonances are also present and can be seen on a logarithmic scale. In contrast, only slight evidence of radiation ripple and no sign of the first resonance is seen in the profiled system over this propagation distance.

Further evidence of the improvement in soliton stability is shown in figures 3.10(a-c), where details for calculations of the two-fold optimal profiling have also been included. Figure 3.10(a) shows the stabilisation of the initial pulse width with increasing n, indicating the increasing facility of the profiled systems to allow propagation of shorter pulses. This is confirmed in figure 3.10(b) which measures the fractional energy carried in an interval of $\pm$ 50 ps around the initial pulse centre.

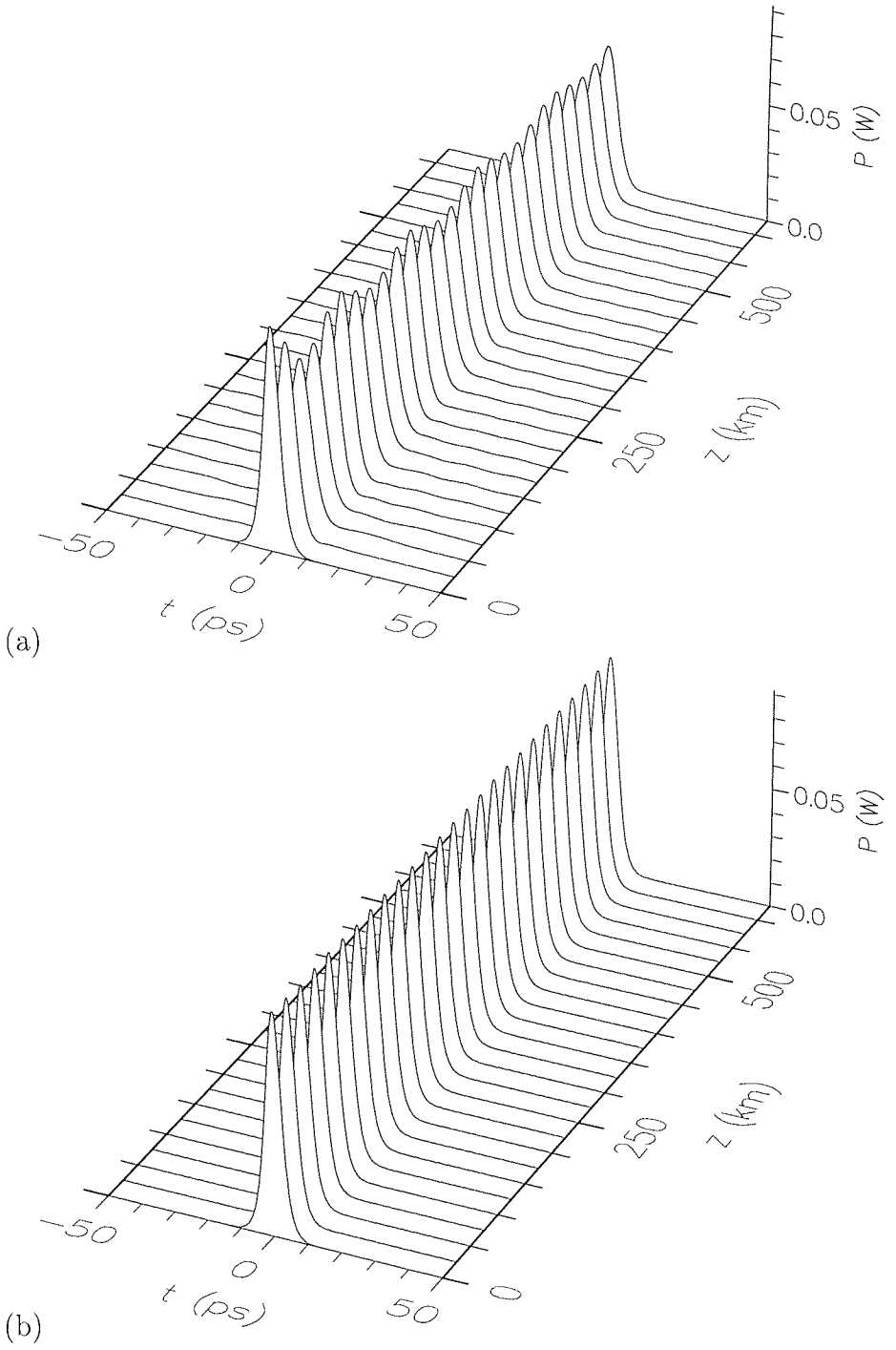

Figure 3.8: Pulse profile evolutions of average N = 1 solitons over 25 amplifier periods (625 km) with 6-dB periodic loss and initial pulse widths of 5.62 ps in (a) unprofiled fibre and (b) four-fold optimally profiled fibre, ie. profile steps at Z_{1-3} = 4.82, 10.39, 16.96 km and D_{1-4} = 1.62, 1.22, 0.87, 0.58 ps/nm/km.

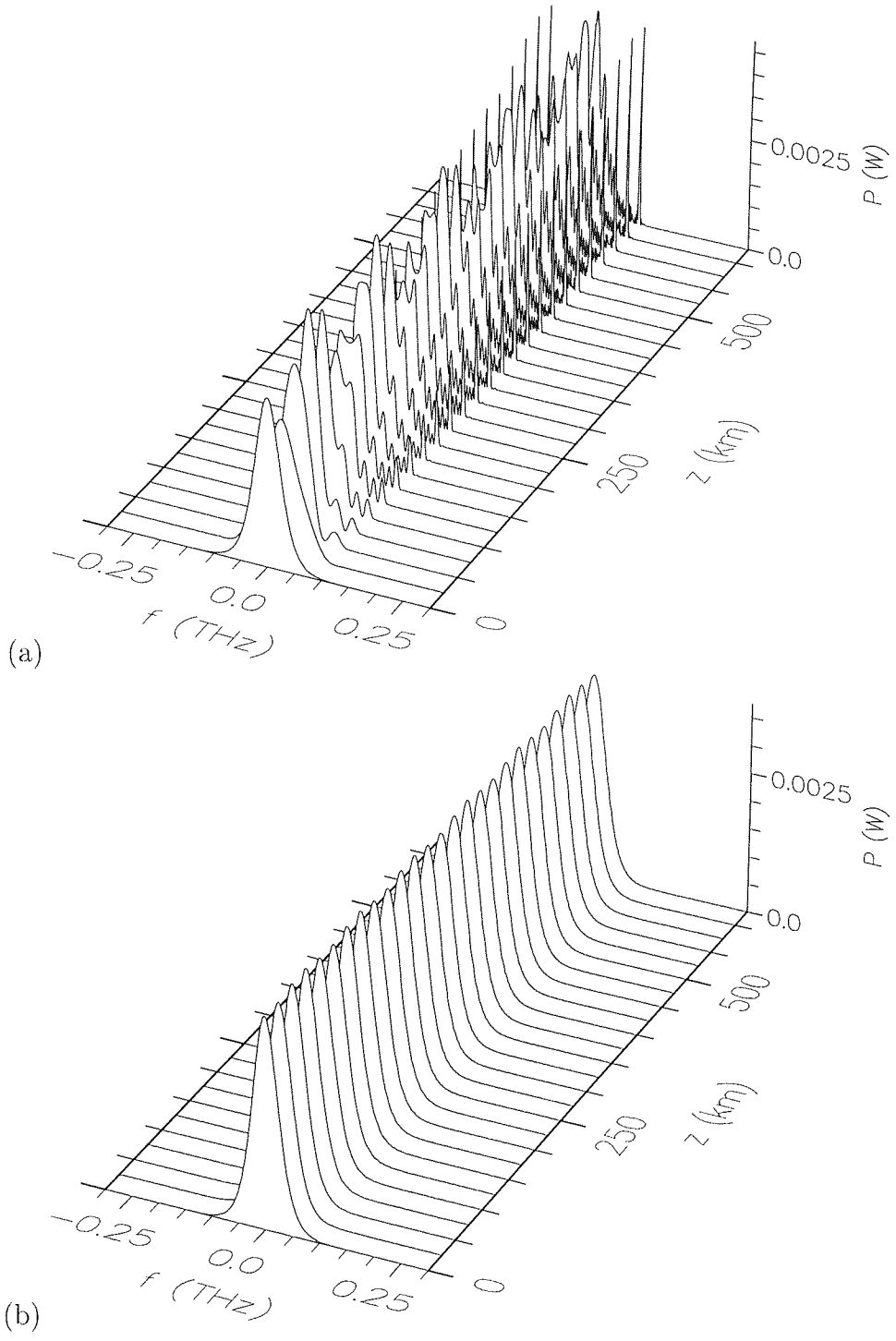

Figure 3.9: Spectral profile evolutions corresponding to the temporal profiles in figure 3.8 for average N = 1 solitons over 25 amplifier periods (625 km) with 6-dB periodic loss and initial pulse widths of 5.62 ps in (a) unprofiled fibre and (b) four-fold optimally profiled fibre.

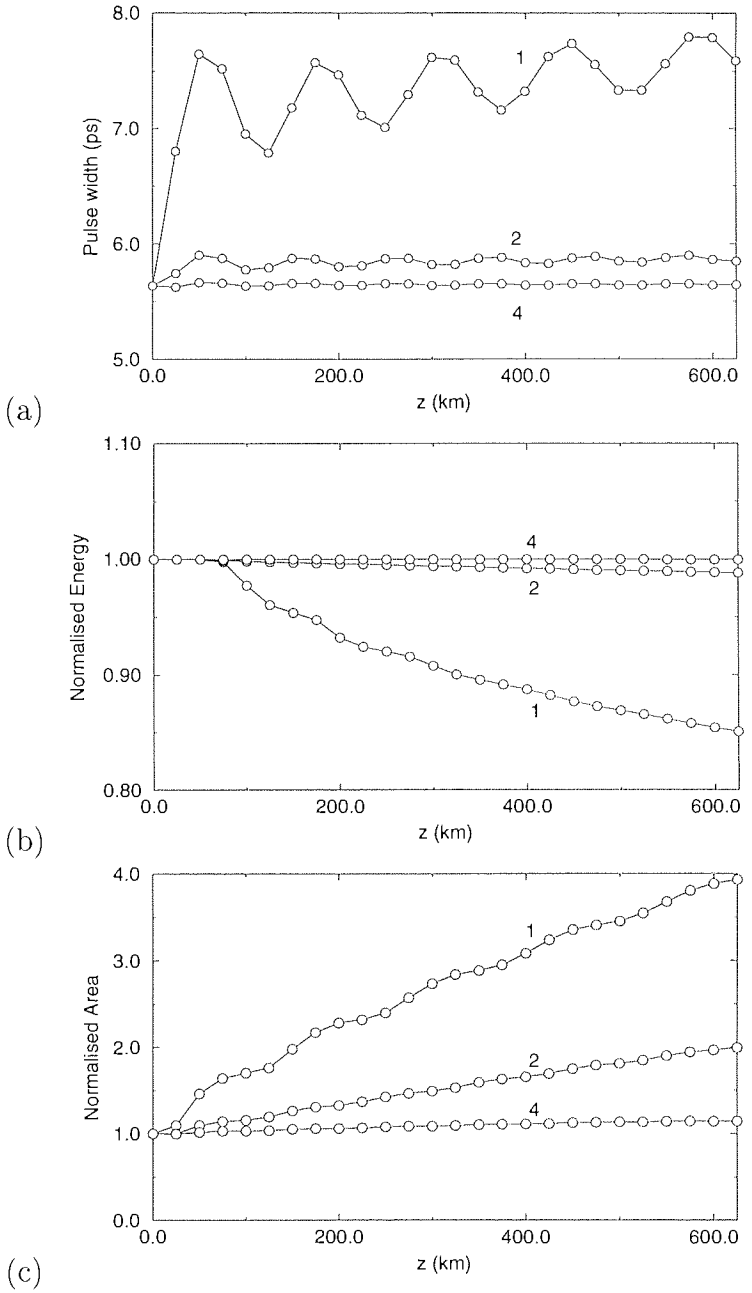

Figure 3.10: Evolutions of the pulse (a) width, (b) energy and (c) area, against propagation distance, in n = 1 (unprofiled), 2- and 4-fold optimally profiled fibre systems for 5.62 ps solitons over 25 amplifier periods (625 km) with 6-dB periodic loss.

For the unprofiled fibre, this fraction is quickly reduced below unity beyond 75 km, as dispersive wave radiation shed by the soliton crosses these boundaries. With an increase in n, the radiative component of the propagation is diminished and at n = 4, 99.8% of the initial soliton energy is still within this window after the 600 km propagation. This computation has been confirmed to 6000 km, after which the pulse width was virtually unchanged, confirming the stability of the propagation over long distances. Figure 3.10(c) shows the evolution of the pulse area, often used as a sensitive measure of pulse distortion as it remains constant for perfect soliton propagation [26, 27, 124], which also reflects increasing pulse stability with profiling.

In the above example, the potential of stepwise dispersion profiling for operating soliton communication systems with shorter pulses was examined. To study the facility to operate with increased amplifier spacings we consider a second and more extreme example, using identical an 5.62 ps soliton source to that above, but double the amplifier spacing to 50 km ($Z_0 = L_a/4$). Figure 3.11 shows pulse evolutions of such a system using unprofiled fibre, optimal two-fold and four-fold stepwise profiling. The unprofiled fibre is unable to support propagation of the initial pulse which breaks up into two main sub-pulses that separate symmetrically, rapidly distributing energy over a wide temporal region. Although the two sub-pulses appear to be reasonably stable, and may ultimately emerge as solitons, they are accompanied at these early stages by a significant quantity of low level radiation, particularly between them. Improved propagation characteristics are obtained with increased profiling. The two-fold profiled system shows similar behaviour to that shown in figure 3.8(a), rapidly shedding radiation over the first few amplification periods and leaving behind a diminished and oscillatory damping soliton. The quantity of radiation shed would certainly disrupt a potential communications system. However, the four-fold profiled system shows almost distortionless transmission in the time domain, with negligible pulse width increase over the first 1200 km propagation. Decreasing evidence of pulse distortion in the corresponding frequency spectra was also noted.

Finally, compare the computation shown in figure 3.8(a) for $L_a = 25km$ and for figures 3.11(a-b) for $L_a = 50km$. The improvement in soliton propagation

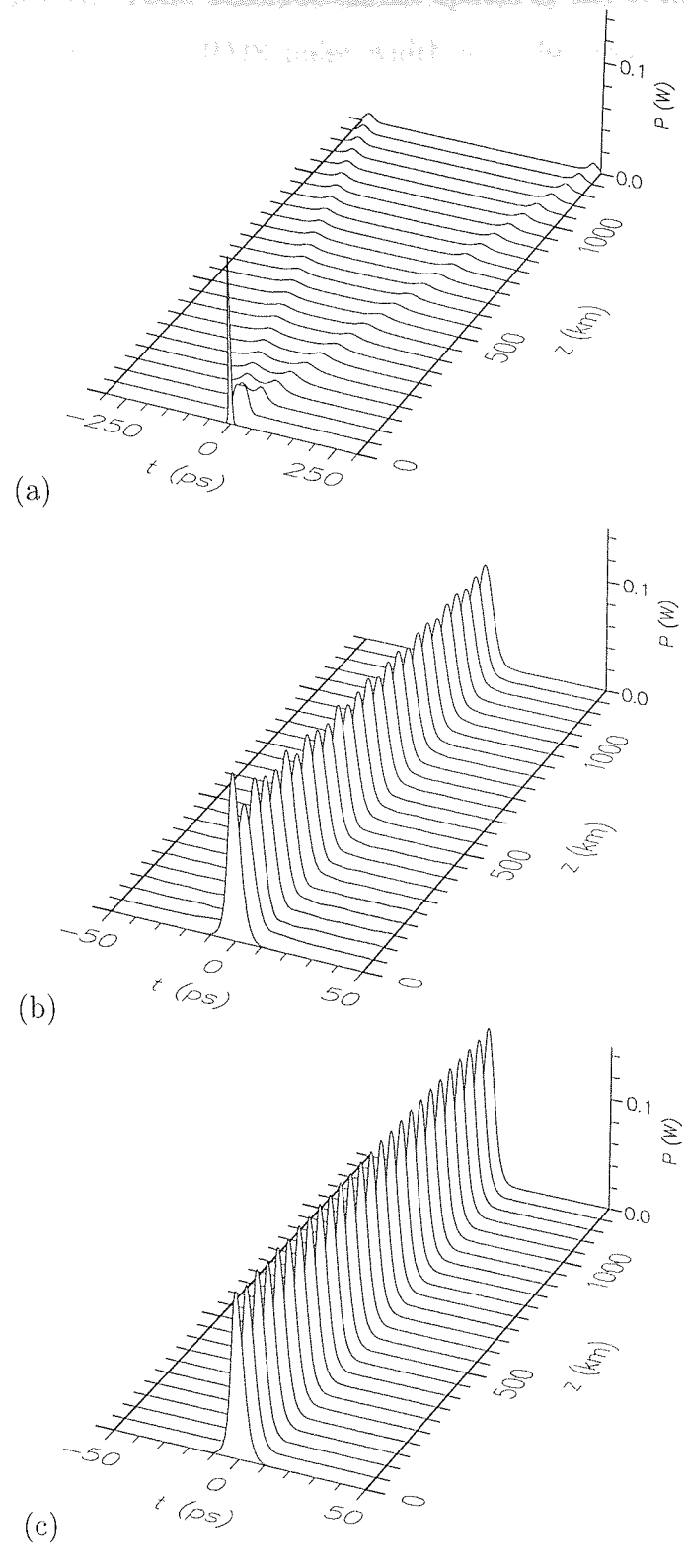

Figure 3.11: Pulse profiles evolutions over 25 amplifier periods (1250 km) with 12-dB periodic loss and initial pulse widths of 5.62 ps in (a) unprofiled fibre, (b) n = 2 fibre (Z_1 = 17.2 km and D_{1-2} = 1.90, 0.53 ps/nm/km) and (c) n = 4 fibre (Z_{1-3} = 7.53, 17.04, 29.95 km and D_{1-4} = 2.41, 1.51, 0.82, 0.34 ps/nm/km.

obtained by either halving L_a or by two-fold optimal dispersion profiling are almost equivalent, as expected. These observations are upheld by any of the usual measures of perturbation, such as the RMS pulse width or pulse area. However, careful comparison of the rate of growth of the pulse areas shows that in the two-fold optimally profiled system are marginally less perturbed than in the system with halving the amplifier spacing. This behaviour is in keeping with the marginal differences in the perturbation function A_n for these cases, as described above, and confirms its validity as an accurate monitor of average soliton perturbations.

3.5 Conclusions

We have shown that stepwise dispersion profiling in periodically amplified systems allows stable propagation in regimes normally forbidden to the average soliton. In particular, n-fold optimal dispersion profiling yields an equivalent reduction in perturbations as n-fold reduction of the amplifier spacing. Thus, in general, if stable propagation is achievable for a system with amplifier spacing L_a and pulses of soliton period Z_0, n-fold optimal profiling will permit extension of the amplifier spacing to nL_a. Equivalently, for the same amplifier spacing, it will allow stable propagation of solitons with period (Z_0/n), yielding corresponding $\sqrt{n}$ increases in the achievable data rates. Given the improved propagation found using dispersion profiling to a given average dispersion as against a single fibre with that dispersion, it seems reasonable to assume that profiling will give significant improvements over reducing the dispersion of a given amplifier span, especially as the SNR problems found with low dispersions are avoided. Therefore, in practical periodically amplified systems, stepwise profiling could be utilised to increase single channel data rates well beyond 10 Gbit/s or to reduce the number of amplifier stations, provided the associated noise penalties are relatively unimportant, as in short-haul systems, or provided the Gordon-Haus effect can be controlled in long-haul systems.

To analyse the optimum dispersion profile a simple and intuitive measure of the perturbations which arise from the discontinuous balance between dispersion and nonlinearity was used. The validity of this perturbation function has been verified numerically and, based on it, a straightforward algorithm for determining

optimal n-fold profiles has been presented. Using this method, n-profile design diagrams in terms of the path-averaged system dispersion and net periodic loss are readily obtainable and examples for two-fold and four-fold profiling have been given. In practice, only a limited set of fibres with different dispersions will be available. Nevertheless, the same approach could be used to optimise system design for the fibre available.

The results presented above apply only to unidirectional transmission. They are however equally applicable to unidirectional, mode-locked erbium fibre soliton lasers. In these lasers, the cavity must be sufficiently long for the nonlinear mode-locking mechanism to operate effectively. As a result, the pulse width is limited via the same average soliton condition and unwanted frequency sidebands are often generated. Therefore, stepwise dispersion profiling of the gain medium could also be used to suppress sideband generation and to stabilise the mode-locking of shorter solitons. In either case, the profiling required is simple to implement and, with the benefits found, should provide a useful method of improving soliton propagation in systems outwith the usual average soliton limit.

Chapter 4

Soliton transmission over standard fibre

4.1 Introduction

Of the ~50 million kilometres of optical fibre installed world-wide, most is so called *standard fibre*, with low-loss in the 1.3 and 1.55 μm wavelength regions, the second and third communications windows, and low dispersion in the 1.3 μm window. Generally, current systems work in this second window using electronic regenerators to re-time, reshape and amplify the optical signal periodically to maintain the data over the system length. The major drawback of these regenerators is that they operate at a fixed data rate which necessitates their replacement if the system is to be upgraded to higher data rates. Recently, interest has turned to replacing these regenerators with erbium-doped fibre amplifiers (EDFAs), which have a wide-bandwidth and therefore are in principle data rate transparent. However as they do not re-time or reshape the optical signal they introduce other system design problems that must be addressed [125], mainly due to the higher dispersion of the optical fibre in this window.

Several methods of coping with the dispersion problems have been suggested, including the use of dispersion compensating fibre [5, 6, 126]–[130], optical phase conjugation [131]–[134], pulse pre-chirping [18, 135, 136] and duobinary transmission [137, 138]. Of these, phase conjugation is a complex process to implement efficiently and pulse pre-chirping and duobinary coding are limited in the

distance over which they can be effective to around 150 km. Dispersion compensation is simple and effective, but requires large additional fibre lengths, greater optical gain leading to additional amplifier noise and a reasonable degree of accuracy. However, as well as being supported by the fibre dispersion in the erbium gain band, solitons have two major advantages over linear propagation in standard fibre. The existing standard fibre was mostly made before polarisation mode dispersion (PMD) could be reasonably well controlled in the manufacturing process. While this is a major problem for linear propagation techniques solitons by their very nature can cope with a reasonable degree of PMD (see section 2.7). Additionally, solitons are compatible with all optical switching and routing technologies proposed to overcome the electronic bottle-neck problems encountered at switching nodes with the high data rates currently being considered [139]–[142].

In this chapter, we study the problems associated with using solitons to upgrade embedded standard fibre systems with EDFAs. In particular we study systems where the existing amplifier spacings are >30 km with a view to upgrading the data rate to 10 Gbit/s, which is a specific but important technological challenge relevant to the current European optical network [85]. The soliton system design constraints are discussed and investigated by numerical simulation. We show that soliton propagation should be possible in standard fibre systems to distances of around 200 km, and that phase modulation and alternating amplitude codings are detrimental in such highly perturbed systems. In order to extend this distance a novel method of improving soliton propagation in standard fibre systems is examined. This investigates the use of dispersion compensating fibre, incorporated as part of each amplifier, to reduce the average dispersion of each system link. This scheme should lead to soliton propagation for greater than 2000 km.

4.2 Solitons in standard fibre

The design constraints for soliton systems were discussed in chapter 1. For such short systems as those considered here, two of the constraints, the Gordon-Haus jitter and the required signal-to-noise ratio are unimportant as neither has sufficient distance in which to accumulate to any significant degree. The soliton interaction and average soliton constraints must however be balanced to give a stable prop-

agation. The average power requirement can also be an issue, due to the high dispersions of these systems.

In order to illustrate and assess these constraints, we shall consider a particular system. The standard fibre was taken to have a dispersion of 15 ps/nm/km and a loss of 0.2 dB/km at the 1.55 μm signal wavelength, and the data rate was 10 Gbit/s. It was assumed the EDFAs could provide the optical powers and gain necessary for soliton propagation, with the amplifier output power in the range 5–15 mW. Figure 4.1 is the design diagram for these system parameters resulting from the constraints outlined above. The average soliton (AS) and average power (AP = 5, 10 and 15 mW) constraints are minima, whereas the soliton interaction (SI) constraints for system lengths of 144 km and 360 km are maxima. The design diagram identifies an acceptable region of parameter space for a 144km system with 10 mW optical amplifier output powers and amplifiers spacings below 12 km, as highlighted by the shaded region around 25 ps. Similarly, for system lengths of 360 km, these constraints dictate higher average powers of 15mW, shorter pulse widths of around 15 ps and impractically short amplifier spacings below 6 km.

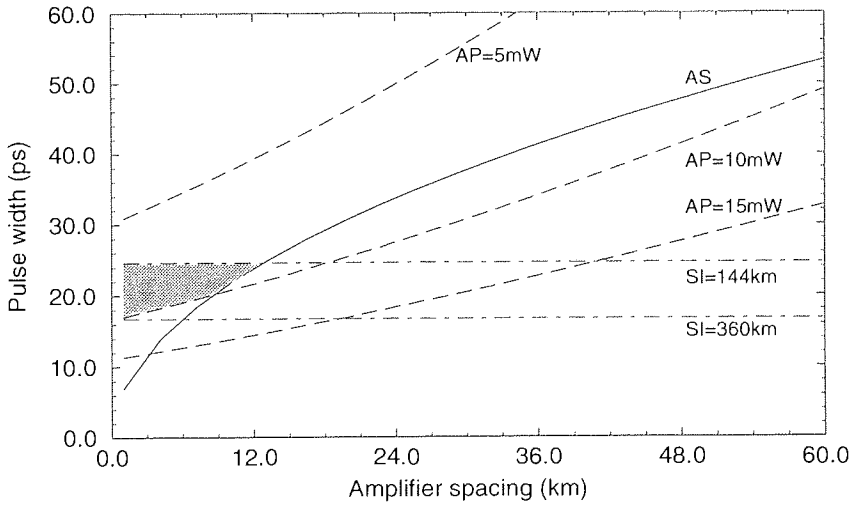

Figure 4.1: Design diagram for a 10Gbit/s standard fibre system. Solid line (AS) is the average soliton constraint, dashed lines are the average power (AP) constraints for 5, 10 and 15 mW and the dot-dashed lines are the soliton interaction (SI) constraints for system lengths of 144 and 360 km. The region of operation for a 144 km system with 10 mW average amplifier output powers is shaded.

The upgrade of existing systems means that ideally the original amplifier spacings should be maintained. In this section, we focus on the use of 36 km

original amplifier spacings for total system lengths up to 360 km (see figure 4.2), corresponding closely to the current European optical communications network [85]. Since operation of soliton systems at 10 Gbit/s necessarily prohibits soliton widths greater than approximately half the bit interval of 50 ps, the associated soliton periods in standard fibre are only a few tens of km. As $L_a \approxeq Z_0$, average soliton perturbations are severe and the system design is closely squeezed between the competing requirements of the soliton-soliton interaction and average soliton constraints. As a result, any potential system is highly perturbed and as shown in the design diagram of figure 4.1 there is now allowable region of operation, according to the simple design rules above. However, these design rules are based on long-haul system considerations which use conservative guidelines to completely avoid perturbations. Therefore, in order to probe these constraints more closely and identify the limits more precisely, we have performed extensive sets of numerical simulations using full NLSE propagation, as described in the following section.

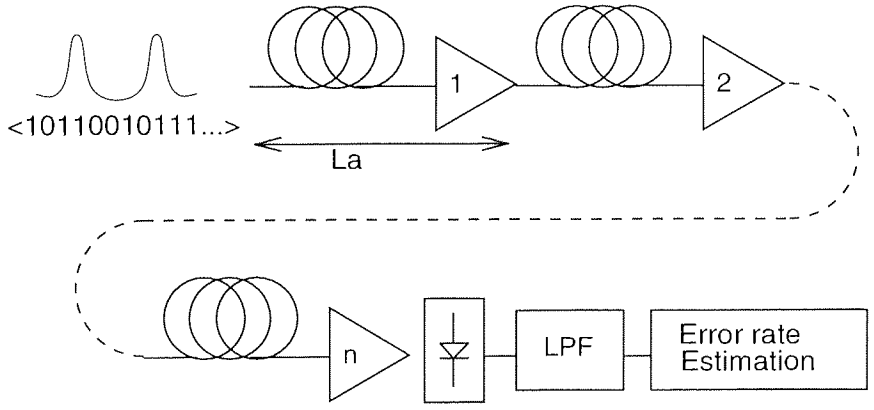

Figure 4.2: Schematic diagram of the system under consideration. L_a is the amplifier spacing of 36 km. LPF is a raised cosine electrical low pass filter. n is number of amplifier sections.

4.2.1 Standard fibre system simulations

The system was simulated by propagating a random bit sequence of 144 data bits, 50% data ones, at 10 Gbit/s, via the split-step Fourier method along 36 km of standard fibre, before being amplified by gain equal to the previous loss. Amplified spontaneous emission (ASE) noise was included, for an amplifier spontaneous emis-

sion factor $N_{SP} = 1.4$. Output could be obtained after each amplifier. The receiver was simulated as a fast photodiode followed by an electronic filter with a bandwidth of half the data rate to convert the return-to-zero (RZ) soliton data to non-return-to-zero (NRZ) format. It was then possible to estimate the bit-error ratio (BER) from the received eye diagram through the Q parameter method [143]–[145], where Q is given by,

$$Q = \frac{\mu_1 - \mu_0}{\sigma_1 + \sigma_0}, \tag{4.1}$$

for means $\mu_{1,0}$ and standard deviations $\sigma_{1,0}$ of the data 1's and 0's. The BER is then estimated according to,

$$BER = \frac{1}{\sqrt{2\pi}} \frac{exp\,(-Q^2/2)}{Q}. \tag{4.2}$$

For each BER computation, the 144 data bits were propagated in 9 sets of 16 bits for speed of simulation, as it was found that the BER estimated was the same using this method or a single 144 bit propagation. We note that determination of the BER by this method is normally performed for a set of single, isolated pulses to avoid an under-estimate of the Q from patterning effects. However, in this work we expect strong soliton interactions, the nature of which will be pattern dependent, necessitating the inclusion of patterning in the BER estimate.

4.2.2 System performance results

Simulations were performed for pulse widths of 10-50 ps to test the maximum transmission distance for which data could be recovered. Figure 4.3 shows a typical simulation result taken at each amplifier output for 30 ps pulses propagating to 360 km. After only a few amplifications the pulse train begins to distort and by the end of the simulation the data has been lost. However up to around 200 km, although the pulse shapes have been corrupted, the energy associated with each data one largely remains in the appropriate bit slots. This is not obvious from figure 4.3 but is clearly seen in the filtered eye diagrams of figure 4.4. These show that as the pulses propagate, the initially clean eye (a) is gradually degraded (b-d) but remains open to 216 km. However, by the next amplification at 252 km (e), the eye is beginning to close, giving significant errors at the receiver, and by 360 km

(f) the eye has completely closed. Thus, we see that although the pulse shapes are changed, the data can be recovered to a distance of 216 km, corresponding to 6 amplifier spans.

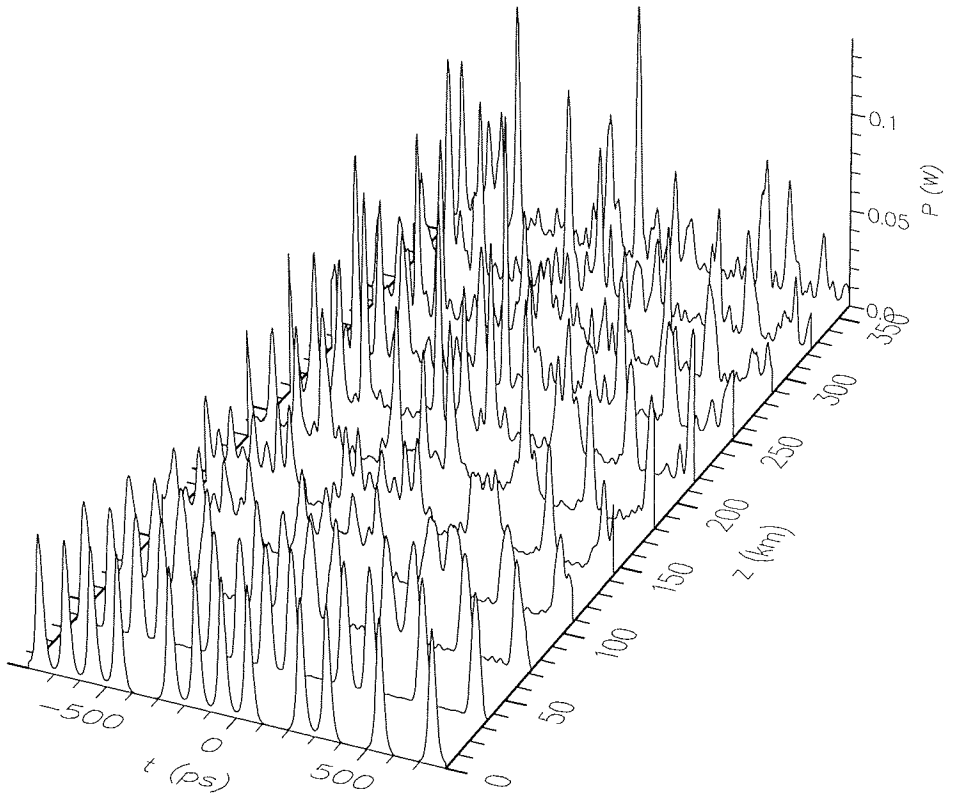

Figure 4.3: Example simulation of a 30 ps pulse train over 360 km of standard fibre with data < 1111011110110101 >.

This is also shown in figure 4.5, which summarises the BERs for the range of pulse widths from 10 to 50 ps with increasing distance. We note that the estimated BER values are somewhat optimistic. However, these numerically obtained error rates do not take account of effects not attributed to the soliton propagation through the fibre and EDFAs, such as source and receiver noise. This diagram does not therefore attempt to predict experimentally measurable error rates but to indicate where the system might reasonably be expected to operate.

Figure 4.5 shows that there is a small parameter region in which solitons

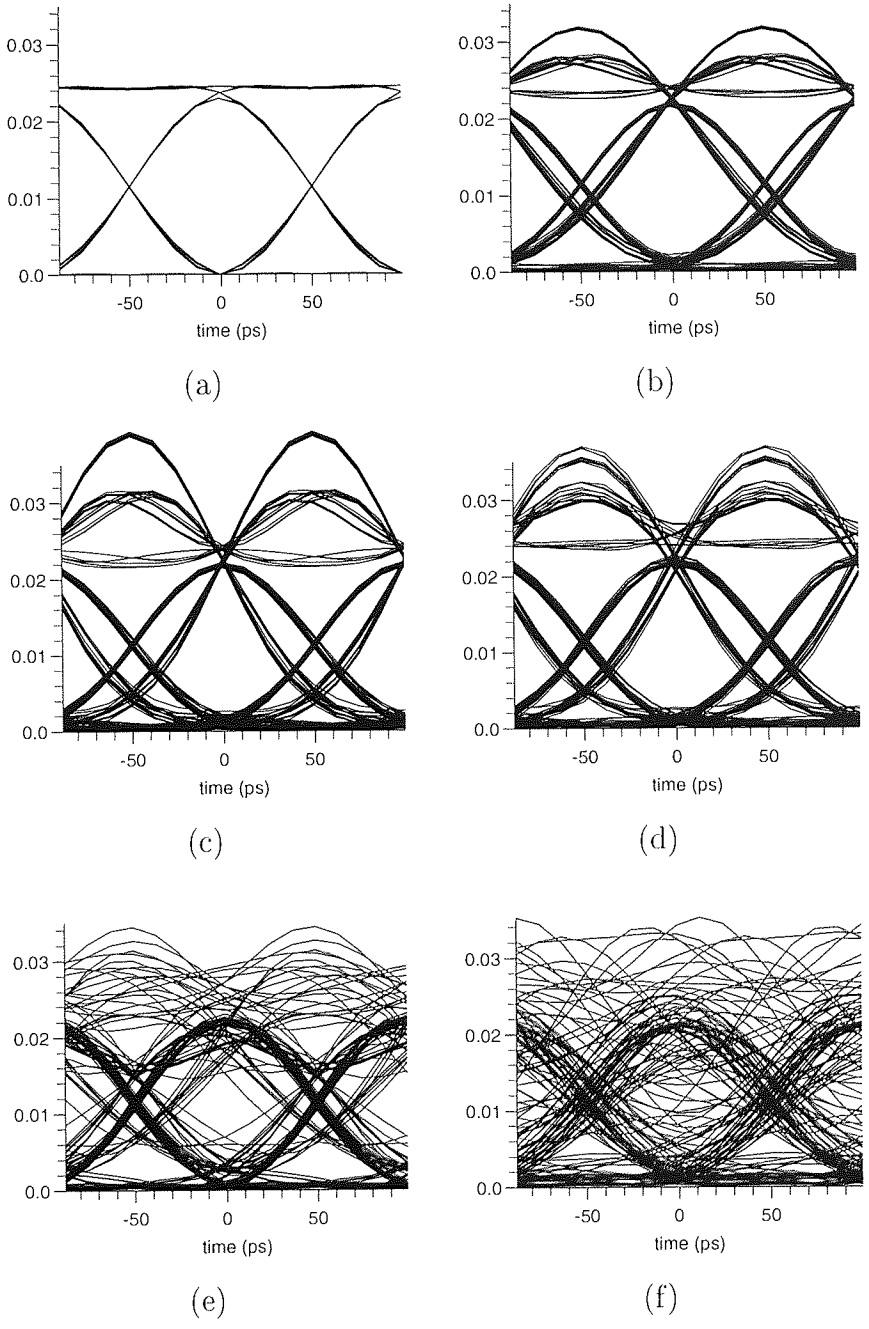

Figure 4.4: Filtered simulation eye diagrams corresponding to figure 4.3 after system lengths of: (a) 0 km (b) 144 km (c) 180 km (d) 216 km (e) 252 km (f) 360 km.

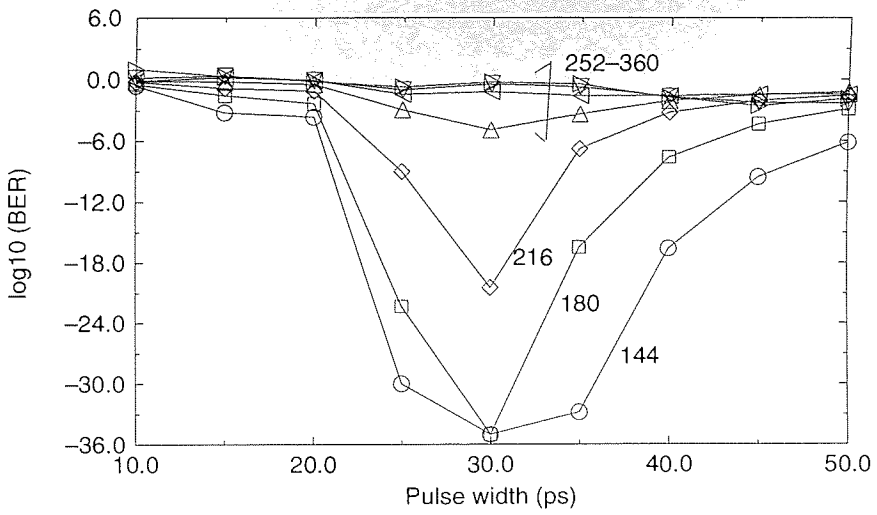

Figure 4.5: $Log_{10}(BER)$ versus pulse width for propagation in standard fibre to distances of 144–360 km. Output is taken after each 36 km spaced amplifier.

can propagate for pulse widths of around 30 ps. For a system of length 144 km, data streams with pulses in the range 22 – 38 ps propagate with acceptable error rates. As the distance increases, so the range of pulse widths diminishes until no pulse width will propagate. However, this is substantially better performance than anticipated by the design diagram of figure 4.1.

4.2.3 Phase and alternating amplitude modulation

In these simulations, the initial solitons were generated in-phase. It was noted in section 2.8.1 that a stream of pulses alternating in phase by π (anti-phase) could in principle stabilise their positions against soliton interactions by mutual repulsion from the pulses on either side, and that phase quadrature ($\pi/2$ difference) does not give any soliton interactions, but is an unstable operating point. It has been suggested that the anti-phase condition could in principle constitute the most stable operating condition for soliton transmissions [84, 85, 146]. To examine these possible phasing schemes, figure 4.6 shows simulation results for the variation of BER with initial phase separation of adjacent bits for 30 ps pulses at 144 and 180 km.

We find that the error ratios are lowest for pulses which are in phase or nearly in phase. While the error ratio is also reduced where the pulses are in anti-

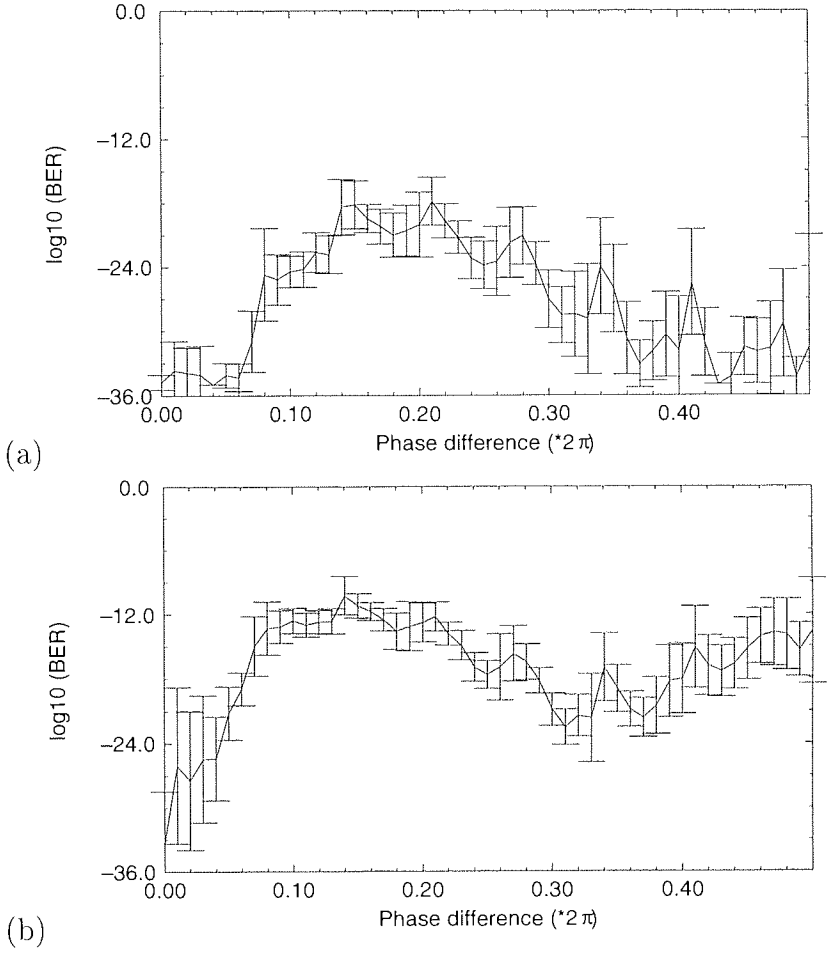

Figure 4.6: $Log_{10}(BER)$ versus initial intra-pulse phase separation ($\times 2\pi$ radians) for 30 ps solitons in standard fibre for system lengths of (a) 144 km and (b) 180 km.

phase for 144 km, the deviation obtained for the value of Q is larger indicating a worse operating point. This is more obvious one amplifier span later at 180 km. Thus, in this system varying the initial intra-pulse phase difference does not improve the system BER performance and in particular there is no indication of improvement for soliton phasing in quadrature or anti-phase. Therefore we see that when using amplitude-shift keying (ASK), the normal on/off bit modulation format for solitons, the missing pulses (data zeros) mean that the mutual repulsion between neighbouring solitons required for phase quadrature ($\pi/2$ phase difference) does not exist for all pulses, confirming that it is an unstable operating point. Hence we conclude that phase modulation does not offer any advantages in such highly perturbed systems.

Similarly, in figure 4.7 we summarise a set of simulations to test the effect of using solitons of alternating amplitudes, which in principle could also reduce the effect of soliton-soliton interaction [86]. As above, it was found that in this heavily perturbed system no benefit could be gained from using this scheme. Typically, a pulse-to-pulse amplitude difference of around 10% is required to significantly reduce the interactions. Variations of up to this level were tested, but in every case a significant degradation in the system BER performance was observed.

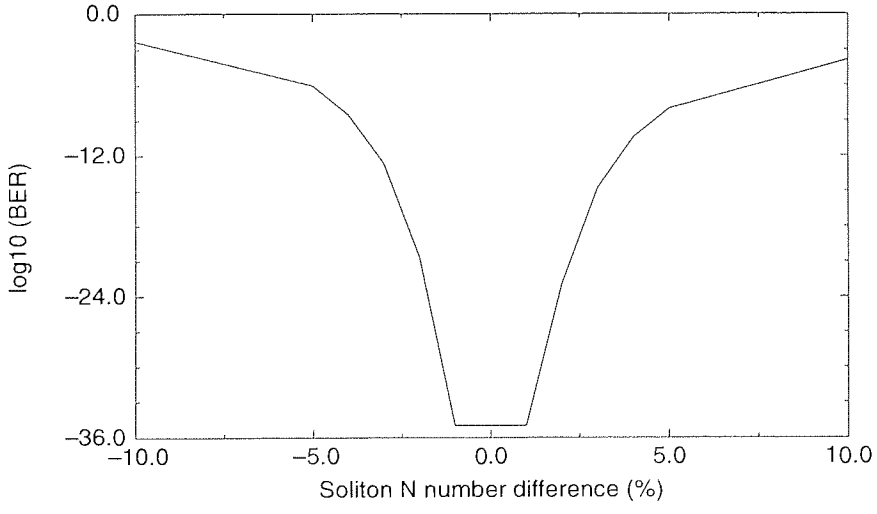

Figure 4.7: $Log_{10}(BER)$ against the difference in the soliton N number for 30 ps alternating amplitude solitons in standard fibre to 144 km.

4.3 Dispersion compensation with solitons

We have shown that it is possible to operate solitons over short standard fibre systems for up to 216 km. A remaining problem, however, is that optical powers of around 12 mW are required from the output of each EDFA. In addition, this system is limited in maximum distance, with an increasingly narrow range of tolerable pulse widths. In order to alleviate these distance and pulse width constraints, it is necessary to do more than install EDFAs and propagate solitons. The approach we consider here is to reduce the *average* dispersion and optical power by dispersion compensation. We adopt this approach as, even though it is possible to dispersion compensate NRZ systems in this way, solitons may be more resilient to the perturbations of such compensated systems. Furthermore, solitons do not require complete dispersion compensation as NRZ systems do, merely a reduction in the average dispersion. Given that we are attempting to upgrade standard fibre systems whose exact dispersion may not be known and which may vary along a system or even amplifier span, these soliton advantages over NRZ may represent a more flexible upgrade path.

There are several methods of dispersion compensation available, including optical fibre Bragg reflection gratings [147, 148]. Here we consider the use of dispersion compensating fibre [5, 6, 127, 128]. Such fibre is commercially available and has high negative group delay dispersion (GDD) in the 1.55 μm region. By incorporating a length of this fibre prior to the active fibre as part of each amplifier node, the average dispersion of each amplifier link is reduced. This should lead to reduced perturbations to the solitons alongside reduced average powers. The actual dispersion compensating fibre simulated here was not of the optimum dispersion and loss now available [10], but of a more modest dispersion value of -50 ps/nm/km. While dispersion compensating fibres generally have slightly higher loss than standard fibre, the same value of 0.2 dB/km as for standard fibre was used as improvements are still being made to the loss figures of these fibres. In addition, as we shall show in section 4.3.3 the loss of the fibre may not be too significant in short systems (where ASE noise is not an issue) provided the compensating fibre is placed in the low power, dispersion dominant part of the soliton propagation cycle.

4.3.1 Dispersion compensation scheme

The average dispersion of the amplifier link with the addition of the compensating fibre is found from considering the total dispersion across the link. For a standard fibre section of dispersion D_s and length L_s, concatenated with a compensating fibre of dispersion D_c and length L_c, the average dispersion D_a is,

$$D_a = \frac{D_s L_s + D_c L_c}{L_s + L_c}. \tag{4.3}$$

Thus, in order to reduce the average dispersion of an amplifier link to 6.0 ps/nm/km an additional 5.8 km of compensating fibre must be added to each amplifier. The amplifier gain and the launch powers are then adjusted to take account of the extra periodic loss and lower average dispersion. Figure 4.8 shows a schematic diagram of such a compensating amplifier with the variation of the fibre dispersion under such a reduction of the average dispersion to 6.0 ps/nm/km.

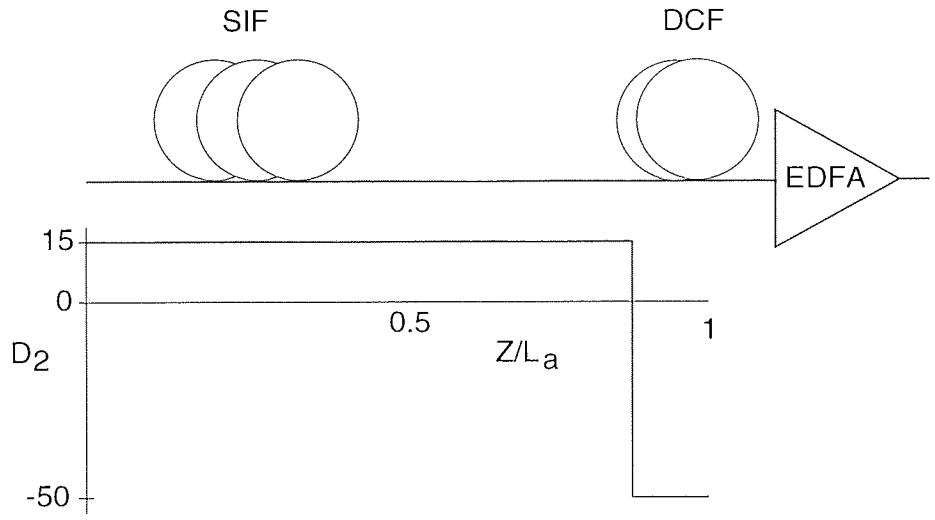

Figure 4.8: Schematic diagram of the dispersion compensating amplifier link and the variation of dispersion with distance over one transmission link for $D_a = 6.0$ ps/nm/km. SIF is 36 km of step index fibre, $D_2 = 15ps/nm/km$, DCF is 5.8 km of dispersion compensating fibre, $D_2 = -50ps/nm/km$.

In order to assess the likely impact of such a compensation scheme it is helpful to consider an extension of the simple design diagram of figure 4.1. Previously, the system dispersion was fixed and the amplifier spacing varied. Now we consider a fixed standard fibre length between amplifiers of $L_s = 36$ km but vary

the dispersion, so the x-axis is the average system dispersion. Account has to be taken of the additional length of the compensating fibre in the calculations, but it is considered an integral part of each amplifier, rather than an addition to the total length of the propagation fibre.

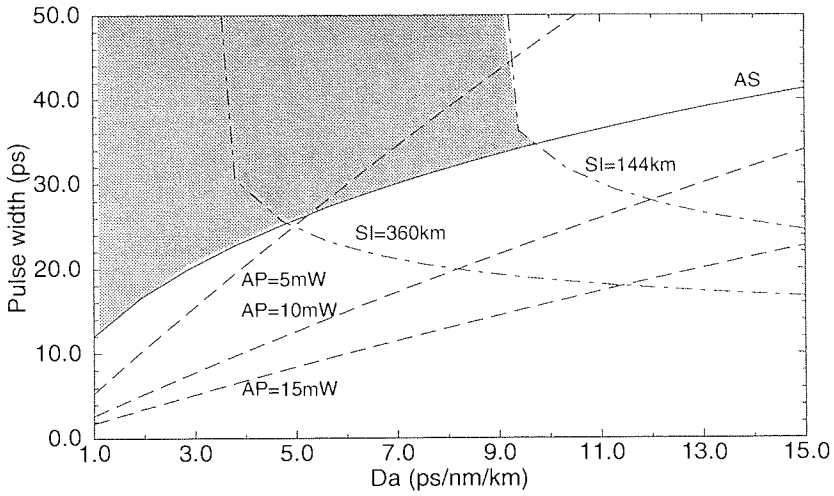

Figure 4.9: Dispersion compensation design diagram of pulse width against average dispersion D_a. Solid line (AS) is the average soliton constraint, dashed lines are the average power (AP) constraints for 5, 10 and 15 mW and the dot-dashed lines are the soliton interaction (SI) constraints for system lengths of 144 and 360 km. The region of operation for a 144 km system with 10 mW average amplifier output powers is shaded.

Figure 4.9 shows that as the dispersion is reduced, the minimum pulse width limits from the average soliton and average power constraints decrease, whilst the maxima from the soliton interaction constraint increase. We see that if the dispersion is decreased below 9 ps/nm/km a region of operation opens for a system of length 144 km. However, we have already seen that for such short distances, the region of operation is considerably greater than estimated from these simple design rules and soliton propagation is possible over 200 km of standard fibre without dispersion compensation. Therefore, in the following section we repeat the simulation exercise above, to obtain more accurate design limits.

4.3.2 Dispersion compensation simulation results

Simulations were carried out as before for pulse widths of 5–45 ps over the range of average dispersions from 1 – 15 ps/nm/km. A sample simulation output is shown

in figure 4.10 for a system compensated to 6.0 ps/nm/km and clearly shows the improvement in the results compared to figure 4.3. Although there are still perturbations and distortions, the data is still clearly seen after many more amplification periods. This is reflected in the corresponding eye diagrams, shown in figure 4.11, which indicate that the data can be recovered over the whole 360 km system length.

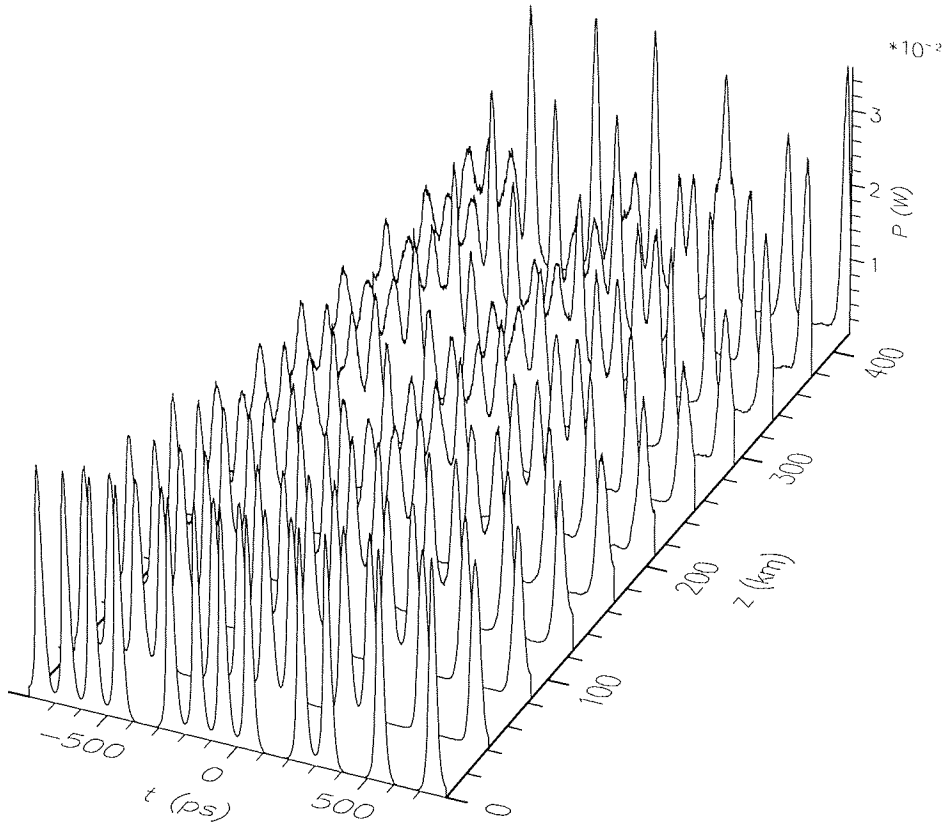

Figure 4.10: Example simulation of 30ps pulse train in a system compensated to 6.0 ps/nm/km, with data < 1111011110110101 > as for figure 4.3.

From simulations such as figure 4.10 it was possible to obtain a dispersion design diagram to improve on the previous version of figure 4.9, the results of which are shown in figure 4.12. This shows that as the dispersion is reduced from 15.0 ps/nm/km, the operable range of pulse widths increases from 22–38 ps to 10–40ps. Note that a limiting maximum pulse width is found for longer pulse widths. This is due to the large degree of pulse overlap for relatively broad pulses, so that

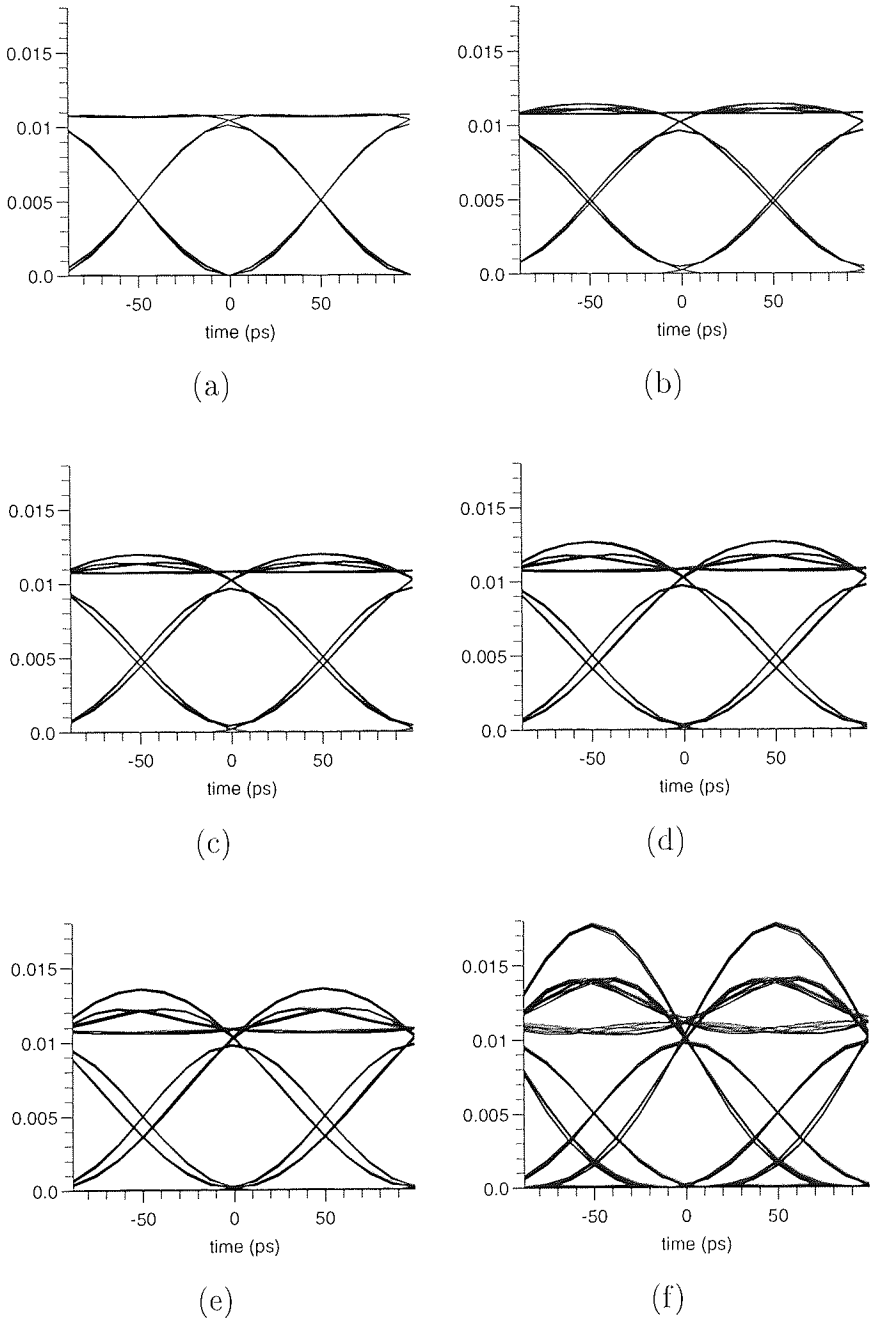

Figure 4.11: Filtered simulation eye diagrams corresponding to figure 4.10, at distances: (a) 0 km (b) 144 km (c) 180 km (d) 216 km (e) 252 km (f) 360 km.

adjacent solitons cannot be considered as individual entities and do not propagate as stable pulses. Also shown in figure 4.12 is the increase in propagation distance attainable using this scheme. As the dispersion is reduced, so the propagation distance achievable by the mid-range pulse widths increases. We see that as the dispersion is reduced below 12.0 ps/nm/km a distance of 252 km is possible and below 9.0 ps/nm/km the full 360 km propagation distance considered is attainable. Note that along with these improvements in propagation distance, the reduction in average dispersion also reduces the average power required to support the solitons (see equation (2.68)).

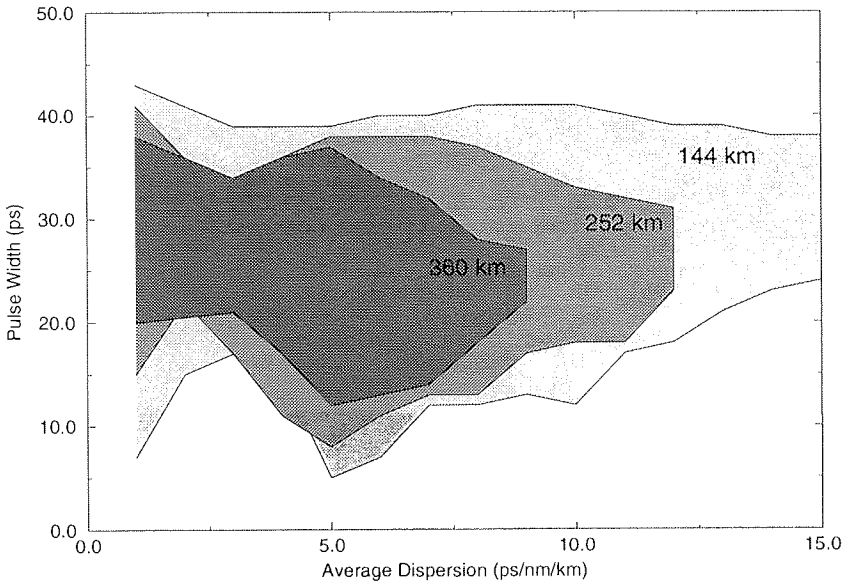

Figure 4.12: Dispersion compensation design diagram from simulations for system lengths of 144, 252 and 360 km. Acceptable BER was chosen as 10^{-24}. Region of operation lies between each pair of curves. Accuracy was limited by the computing time required.

Once the dispersion has been reduced below around 5 ps/nm/km, figure 4.12 becomes more difficult to interpret. We believe that in this region, the perturbations caused by the large additional lengths of compensating non-soliton supporting fibre become significant leading to large errors in the results. To investigate this region further, simulations were performed for 20 ps solitons in a system compensated to 1 ps/nm/km over a range of input pulse powers, in order to test whether higher input powers would assist coupling into the stable propagation mode of the transmission line. Figure 4.13 shows the received BER against input soliton N

number (calculated using the dispersion D_a) and distance for an average dispersion of 1 ps/nm/km. From the average soliton model the input N number should be 1.55, but as clearly seen in this figure, increasing N to around 2.60 significantly improves propagation fidelity, allowing transmission to distances of over 2000 km. This corresponds to an average power of 0.38 mW, far below that required for the uncompensated system average power of 14.2 mW for the same 20 ps pulses. It is important to note that the window of acceptable powers for soliton transmissions beyond, for example, 1000 km (suitable for European trunk networks) is wide. This indicates that the solitons will be robust to both the exact launch powers and the exact dispersion of the installed standard fibre (as $P_{av} \propto D_2$) allowing wide tolerances in the design of such dispersion compensated soliton system upgrades.

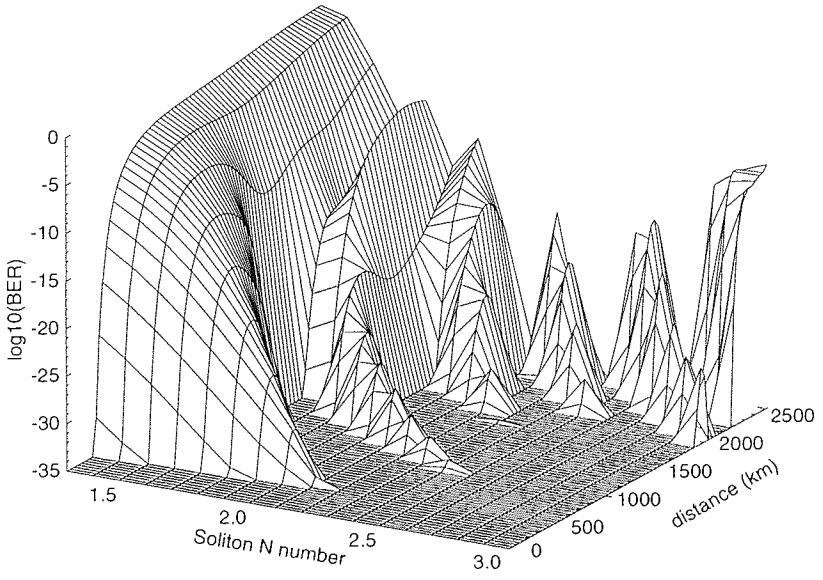

Figure 4.13: $log_{10}BER$'s against input soliton N number and distance for 20 ps pulses and 1 ps/nm/km average dispersion. At 2268 km for N=2.60 the BER was still unchanged at the simulation minimum of 10^{-35}.

4.3.3 Compensating fibre placement

A final point concerns the placement of the dispersion compensating fibre within the periodic loss and gain cycle of the propagation. Thus far, we have assumed the compensating fibre simply reduces the average dispersion, implying that its positioning within the cycle is unimportant. Figure 4.14 compares BERs for 30 ps

solitons for systems where the compensating fibre is placed immediately before and after the amplifier, with the equivalent uncompensated system.

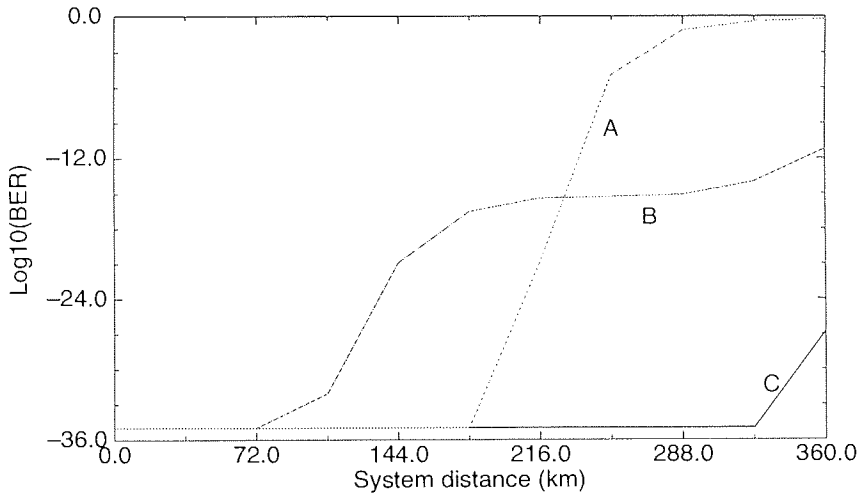

Figure 4.14: BER versus propagation distance for 30 ps pulses (A) without dispersion compensation, (B) with 5.8 km DCF after the amplifier (figures 4.3 and 4.4):, and (C) with 5.8 km DCF before the amplifier (figures 4.10 and 4.11). The input power in each case was the average soliton prescription value of $N = 1.50$ at $D_a = 6ps/nm/km$, other parameters also as figure 4.10.

We find that placing the fibre immediately after the amplifier actually reduces the error free propagation distance from that of the uncompensated system. Attempting to equalise the dispersion in the part of the cycle where fibre nonlinearity, through self-phase modulation, is dominant, actually introduces additional perturbations, which exceed any benefit from the reduction in average dispersion. This clearly shows that it is necessary to put the fibre in the dispersion dominant, low power section of the soliton propagation cycle. As nonlinear effects are undesirable within the dispersion compensating fibre, so the power requirement in this fibre is that it be low enough to negate nonlinear results. As such, insertion loss and fibre attenuation will not be an issue other than for the usual SNR constraint, as pure dispersion is unaffected by the optical power (section 2.3) justifying our use of $\alpha = 0.2dB/km$ in our simulations.

4.4 Conclusions

We have shown that it is possible to upgrade short standard fibre systems to 10 Gbit/s by replacing electronic regenerators with erbium doped fibre amplifiers and using solitons. Despite the fact that the perturbations to the solitons are large, error-free operation is possible to around 200 km using relatively long, 36 km amplifier spacings, pulse widths of around 30 ps and optical powers of 12 mW. The best operation is obtained, for this heavily perturbed system, with solitons which are initially in phase and of equal amplitude.

In order to reduce the powers required and increase both the maximum transmission distance and the range of pulse widths over which operation is possible, a simple, passive dispersion reduction scheme was studied. By introducing a section of dispersion compensating fibre immediately before each amplifier, the average dispersion could be reduced. Reduction of the dispersion, in what is for solitons a novel method, to 6.0 ps/nm/km increased the total transmission distance to in excess of 360 km, extended the range of tolerable pulse widths by a factor of three from 25-35 ps to 10-40 ps for the 144 km system, and reduced the average power requirement to 5 mW. Dispersion compensation below 6 ps/nm/km did support propagation using average soliton prescription input powers, but propagation fidelity was much improved by increasing the input pulse power . This unexpected result allowed propagation to over 2200 km for 20 ps solitons in fibre compensated to an average of 1 ps/nm/km. It was noted that the dispersion compensating element must be placed in the part of the soliton propagation cycle where dispersion is dominant. This technique divides the process of dispersion equalisation required in standard fibre between linear dispersion compensation and nonlinear soliton propagation. The resultant scheme is simple to implement and offers the robustness to perturbations, such as the exact dispersion of the installed standard fibre, and WDM compatibility inherent to soliton transmission.

With their suitability to all optical processing and routing technologies and resilience to polarisation mode dispersion, solitons are fast becoming a realistic alternative to NRZ transmission. In this chapter, we have shown that solitons should be considered for the future upgrade of standard fibre communication systems.

Chapter 5

Improved launch condition for the average soliton

5.1 Introduction

As discussed in chapter 2, the average soliton model for soliton propagation in a periodically amplified transmission line holds well, provided the amplifier spacing is short compared to the soliton period ($L_a \ll Z_0$, or equivalently $z_a \ll z_0 = \pi/2$ in soliton units). No significant pulse shape changes occur on the length scale of energy fluctuations which can then be averaged over each amplification period. The average soliton condition simply requires that the soliton launch power is chosen such that the path average power is equal to the usual lossless soliton power, with equation (2.53) giving the input peak power Λ_0^2. In systems that satisfy $z_a \ll z_0$, pulse shape variations due to the periodic loss-gain cycle are indeed small and therefore the launch position relative to the periodic cycle is arbitrary and usually considered to coincide with an amplifier node, as befits comparison with experimental recirculating loop systems [149]–[151]. However, as z_a is increased towards z_0, the perturbations due to the system periodicity become increasingly evident, resulting in the generation of spectral sidebands [62, 152] and dispersive radiation [153]. Moreover, non-negligible pulse shape changes occur in response to the varying influence of fibre nonlinearity over dispersion across each inter-node spacing.

The problems encountered are exacerbated in standard fibre systems as the

high dispersion leads to a short soliton period. In particular, as shown above, when considering the upgrading of an existing standard fibre system the soliton period may even be less than the amplifier spacing, leading to significant pulse shape changes with propagation. These pulse shape changes are shown below to essentially mean that at an amplifier the propagating pulse is not a perfect $sech^2$ soliton but slightly chirped. As the nonlinear and dispersive length scales are now significant compared to amplifier span, the mismatch in their effects along the span will cause chirping first from SPM while the power is high then later from GVD once the power has dropped. As these competing effects periodically switch over there are two points in the power cycle where the pulse is a perfect soliton. We therefore assess these two points and show that by launching a perfect soliton at one, by the addition of the appropriate length of fibre prior to the first amplifier node, initial propagation variations can be reduced.

We use the operator splitting technique [24, 62] to calculate the local error in the average soliton to $O(z_a^3)$ and show how the term of $O(z_a^2)$ can be minimised by an appropriate choice of initial launch point. The resulting improvement in the evolution of the average soliton arises from effectively averaging over pulse shape variations in addition to pulse energy variations. The improvement is in the initial condition and reduces the initial radiation but does not affect the generation of sidebands in the spectra resulting from the periodic amplification. Thus the approach is of particular benefit for relatively short systems. We also show that these results can be related to results in refs. [23] and [25] which use the Lie transform technique.

5.2 Operator analysis

The fields and positions in the generalised periodic cycle are shown in figure 5.1. Working once more in normalised units (see chapter 2), we consider a unit cell of length, $z_a = L_a/L_D$, with loss, $\Gamma = \alpha L_D/2$, and an amplifier of gain, $G = e^{2\Gamma z_a}$. In a periodic system, the origin of the unit cell is indeterminate and we can consider the period to be arbitrarily divided about the amplifier, which is placed a distance z from the end of the fibre. We follow the operator approach of ref. [24] and write

the dissipative NLSE (equation (2.47))

$$i\frac{\partial u}{\partial z} + \frac{1}{2}\frac{\partial^2 u}{\partial \tau^2} + |u|^2 u + i\Gamma u = 0 \tag{5.1}$$

in terms of the dispersion operator $\hat{D}$, the nonlinear operator $\hat{N}$ and the loss operator $\hat{L}$, where,

$$\hat{D} = -\frac{i}{2}\frac{\partial^2}{\partial \tau^2} \quad , \quad \hat{N} = -i|u|^2 \quad , \quad \hat{L} = \Gamma. \tag{5.2}$$

We then calculate the next order error term as a function of z.

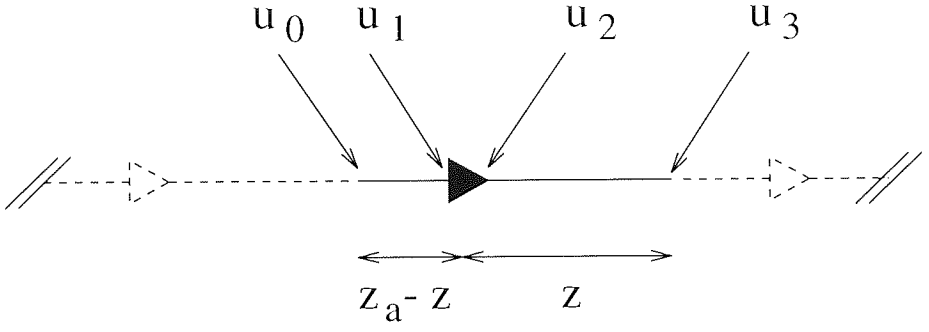

Figure 5.1: Definition of fields in the unit cell for the average soliton.

At the end of the first fibre section, the field u_1 is given by,

$$u_1 = \exp\{(\hat{D} + \hat{N} + \hat{L})(z_a - z)\}u_0, \tag{5.3}$$

and u_2 is related to u_1 in the usual way,

$$u_2 = \exp\{\Gamma z_a\}u_1, \tag{5.4}$$

to exactly balance the periodic loss and gain. In [24], the average soliton condition was derived to $O(z_a^2)$, by using an operator splitting accurate to the same order. To derive the errors induced by the system to $O(z_a^2)$, we use an operator splitting accurate to $O(z_a^3)$. Thus eqn. (5.3) becomes,

$$u_1 = \left\{\exp\{\hat{D}(z_a - z)/2\}\exp\{(\hat{N} + \hat{L})(z_a - z)\}\exp\{\hat{D}(z_a - z)/2\}\right. \tag{5.5}$$

$$\times \quad \exp\{O(z_a - z)^3\}\Big\}\, u_0, \tag{5.6}$$

where, as before, the nonlinear and loss terms have been kept together. In the following we omit terms of $O(z_a^3)$.

The combination of loss and nonlinearity in eqn. (5.6) can be expressed exactly in terms of a renormalised nonlinearity [24, 62] to give,

$$u_2 = \Big\{\exp\{\Gamma z_a\}\exp\{-\Gamma(z_a - z)\}\exp\{\hat{D}(z_a - z)/2\}\exp\{\Lambda_2^{-2}\hat{N}(z_a - z)\} \tag{5.7}$$

$$\times \quad \exp\{\hat{D}(z_a - z)/2\}\Big\}\, u_0, \tag{5.8}$$

where,

$$\Lambda_2^2 = \frac{2\Gamma(z_a - z)}{1 - e^{-2\Gamma(z_a - z)}}. \tag{5.9}$$

Similarly, u_3 can be written in terms of u_2 as,

$$u_3 = \exp\{-\Gamma z\}\exp\{\hat{D}z/2\}\exp\{\Lambda_1^{-2}\hat{N}z\}\exp\{\hat{D}z/2\}u_2, \tag{5.10}$$

where,

$$\Lambda_1^2 = \frac{2\Gamma z}{1 - e^{-2\Gamma z}}, \tag{5.11}$$

and thus u_3 can be expressed in terms of the initial field u_0 by combining eqns. (5.8) and (5.10). This rather lengthy expression can be simplified to re-order the operators while collecting the resulting commutators to give,

$$u_3 = \Big\{\exp\{\hat{D}(z_a + z)/2\}\exp\{\Lambda^{-2}\hat{N}z_a\}\exp\{\hat{D}(z_a - z)/2\}\exp\{-\frac{zz_a}{2\Lambda_1^2}\} \tag{5.12}$$

$$\times \quad \exp\{2\Gamma z\left[\hat{D}, \hat{N}\right]\}\Big\}\, u_0, \tag{5.13}$$

where,

$$\Lambda^2 = \frac{2\Gamma z_a}{(1 - e^{-2\Gamma z_a})}e^{-2\Gamma z} = \Lambda_0^2 e^{-2\Gamma z} \tag{5.14}$$

as before.

To obtain a second order split step form for the NLSE we make one further operator move ($e^{-\hat{D}z/2}$) to balance the dispersive contributions around the

nonlinearity and obtain,

$$u_3 = \left\{\exp\{\hat{D}z_a/2\}\exp\{\Lambda^{-2}\hat{N}z_a\}\exp\{\hat{D}z_a/2\}\exp\{-f(z)\left[\hat{D},\hat{N}\right]\}\right\}u_0, \tag{5.15}$$

where,

$$f(z) = \frac{zz_a}{2}\left(\frac{e^{2\Gamma z}}{\Lambda_1^2} - \frac{1}{\Lambda^2}\right). \tag{5.16}$$

A renormalisation of the fields in a similar way to ref. [24], i.e.,

$$u_0 = \Lambda q_0 \ , \ u_3 = \Lambda q_3, \tag{5.17}$$

allows us to make contact with the lossless NLSE, giving,

$$q_3 = \left\{\exp\{\hat{D}z_a/2\}\exp\{\hat{N}z_a\}\exp\{\hat{D}z_a/2\}\exp\{-f(z)\Lambda^2\left[\hat{D},\hat{N}\right]\}\right\}q_0. \tag{5.18}$$

The first three terms in the parenthesis constitute the split-step representation of the lossless NLSE accurate to $O(z_a^2)$ as required. Thus we can write,

$$q_3 = \left\{\exp\{(\hat{D}+\hat{N})z_a\}\exp\{-f(z)\Lambda^2\left[\hat{D},\hat{N}\right]\}\exp\{O(z^3)\}\right\}q_0, \tag{5.19}$$

where the second order commutator, $\left[\hat{D},\hat{N}\right]$, now represents the error induced by the system periodicity. There is a simple prescription for eliminating the effects of this term.

5.3 Discussion

The pre-factor of the commutator is given by,

$$F(z) = f(z)\Lambda^2 = \frac{z_a}{2}\left\{z_a\left(\frac{1-e^{-2\Gamma z}}{1-e^{-2\Gamma z_a}}\right) - z\right\}, \tag{5.20}$$

and is plotted in figure 5.2 for $\Gamma = 0.44$ and $z_a = 2.07$. $F(z)$ represents the deviation of the system from the pure NLSE and, as shown in figure 5.2, is always positive. Thus a pulse launched at $z = 0$ (the condition usually considered) will accumulate small distortions as each span of the system is traversed. If, however, we launch a pulse at some intermediate point, then the error will fluctuate about

some initial value. This suggests that we choose launch points z_l such that the system error is equal to its mean, i.e.,

$$F(z_l) = \bar{F} \tag{5.21}$$

where

$$\bar{F} = \frac{1}{z_a} \int_0^{z_a} F(z) dz. \tag{5.22}$$

$\bar{F}$ is also shown in figure 5.2, where we can see that two solutions, z_{l1} and z_{l2}, exist. These are the preferred points at which to launch a bandwidth-limited, soliton-like, *sech*-shaped pulse.

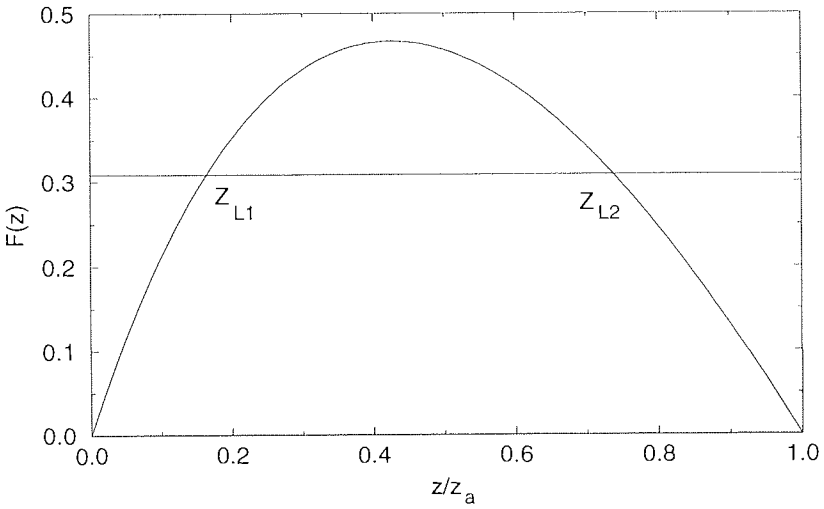

Figure 5.2: The pre-factor of the second order commutator $F(z)$ and its mean value $\bar{F}$ as a function of amplifier position for $\Gamma = 0.44, z_a = 2.07$.

We note that the function $F - \bar{F}$ may be written in the form,

$$F - \bar{F} = \frac{z_a}{2} \left\{ \frac{1}{2\Gamma} + \frac{z_a}{2} - z - \frac{z_a e^{-2\Gamma z}}{1 - e^{-2\Gamma z_a}} \right\}. \tag{5.23}$$

It is possible to make contact here with the Lie transform approach used in ref. [23]. The function $F - \bar{F}$ is identical to the quantity $A_1(z)$ of [23] (apart from our pre-factor $z_a/2$), which is a measure of the lowest order, rapidly varying correction to the guiding centre soliton. Thus choosing an initial point to set $A_1(z)$ to zero in [23] leads to the same result as that presented here.

5.4 Numerical example

The effectiveness launching a pulse at an improved launch point is illustrated in figure 5.3 which shows the pulse evolution with distance over 10 amplifier spacings of $L_a = 40$km for two identical systems. Figure 5.3(a) shows the usual average soliton prescription evolution starting from an amplifier node, whereas in figure 5.3(b), the 10 amplifier span is preceded by a 10.51 km length of fibre and the power is adjusted appropriately, to correspond to launch from z_{l2}. To elaborate on the pulse shape changed noted in figure 5.3, figure 5.4 shows the corresponding evolution of the soliton pulse width (FWHM). In figure 5.4(b), the launched $sech^2(t)$ pulse is chirped and broadened on propagation in this initial link and the pulse emerging from the first amplifier *couples into* the propagating mode of the system much more closely than the $sech^2(t)$ pulse launched from $z = 0$ in figure 5.4(a). The width of the resulting pulse oscillates regularly over each period as it compresses and broadens in phase with the excess nonlinearity and dispersion it experiences during each periodic cycle. However, despite these large excursions, which measure 25% of the mean pulse width, the mean pulse width itself increases by less than 10% over the system span. Furthermore, in figure 5.4(b) there is little evidence of the $8Z_0$ instability [27, 154] seen in figure 5.4(a), which is seeded in that case by over-compression during the first half-cycle.

In these calculations, the fibre dispersion and loss were 16 ps/nm/km and 0.2 dB/km respectively, and the launched pulse width was 35 ps FWHM, giving a soliton period of 30.3km and normalised parameters, $\Gamma = 0.44$ and $z_a = 2.07$. These parameters, which are relevant to soliton transmission of 10Gbit/s signals over standard fibre [85, 125, 155], and if re-scaled to dispersion shifted fibre with $D = 0.5$ps/nm/km, correspond to pulse widths of 6.2ps, which are considerably shorter than those used in recent recirculating loop experiments [149]–[151], were chosen to exceed the usual average soliton limit and therefore to generate significant nonlinear phase shifts and perturbations per period. Consequently, in both cases, some dispersive radiation is shed by the emerging average soliton [153] and therefore our simulations have included dissipative boundary conditions [156] to minimise returning radiation (alternatively, the calculation boundaries could have been extended), allowing us to concentrate on the evolution of the parameters of

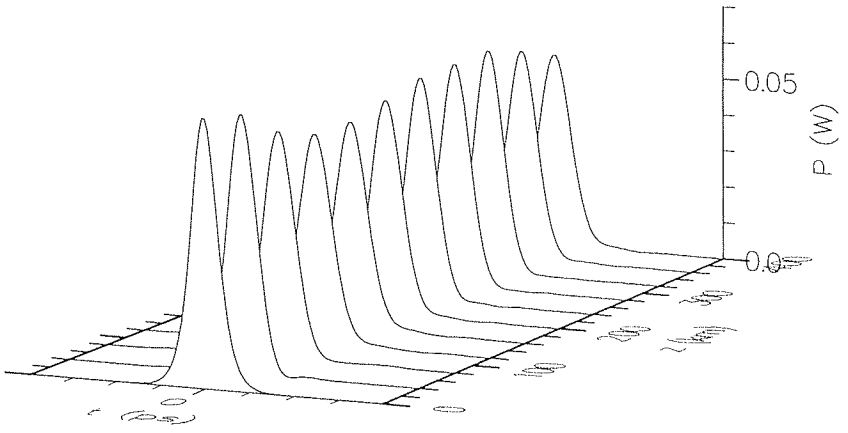

(a)

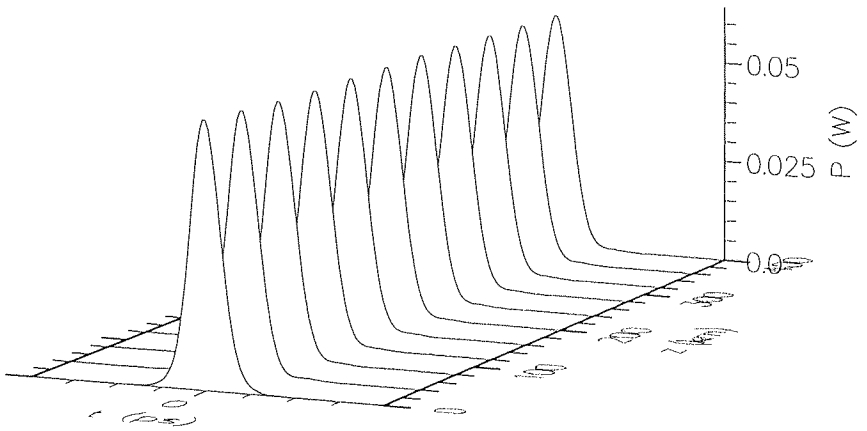

(b)

Figure 5.3: Evolution of the pulse shape over 10 amplifier spans for 35 ps solitons launched at (a) the amplifier node ($z = 0$) and (b) an improved launch point ($z = z_{l2}$). Calculation parameters: D = 16 ps/nm/km, fibre loss 0.2 dB/km and $L_a = 40$ km.

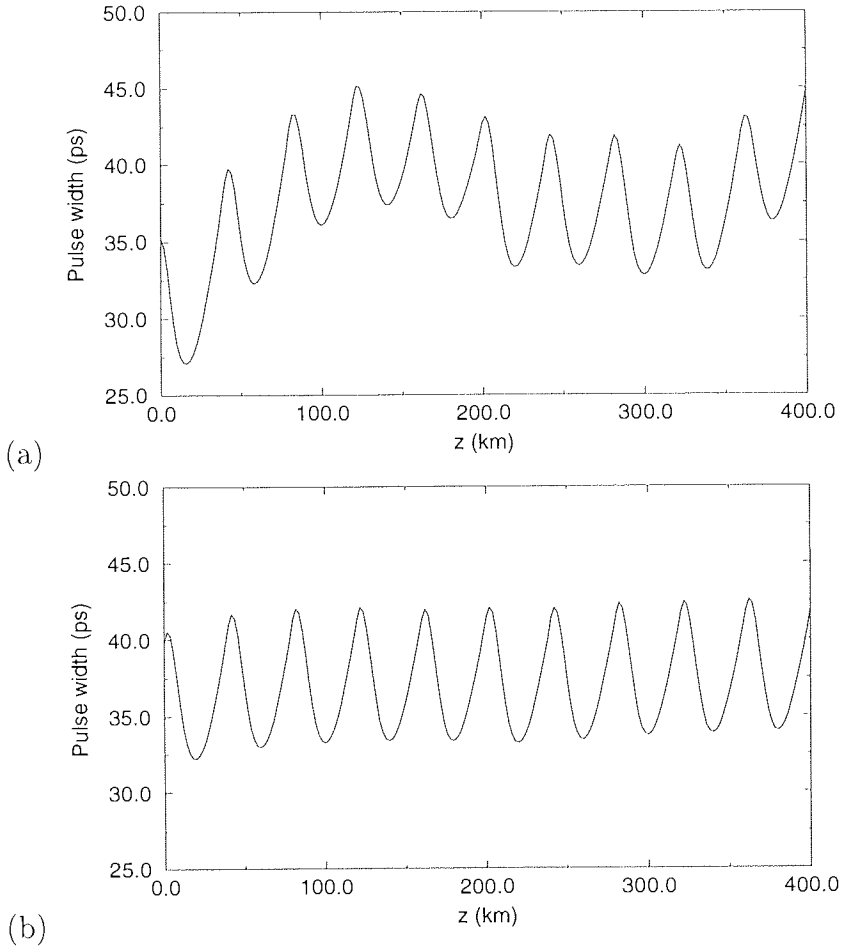

Figure 5.4: Evolution of FWHM pulse widths corresponding to figure 5.3.

the emerging average soliton.

The improved regularity in the evolution of average soliton parameters is also reflected in figure 5.5 which shows the time-bandwidth product of the emerging pulses. As above, it is clear that the oscillation is considerably stabilised by launch from z_{l2}, indicating that the amount of initial dispersive radiation should also be reduced.

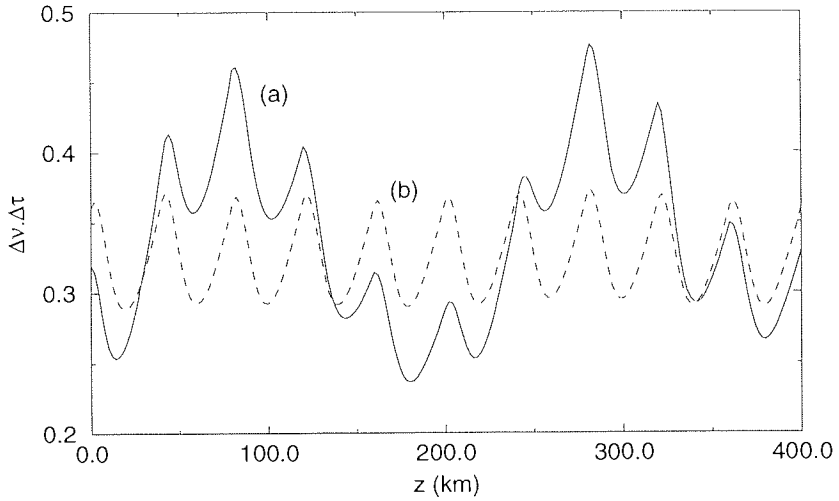

Figure 5.5: Evolution of the time-bandwidth product for launch from (a) $z = 0$ and (b) $z = z_{l2}$, corresponding to figure 5.4.

5.5 Conclusions

We have determined improved launch conditions for the average soliton, which are useful in strongly perturbed systems, operating close to the average soliton limit. Using the operator approach, we have identified two points within the periodic cycle for optimal launch of a bandwidth-limited, *sech*-shaped pulse. These points ensure optimal coupling of the launched pulse to the propagating mode and hence the minimisation of initial pulse distortion and associated dispersive wave radiation. In previous prescriptions for the average soliton, only the amplitude variation across the amplifier link was considered. Our improved prescription utilises an additional degree of freedom, by phasing the launch position with respect to the periodic cycle, and effectively averaging subsequent pulse shape changes. In the strongly perturbed regime, the resulting average soliton changes periodically throughout the

span, not only in amplitude but also in shape. Therefore, this prescription may be considered equivalent to pulse launch at an amplifier node with the next order *correctly shaped* pulse, as envisaged in [23] and [153], but is simpler to implement, since it takes advantage of propagation within the system to perform the desired pulse shaping.

We note that our result is somewhat analogous to the numerical, second order, split step operator technique, in which the dispersion step is placed equally about the nonlinear step to increase the order of accuracy of the integration [4],pp.44. As such, its importance increases as the total number of amplifier sections decreases [157]. Therefore, it has little relevance to long haul soliton systems comprising hundreds of amplifiers, where fine tuning of the initial condition has negligible influence ultimately over accumulating nonlinearities. Nevertheless, in relatively short haul systems, comprising a handful of amplifier stages with relatively longer amplifier spans, such as those of the European optical network [85], it may prove a useful performance enhancement technique.

Chapter 6

Soliton pulse sources

6.1 Introduction

An important requirement for soliton transmission systems is a source of short $sech^2(t)$ pulses at the desired data rate. The laser must repeatably produce identical pulses at a fixed repetition rate with the minimum of intervention from the system operator. Naturally, the simpler the laser the more likely this maintainence criteria will be satisfied.

There are many methods available for producing a soliton laser. Whilst there are a number of linear cavity soliton lasers [158]–[161], a lot of attention has focussed on a ring cavity structure [162]–[171]. Such uni-directional ring lasers often find preference due to their analogy with optical transmissions, as in the anomalous dispersion regime their behaviour is governed by the NLSE, with gain interchanged with loss but which again can be removed through the average soliton prescription. The pulse shaping characteristics are therefore well understood allowing for easy design, provided the pulses can be maintained in the appropriate positions, as Gordon-Haus jitter and so forth will also apply. However, to obtain the required fixed repetition rate desired some mode locking mechanism must be applied at that rate, so this temporal jitter is generally suppressed. Other methods of producing the required pulses include external shaping of gain-switched or modelocked semiconductor device pulses [172], pulse shaping of the beat signal produced by two c.w. signals separated spectrally by the required repetition rate through dispersion decreasing fibre [60, 173] and though cross-phase modulation of a c.w. signal [174].

There is also development work into single chip integrated laser/modulator devices producing an RZ data stream directly from the laser [175].Such devices probably represent the most likely candidate for a deployable soliton laser source if they reach the required data rates (this paper has a printing error in the title, with the data rate achieved 2.5 Gbit/s, not 12.5 Gbit/s) and commercial availability.

This chapter investigates experimentally three potential laser pulse sources. Two are based around the concept of the ring laser, the third is a gain switched DBF laser with external pulse shaping. The goal for all three lasers in to produce time-bandwidth limited $sech^2(t)$ pulses at the selected repetition rate.

6.2 Phase-modulated ring laser

The first laser investigates the use of a travelling wave phase modulator in a ring laser cavity [151, 165]. The original desire was that this laser should produce short, time-bandwidth limited $sech^2(t)$ pulses at a repetition rate of 5 GHz. Typically for soliton propagation experiments at 5 GHz pulse widths in the range 10 – 25 ps are required from average soliton and soliton interaction considerations. For reasons discussed below the repetition rate goal could not be met, although the laser would produce high quality, sufficiently short pulses at other repetition rates.

The role of the phase modulator, as with all modelockers, is to fix the pulses at the desired repetition rate and induce pulse shaping. By contrast with an amplitude modulator, a phase modulator will not directly impose a pulse shape on the passing signal but instead induce a frequency chirp. In order for this imposed chirp to produce a pulsed soliton source, the signal must propagate through a soliton supporting medium to allow pulse shaping effects. The choice of a ring cavity allows the initial pulse shaping from the c.w. signal of the unmodulated laser to accumulate as the signal is fed back around the cavity without again passing through the phase modulator. While it is not certain what the effect of a signal passing against the travelling wave of the phase modulator in a linear cavity configuration would be, it is probable that some undesired chirp would be imposed, potentially resulting in pulse break-up.

Once pulses have been formed after a few round trips, it is possible for them to pass through the phase modulator without gaining any significant chirp

across the pulse, provided they arrive at the peak of the modulation cycle. If a pulse arrives outside this modulation peak a chirp will be imposed on the it, the strength of which will depend on the deviation from the centre of the modulation peak. This will have the effect, through the interaction with dispersion, of guiding the pulse back to the peak of the modulation cycle, and will be stronger for pulses further from their allotted position [176]. Thus the phase modulator performs its two required duties, that of initial pulse shaping, with soliton effects maintaining the pulses thereafter, and repetition rate stabilisation.

6.2.1 Laser configuration

Figure 6.1 shows the schematic diagram of the final laser configuration used. This is a typical ring laser configuration, although various configuration details were tested and changed prior to this setup. In particular, the fibre pigtailed isolator in the pump beam path, between the WDM's, was tried both in the position shown and 10 m into the erbium fibre from this point with no noticeable difference in the results. Placing the isolator part way into the erbium was tested in order to check whether the loss in the 1480 nm pump power of the 1550 nm optimised isolator would cause a significant reduction in the gain saturation of the first few metres of the erbium fibre. In practice it was found that even with loss the co-propagating pump laser could make the required contribution to saturate the gain of the erbium fibre. The other main configuration change was to the SI fibre, which was varied in length from 0 – 60 m, and was also replaced with up to 40 m of dispersion shifted fibre. The longer length of standard fibre was found to give the shortest pulses and best time-bandwidth products, whilst inclusion of the dispersion shifted fibre lead to pulse break-up as there was insufficient average dispersion in the cavity to counteract the self-phase modulation induced.

The modulator used was an 8 GHz lithium niobate phase modulator, fibre pigtailed and anti-reflection coated for operation around 1.55 μm. By studying the electrical spectrum of the c.w. lasing ring laser the cavity resonance of the modulator was found to be 1.7 GHz. This corresponds to a lithium niobate cavity length of around 5 cm, although as the modulator facets were anti-reflection coated there may be an error in this result as the resonance may instead be due

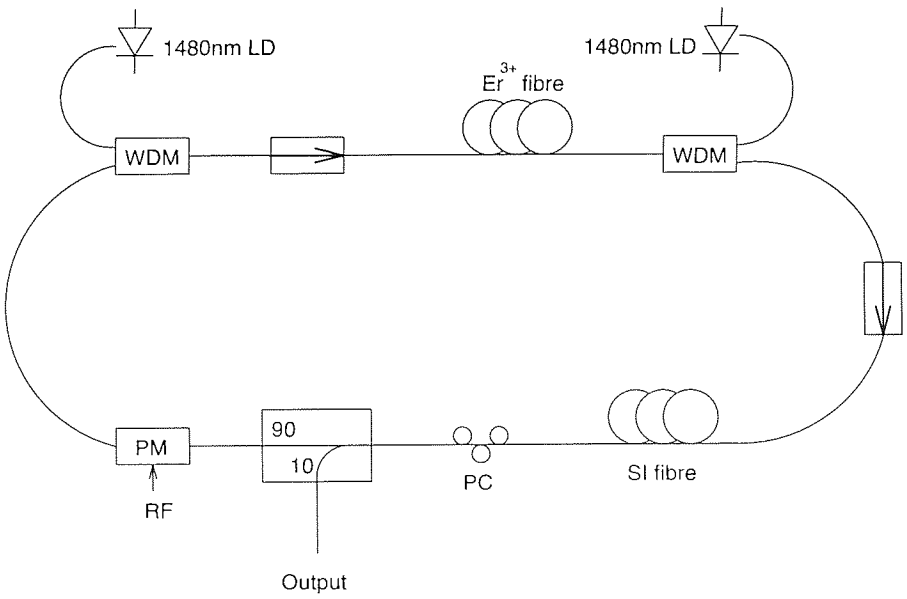

Figure 6.1: Schematic diagram of the phase modulated ring laser. Er^{3+} fibre: 40m erbium doped fibre; SI fibre: (typically) 60m standard fibre; PC; polarisation controller; PM: phase modulator (with RF drive); WDM: 1480/1550 nm wavelength division multiplexer; 1480 nm LD: $\sim$ 30 mW pump laser diodes.

to reflections from the fibre pigtail ends. As described below, this cavity resonance had a significant effect on the performance of the laser.

One significant omission from the ring laser was a spectral filter. Normally some form of wavelength discriminating filter would be included in any erbium fibre laser in order to allow wavelength selectivity and to suppress the 1532 nm erbium gain peak if operation at 1555$\pm$5 nm is required. However wavelength filters can have the detrimental effect of limiting the potential signal spectral width and hence restricting the laser to wider pulses and can introduce unwanted polarisation effects. The problem of the 1532 nm gain peak is simply avoided, provided sufficient pump power is available, by using longer lengths of erbium fibre which will re-absorb the 1532 nm ASE and re-emit the energy at the longer 1550 nm gain peak. Hence as a developmental laser with short pulses required, the filter was omitted and a relatively long erbium fibre length used. Without wavelength selectivity lasing could be found in the range 1552 – 1570 nm, selected through varying the polarisation due to the birefringence in the cavity which mainly came from the phase modulator. Stable modelocked operation was generally found to be at 1562$\pm$2 nm.

6.2.2 Results

As stated above, the original intention of this laser was for operation at 5 GHz with short time-bandwidth limited pulses. However, a major problem with this goal was encountered as it was found that stable modelocking could not be obtained near a harmonic of the fundamental frequency of the phase modulator, 1.7 GHz. Attempts were made to modelock the laser through the range 1 – 6 GHz and stable operation was possible through most of this range except at 1.7, 3.4 and 5.1 GHz $\pm$ $\sim$5%. To illustrate this, the pulse train as measured with a fast photodiode and a sampling oscilloscope is shown in figure 6.2 over this range in 0.5 GHz steps.

As figure 6.2 shows, while reasonable modelocking could be achieved for 4.5 GHz (h) and 5.5 GHz (j), the sampled traced for 5 GHz (i) was noisy as the pulses were not well defined in time (ie. jittered). The pulses the laser formed at 5 GHz were reasonably soliton like, as shown by the autocorrelation trace (figure 6.3(a)) and the spectrum (figure 6.3(b)). They were found to be slightly chirped however, as the pulse width of 14 ps and spectrum of 0.28 nm give a time-bandwidth product of $\sim$0.5, slightly too large for solitons. This pulse break-up is also seen for 3.5 GHz (f) which is too close to the 3.4 GHz modulator harmonic, although 1.5 GHz (b) does appear to be far enough away from the 1.7 GHz resonance. Modelocking at 1.7 GHz gave a similar result as for 3.5 and 5.0 GHz.

The best time bandwidth product was found to be at 1 GHz, as shown in figure 6.4(a), for a pulse width of 14 ps and bandwidth of 0.23 nm. A significant feature of the modelocking at this frequency is that it required a lower power of RF drive to be applied to the modulator, at 18.6 dBm, whereas above 1.5 GHz the maximum available RF power of 27.2 dBm was required. This indicates that the modulator is able to sufficiently chirp the signal at 1 GHz for this cavity length and dispersion. Reasonable time-bandwidth products were also found through the rest of the tested frequency range, with the notable exception of those frequencies too near the modulator cavity harmonics. The measured pulse widths and spectral widths are given in figures 6.4(b) and 6.4(c) respectively.

From earlier experimentation with the additional section of SI fibre, it is to be expected that in order to improve the time-bandwidth products of the higher frequencies, a yet longer length of standard fibre would be useful. This would allow

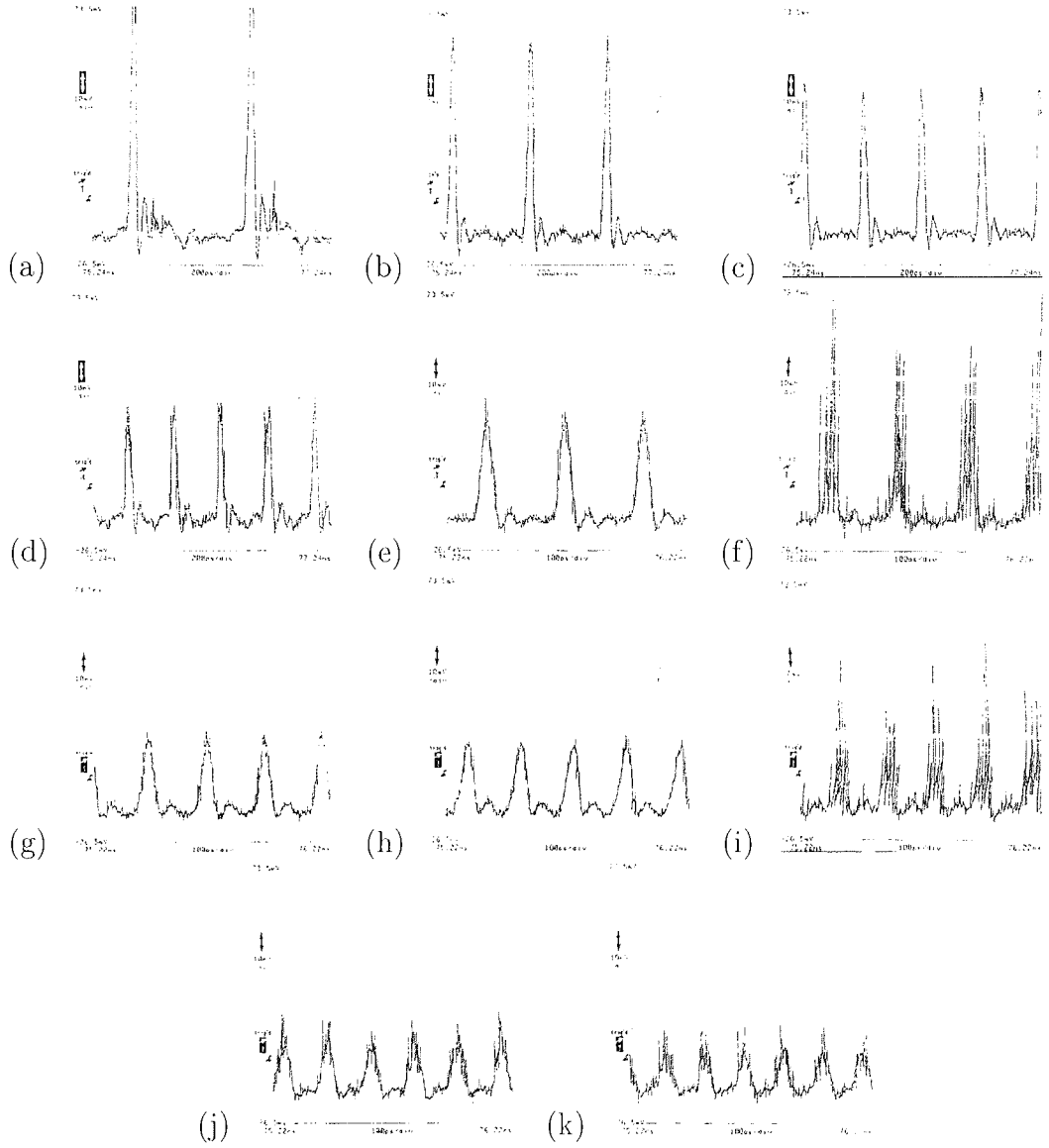

Figure 6.2: Best modelocking achieved on the cavity resonance nearest (a) 1 GHz, (b) 1.5 GHz, (c) 2 GHz, (d) 2.5 GHz, (e) 3 GHz, (f) 3.5 GHz, (g) 4 GHz, (h) 4.5 GHz, (i) 5 GHz, (j) 5.5 GHz, (k) 6 GHz. (Note there is a time-axis scale change from 200 ps/div to 100 ps/div from (e) onwards.)

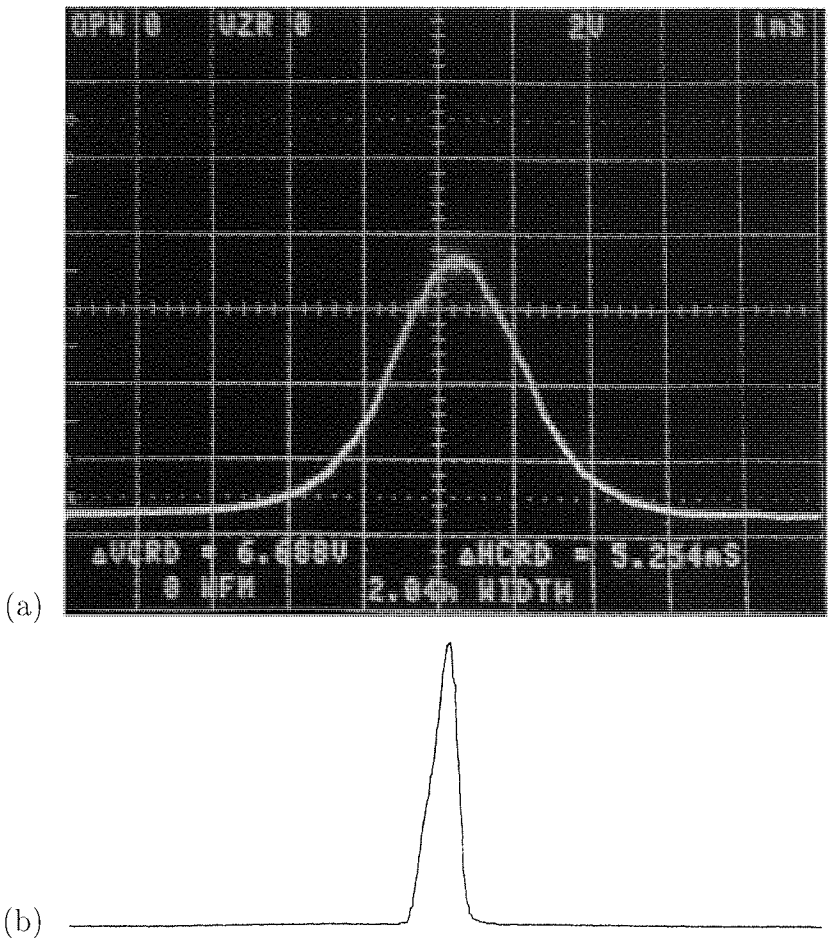

Figure 6.3: (a) Autocorrelation trace of 5 GHz pulses (SHG power (arb. units) versus time (1 ms/div)), pulse width ~14 ps and (b) corresponding spectrum (0-350 μW) versus wavelength (1559.2–1569.2 nm), bandwidth ~0.28 nm

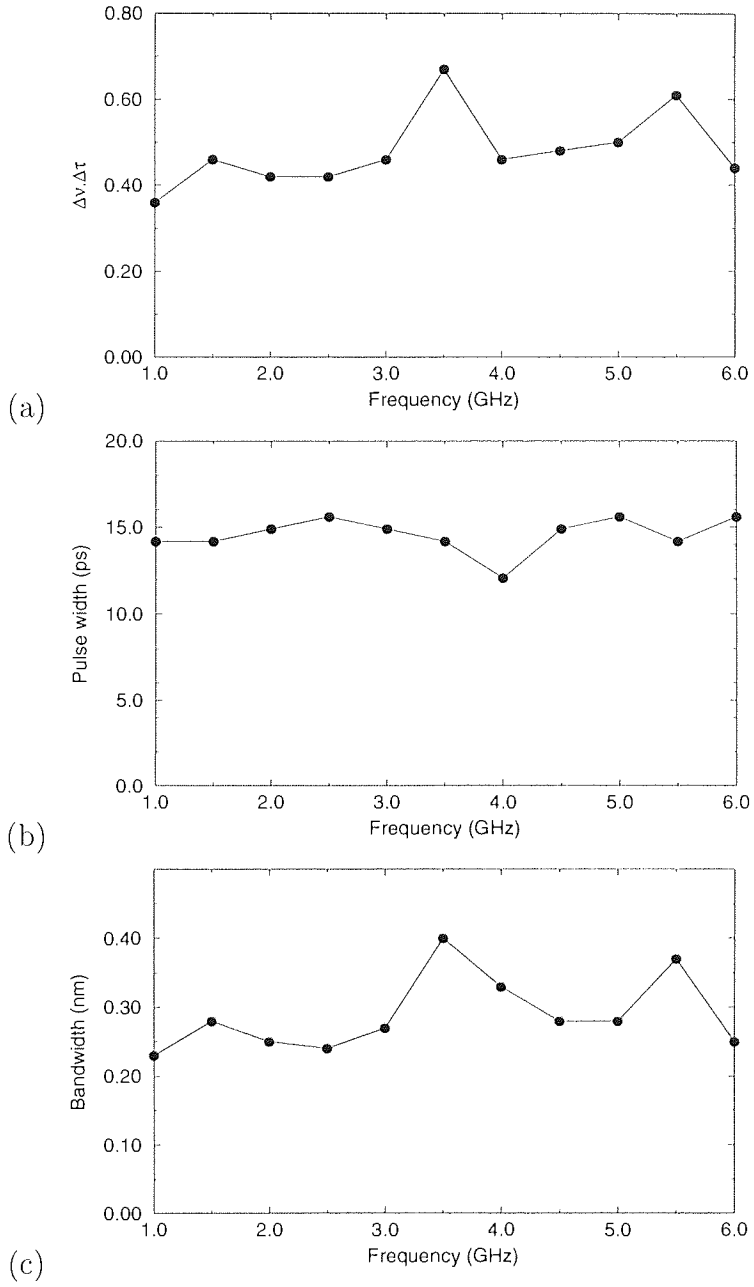

Figure 6.4: Laser characteristics of the phase-modulated ring laser over the mode-locking frequency range 1 – 6 GHz: (a) time-bandwidth products (b) pulse widths (c) spectral widths.

further propagation of the pulses between modulations giving a greater chance of soliton shaping effects improving the pulse shape and bandwidth. However, as the desired laser was a 5 GHz modelocked laser and this could not be achieved with any cavity configuration tested the addition of further standard fibre was not tested. A second, unpackaged but otherwise similar phase modulator was tested but unfortunately it also suffered the same problems as again there was a 1.7 GHz fundamental cavity resonance. However, the laser did work reliably at other repetition rates. If the modulator resonance problem could have been remedied then the laser should have been able to produce suitable 5 GHz time-bandwidth limited soliton source, although some adjustment to the standard fibre length employed for pulse shaping may have been necessary.

6.3 Gain switched DFB laser with pulse compression

Whilst soliton system designers require short $sech^2(t)$ pulse sources at high repetition rates, two important design consideration that are generally overlooked are those of size and simplicity. In the final analysis, if a compact semiconductor device can achieve similar or marginally worse results than a fibre laser, but comes in a far smaller, easily replaced package and only requires electrical drives rather than cavity length and polarisation control, the semiconductor device will be used. One of the more promising semiconductor devices for soliton transmissions is the gain switched distributed feedback (DFB) laser. These devices are not without their problems however, as gain switching is an inexact, partly spontaneous process, which introduces substantial source jitter, the pulse widths tend to be too long for soliton transmission and the pulses are severely chirped by the gain switching process. However if methods can be found to reduce or eliminate these problems DFB lasers will present a strong challenge to fibre lasers for soliton systems.

Here we studied experimentally at an attempt to overcome these problems and produce a very short, modelocked, low jitter pulse source with low chirp. There are three main stages to this work. In the first stage the jitter was reduced by external feedback. Second, the pulse chirp was reduced by propagation in disper-

sion compensating fibre (DCF). The third stage was to effect spectral broadening through the use of a semiconductor laser amplifier, again a compact device requiring only electrical input although usually polarisation dependent, and propagate the hence chirped output pulses through standard fibre to remove this chirp and temporally narrow the pulses.

6.3.1 Theory of spectral broadening through an SLA

The use of semiconductor laser amplifiers (SLAs), in particular travelling wave amplifiers, has been of considerable interest for applications in optical communication systems for several years [143, 177]. The main obstacle to their use as in-line amplifiers in transmission systems is the nonlinearities induced by gain saturation, where the leading edge of a pulse saturates the amplifier reducing the gain seen by the trailing edge [178]. This feature limits their use to outside the saturation regime where the pulse energy may be too low to be practical. Operation within saturation has led to observations of pulse broadening and subsequent compression [179].

The mechanism for these pulse shape changes were shown using a simplified model of pulse propagation in an SLA to be due to self-phase modulation of the signal [180]. Rather than use a numerical simulation to find solutions to the equations governing the evolution of a pulse in an SLA, considerable insight can be gained by making certain approximations and obtaining a closed set of equations. The first approximation is that the loss of the device be essentially zero compared to the gain, which is generally found to be reasonable. It is then possible to obtain the output pulse power P_{out} and phase ϕ_{out} due to the amplifier as [180],

$$P_{out}(t) = P_{in}(t)exp\left[h(t)\right] \tag{6.1}$$

$$\phi_{out}(t) = \phi_{in} - \frac{1}{2}\alpha h(t) \tag{6.2}$$

where P_{in} and ϕ_{in} are the input pulse power and phase. The parameter α is the line width enhancement factor and is typically in the range 3–8 [181, 182]. The function $h(t)$ represents the gain, integrated over the amplifier length, at each point of the pulse. In order to obtain an analytic solution for the function $h(t)$ a second

approximation is made that the input pulse width τ_f is much smaller than the carrier lifetime of the device τ_c which amounts to the pulse being so short that the amplifier gain has no time to recover. In that case we can obtain

$$h(t) = -ln\left[1 - \left(1 - \frac{1}{G_0}\right) exp\left(\frac{-U_{in}(t)}{E_{sat}}\right)\right] \tag{6.3}$$

where G_0 is the unsaturated single pass gain of the amplifier, E_{sat} is the saturation energy and $U_{in}(t)$ represents the fraction of pulse energy in the leading part of the pulse up to a given point t, given by

$$U_{in}(t) = \int_{-\infty}^{t} P_{in}(t')dt'. \tag{6.4}$$

By definition $U_{in}(\infty) = E_{in}$ as the whole pulse will have passed through the amplifier by $t = \infty$.

When considering spectral broadening and pulse compression, it is useful to look at the chirp the pulse experiences on propagation through the amplifier. Using the relationship (cf. equation (2.29))

$$\Delta\nu(t) = -\frac{1}{2\pi}\frac{\partial\phi}{\partial t} \tag{6.5}$$

and the output phase of equation (6.2) we obtain

$$\Delta\nu_{out}(t) = \Delta\nu_{in}(t) + \frac{\alpha}{4\pi}\frac{\partial h}{\partial t} \tag{6.6}$$

where the input pulse chirp is $\Delta\nu_{in}(t)$ if not transform limited. Substituting for $h(t)$ from equation (6.3) we arrive at the output pulse chirp as

$$\Delta\nu_{out}(t) = \Delta\nu_{in}(t) - \frac{\alpha(G_0 - 1)}{4\pi G_0}\frac{P_{out}(t)}{E_{sat}} exp\left(\frac{-U_{in}}{E_{sat}}\right). \tag{6.7}$$

In ref. [180] a Gaussian pulse was used in the derivation and numerical examples. As our interest here is solitons we reconsider using a soliton as the input pulse of the form

$$P_{in}(t) = P_0 sech^2\left(\frac{t}{\tau_0}\right) exp(i\phi_{in}) \tag{6.8}$$

for an peak power of P_0 and soliton width $\tau_0 = \tau_f/2ln(1+\sqrt{2}) = \tau_f/1.763$ as usual

[4],pp.60. This gives the function $U_{in}(t)$ as

$$U_{in}(t) = P_0\tau_0 \left[tanh\left(\frac{t}{\tau_0}\right)\right] \tag{6.9}$$

from which we get

$$h(t) = -ln\left[1 - \left(1 - \frac{1}{G_0}\right) exp\left(\frac{-P_0\tau_0}{E_{sat}} tanh(t/\tau_0)\right)\right] \tag{6.10}$$

which can then be substituted back to obtain the output power (eqn. (6.1)), phase (eqn. (6.2)) and chirp (eqn. (6.7)) to obtain rather unwieldy expressions. It is then relatively straight-forward to use this model to find the effects of the SLA on an input soliton.

To study this model, we took the SLA to have a saturation energy of $E_{sat} = 10pJ$, an unsaturated gain of $G_0 = 1000 = 30dB$ and a linewidth enhancement factor of $\alpha = 8$, reasonably typical values [180] arrived at by comparison with the experimental results below. The input pulse was a perfect time-bandwidth limited soliton ($\phi_{in}(t) = 0$) of 5.5 ps pulse width and a peak power of 500 mW. Using these parameters the model of the amplifier effect on the temporal profile, spectrum (through the Fourier transform) and chirp were found as shown in figure 6.5(a-c), with the input temporal and spectral profiles shown for comparison. The first feature to note was the broadening of the temporal profile experienced by the pulse from the input 5.5 ps to 9.8 ps. As mentioned above, this occurs as the leading edge of the pulse sees greater gain, before the amplifier saturates reducing the gain available to the centre and trailing edge of the pulse. The spectrum of the output pulse (figure 6.5(b)) shows that this temporal broadening is coupled with a red shift of the pulse centre frequency. This frequency shift is due to the SPM-induced frequency chirp imposed on the pulse on propagation through the SLA which is shown in figure 6.5(c). This shows that there is a negative frequency chirp experienced by the entire pulse, hence the red shift, which essentially follows the temporal profile of the output pulse.

Now that there is a chirp imposed on the pulse, with some temporal broadening, we consider pulse compression. The negative chirp imposed on the pulse is essentially linear through the central part of the pulse, $-\tau_0 < t < \tau_0$. This

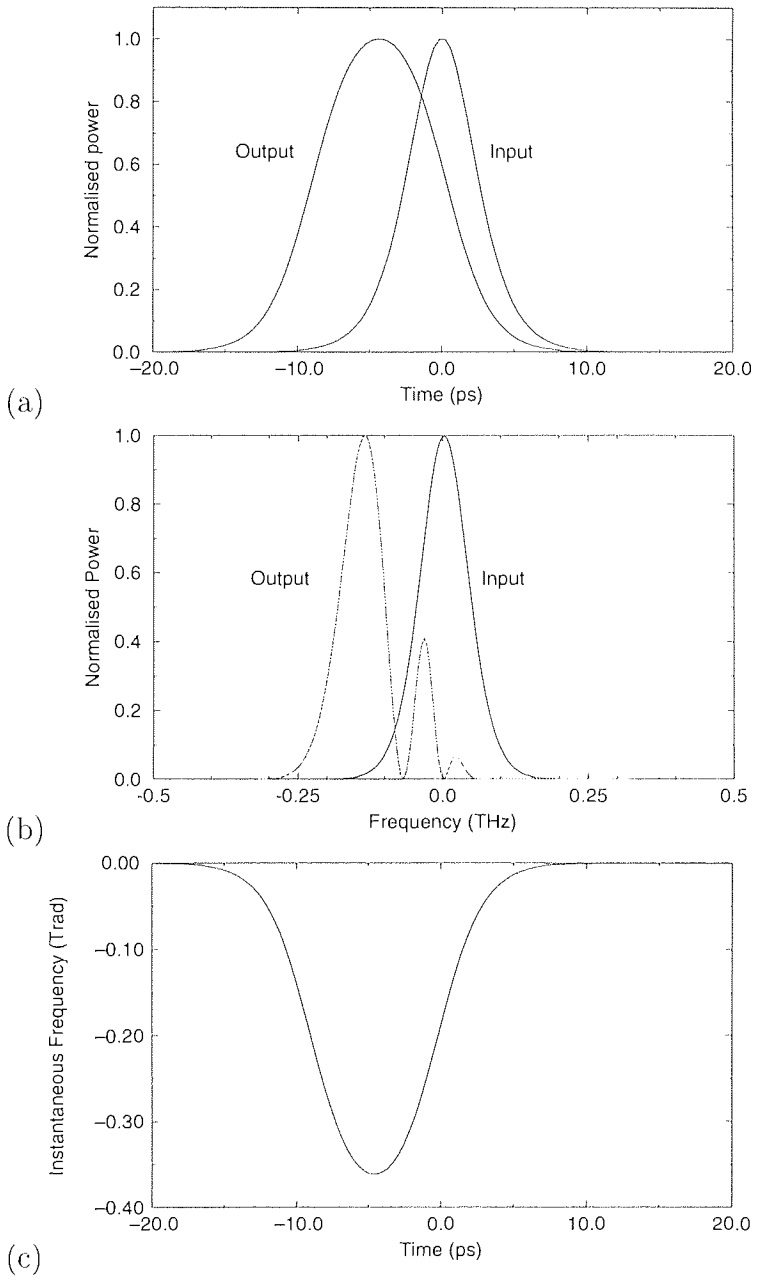

Figure 6.5: Effect of propagation through a saturated SLA on a 5.5 ps soliton for the (a) temporal profile, (b) spectral profile obtained by Fourier transform and (c) frequency chirp. The perfect input soliton has no initial chirp ($\Delta\nu_{in} = 0$).

linear chirp implies that the pulse can be compressed by propagating it through an anomalous dispersive media [4]. We therefore take the modelling one stage further by simulating propagation of the pulse along a length of standard fibre. As we are working a 1.55 μm the standard fibre will have anomalous dispersion of $\sim$17 ps/nm/km for our signal. The results of such a propagation on the temporal profile of the pulse with increasing distance is shown in figure 6.6(a). Here we see as expected that the pulse narrows significantly, reaching a minimum at around a distance of $300m$. This is more clear from figure 6.6(b) which shows the FWHM pulse width against distance and gives the minimum pulse width as 3.76 ps after 270 m. This corresponds to a compression factor of 1.46.

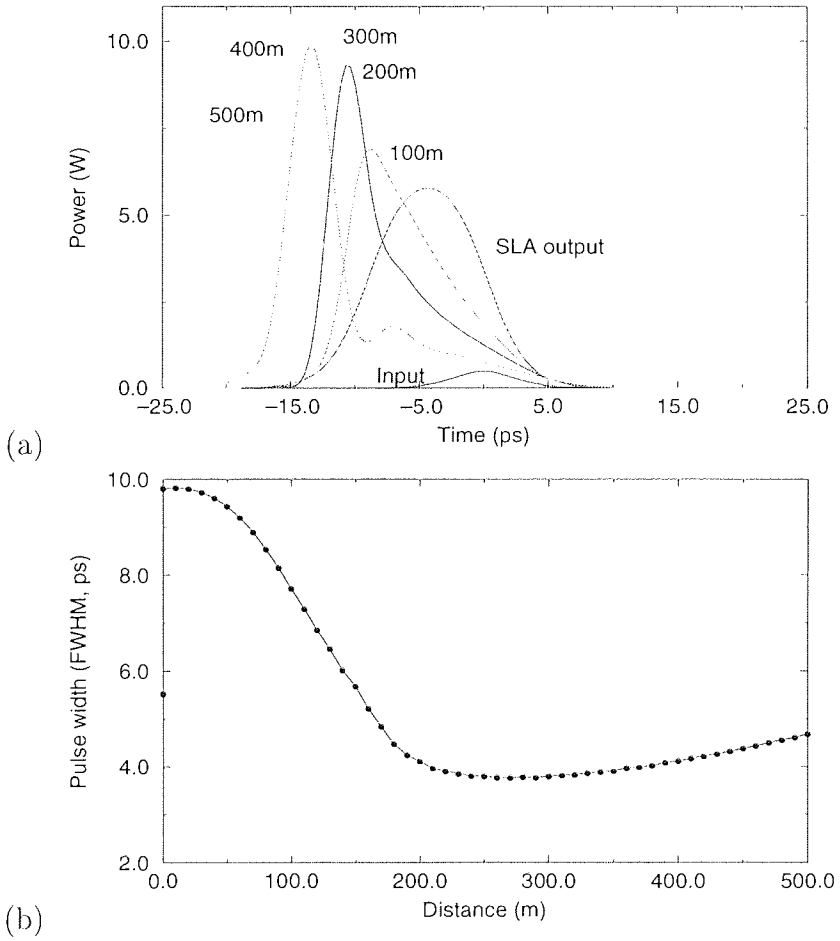

Figure 6.6: (a) Pulse temporal evolution in standard fibre with distance and (b) corresponding pulse widths with distance.

One of the approximations made in the above calculations was that the pulse width was much shorter than the recovery time of the amplifier, the carrier recombination time, ie. $\tau_f \ll \tau_c$. In order to test this assumption, an estimate of

the recombination time was made using the experimental setup shown in figure 6.7. The gain switched DFB laser was modulated at 1.5 GHz and the pulses compressed (described below) before amplification to take their energy into the saturation regime of the amplifier. A second DFB at a different wavelength was driven c.w. and 10 % of this signal injected through the 90:10 coupler to act as a probe beam (this low power was taken both to show the small signal gain of interest and to avoid four-wave mixing effects). As a pulse passes through the amplifier the gain available to the probe beam is reduced by the gain saturation before recovering as the carriers recombine. By filtering out the high power gain switched DFB the effect this has on the c.w. probe beam can be studied on an oscilloscope, as shown in the trace of figure 6.8. The exponential recovery of the probe beam after the gain has been depleted can clearly be seen, although the feature as the gain approaches full recovery is not understood but may be due to gain recovery optically seeded by dispersive wave energy between the DFB pulses due to the pulse compression. From this exponential recovery it was possible to estimate that the carrier recombination time was $\tau_c = 620ps$. For RZ operation at 2.5 GHz the pulse width must necessarily be much less than the pulse spacing of $T_R = 400$ ps and will generally be below 50 ps. The approximation of $\tau_f \ll \tau_c$ can thus be seen to be reasonable.

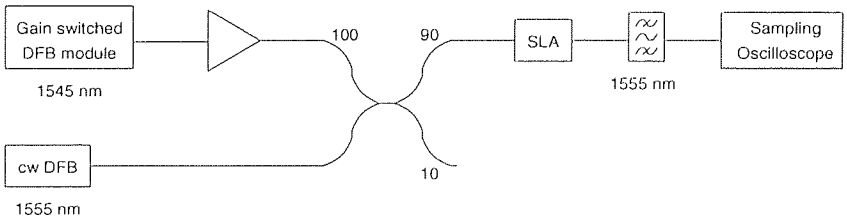

Figure 6.7: Schematic diagram for the experimental setup to measure the carrier recombination time τ_c of an SLA. The DFB module was as in stages 1 and 2 of figure 6.9 below.

6.3.2 Experimental details

The three stages of the final experimental setup is shown in figure 6.9. The first stage was to reduce the DFB jitter by external feedback. The DFB laser used in these experiments could be gain switched at up to 10 GHZ, although

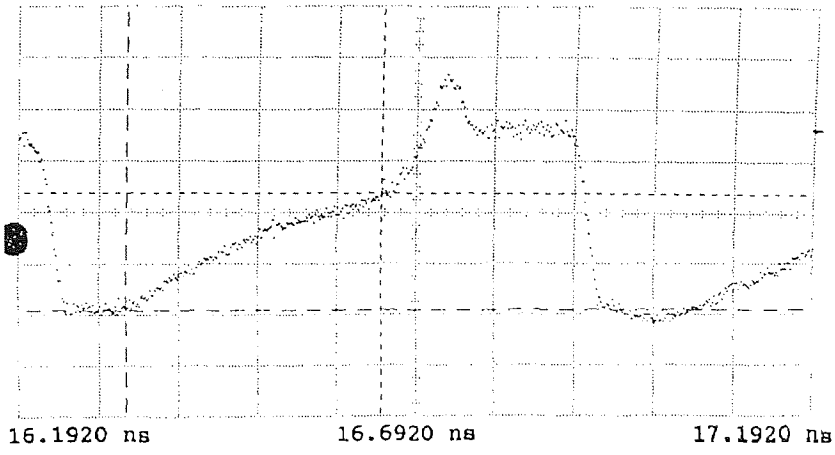

Figure 6.8: Trace obtained from a sampling oscilloscope for the dynamics of the c.w. probe beam due to gain saturation by the gain switched DFB.

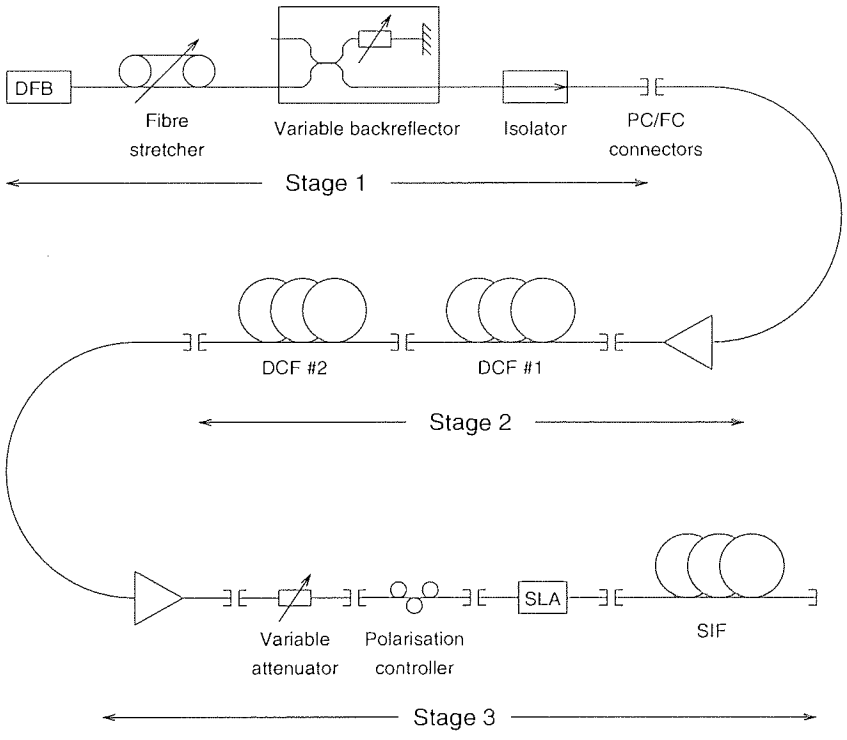

Figure 6.9: Schematic diagram of the three stages for the stabilisation and compression of a DFB laser. Stage 1 is the modelocking of the DFB through an external cavity, stage 2 compresses the DFB by removing the chirp with dispersion compensation fibre (DCF), stage 3 uses SPM from an SLA to chirp the pulses then compress them through standard fibre (SIF).

here the desired repetition rate was 2.5 GHz. At the threshold current of 28 mA application of +27 dBm of RF power would produce heavily jittered pulses ($\sigma \simeq 7ps$) making measuring the pulse width prone to error. In order to reduce the jitter a variable backreflector was introduced in order to externally feedback some of the output signal to seed the gain switching, as shown in stage 1 of figure 6.9, the laser output being taken from the throughput 50 % of the backreflector. A fibre stretcher was also included to set the required phase of the pulse being fed back. This arrangement led to a reduction in the observed jitter to that of the measuring oscilloscope ($\sigma \simeq 1ps$) and allowed measurement of the pulse width of 16-20 ps, depending on the applied bias and drive RF powers. This feedback mechanism also appeared to reduce the output pulse width, as the estimate of the jittered pulse width was $\gtrsim$ 40 ps. Curiously, it was noted that after a break in the fibre between the fibre stretcher and the backreflector was repaired, the amount of backreflection did not matter, although the fibre stretcher still required adjustment. This result was attributed to a bad fusion splice between the fibre stretcher and the variable backreflector which gave sufficient feedback.

These output pulses were heavily chirped as indicated by the lopsided spectrum of figure 6.10(a). The measured halfwidth of this spectrum was found to be 1.06 nm. This corresponded to a pulse width of 19.4 ps (figure 6.10(b)) giving a time-bandwidth product of 2.58. These were obviously not solitons, which have a time-bandwidth product of 0.314, but the positive chirp did allow us to attempt to reduce the pulse width through dispersive compression, stage 2 of figure 6.9. For this the modelocked DFB pulses were amplified then transmitted through a length of dispersion compensating fibre (DCF). To find the optimum compression (ie. best pulse width and time-bandwidth product) several different fibre lengths and hence different dispersion values were used in the various permutations possible to give a selection of group delay values. Figure 6.11 shows the resulting pulse widths and time–bandwidth products against group delay from which it was found that for optimum compression a group delay of around -10 ps/nm was required. In the later experiments the actual group delay used was -11.5 ps/nm from a combination of two compensating fibres, which was marginally the better operating point, giving a pulse width of 5.5 ps and a time-bandwidth product of 0.83. While these pulses

were still not solitons, they were significantly closer. As the pulses had been compressed as far as possible by this method it can be assumed that while some of the energy may be acquired by the pulse through soliton shaping upon transmission, most would probably be lost to dispersive wave radiation.

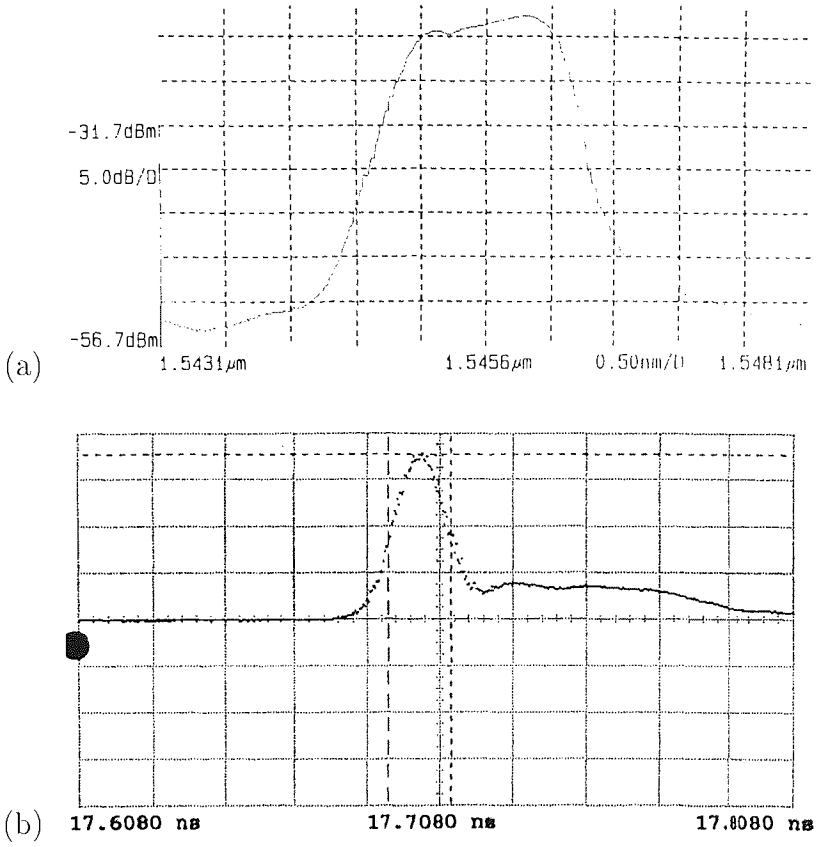

Figure 6.10: Stage 1 output of the DFB laser. (a) Heavily chirped spectrum and (b) corresponding sampling oscilloscope trace, with a slight tail from overdriving the RF power.

The final stage of this experiment was to further reduce the pulse width using SLA spectral broadening and chirping and dispersive compression in standard fibre. To achieve the optical power required to saturate the SLA, a high power amplifier (saturated output power of +14 dBm) was introduced prior to the SLA. In order to adjust the input power for testing a variable attenuator was included, as well as a polarisation controller to optimise the polarisation input to the SLA. The amplifier used in this work was not the same as that used to estimate τ_c in the theory section above, as the fibre-to-fibre gain through that amplifier was rather low, thought to be due to poor fibre-SLA coupling. Instead a similar amplifier was used, but with greater gain, as shown in figure 6.12(a). This amplifier also had a higher gain

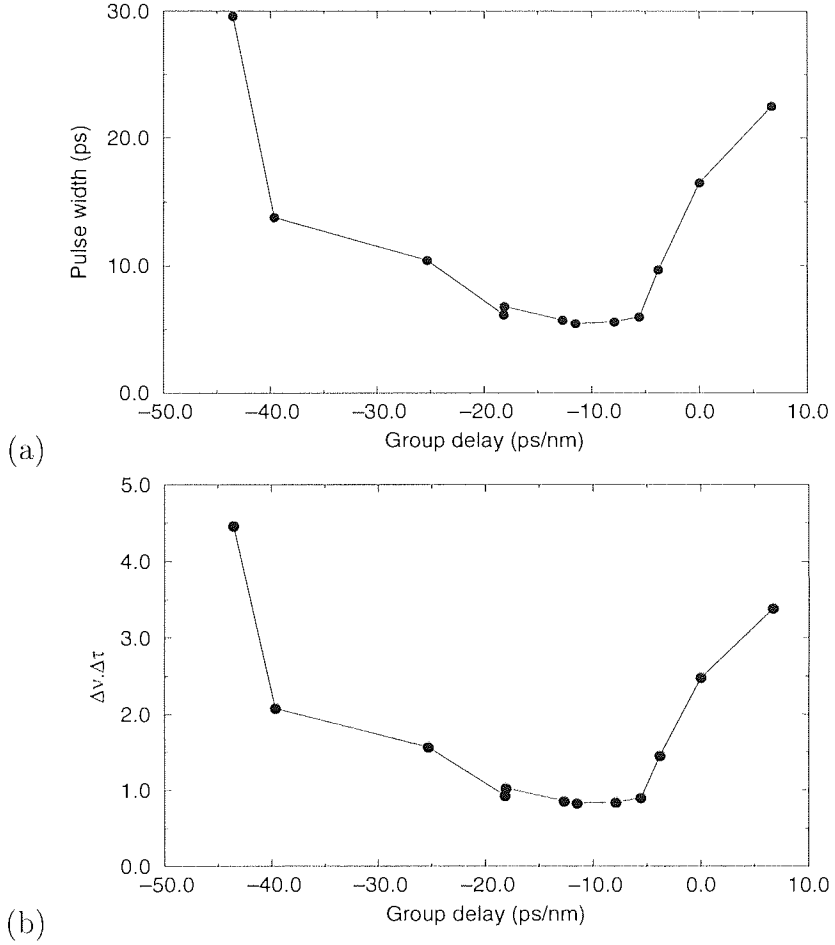

Figure 6.11: DFB compression through DCF. (a) Pulse width versus group delay using the various fibres available in all permutations and (b) corresponding time-bandwidth products.

saturation point, with the gain saturation curves shown in figure 6.12(b).

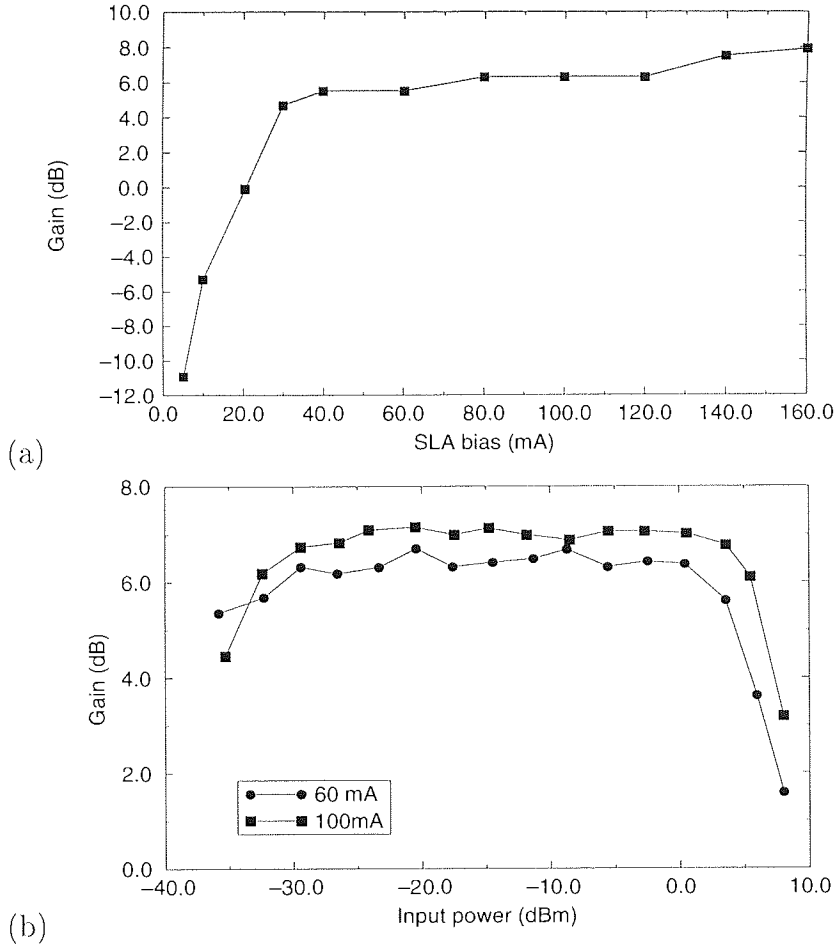

Figure 6.12: Gain characteristics of the SLA: (a) small signal gain against SLA bias current at an input power of -20 dBm, (b) gain saturation curves, against output power, at 60 and 100 mA SLA bias currents.

The experiment was performed in two parts. The first part was to use the amplifier as far into saturation as possible, using the highest available input power from the EDFA of +11 dBm, to test for a suitable length of post-amplifier compression fibre. The pulse width with no compression fibre increased as expected from 5.5 to 6.9 ps upon traversing the SLA. Standard fibre lengths of 200 m, 300 m and 700 m of SIF ($D_2 = 18ps/nm/km$) were tested, as was the 700 m standard fibre length in conjunction with 100 m of DCF ($D_2 = -38ps/nm/km$) to give a larger set of total dispersion values. The output pulse width found is plotted against the group delay experienced in figure 6.13 and shows a broad minimum around 7 ps/nm. The minimum output pulse width achieved with the fibres available was for the 300 m SIF (5.4 ps/nm) at 4.6 ps. This length of fibre was used hereafter.

In order to increase the available input power to the SLA, the polarisation

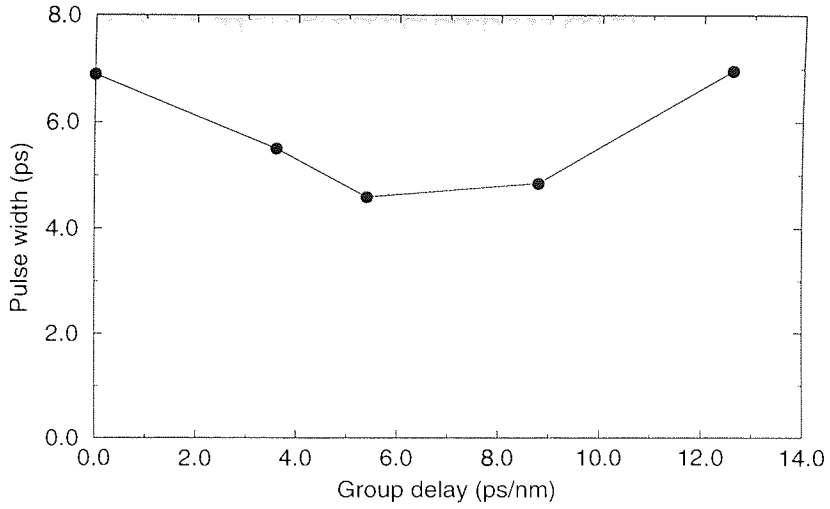

Figure 6.13: Minimum pulse width against the group delay for the DFB pulses after the SLA and compression fibre.

controller was removed from the experiment. While this meant that the input polarisation could not be optimised it did increase the input power by 2 dB to 13 dBm. Transmission through the 300 m of standard fibre at this input power resulted in a pulse width of 3.5 ps, with this autocorrelation trace shown in figure 6.14. This corresponds to a compression factor for this stage of 1.6 (c.f. section 6.3.1), and for the experiment as a whole of 4.6. The optical bandwidth of these pulses was measured to be 1.5 nm, giving a time-bandwidth product of 0.65. Once more, although this time–bandwidth product is too large for these pulses to be solitons, it is closer to the required 0.314 time–bandwidth value than the output of stage 2 ($\Delta\nu\Delta\tau = 0.83$).

The polarisation controller was left out for the second part of the experiment, the variation of the compression factor against input pulse power. The input power was reduced by increasing the attenuation of the variable attenuator, with the compression against power shown in figure 6.15(a). As already indicated, reducing the input pulse power reduces the compression available, due to the reduction in the chirping the pulse experiences. This correlation is confirmed by comparing the compression achieved with the bandwidth of the SLA output for a given input power, as shown in figure 6.15(b). This highlights the spectral broadening responsible for the chirp and thus available for pulse compression.

While this laser configuration does give short, low jitter pulses, the pulses

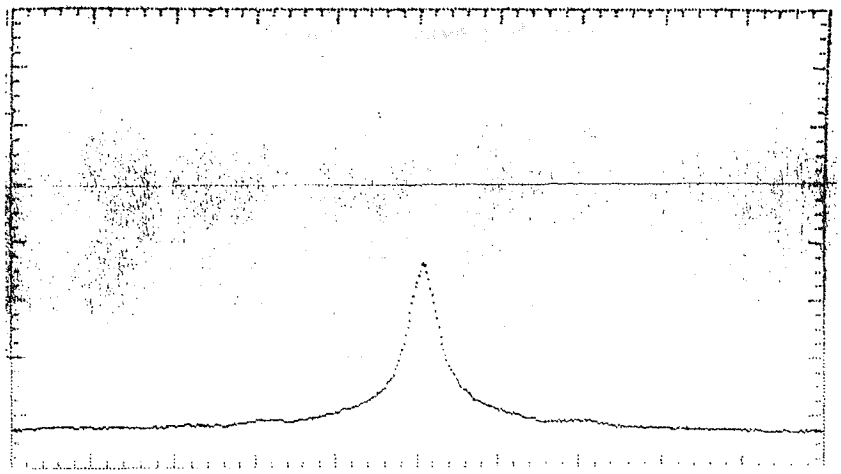

Figure 6.14: Optimum 3.5 ps output autocorrelation trace after the three stages from the DFB laser, SLA and fibre compressions.

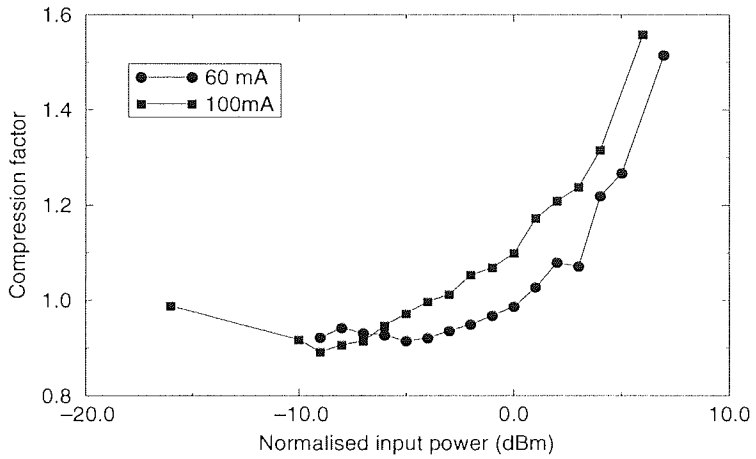

(a)

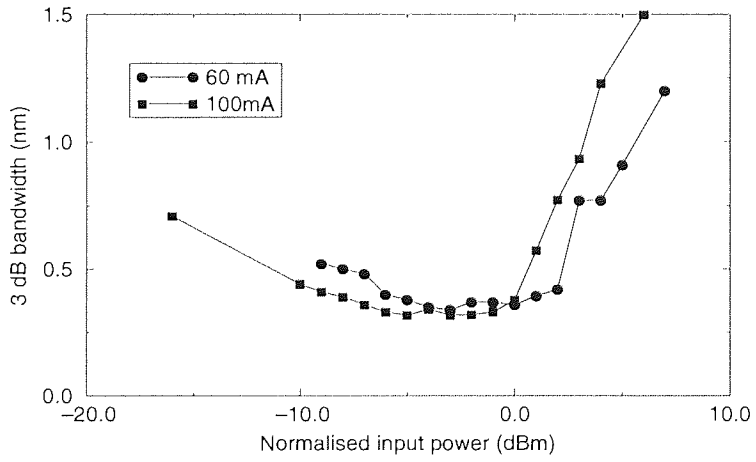

(b)

Figure 6.15: (a) Compression factor against input power, normalised to the saturation power, at 60 mA and 100 mA after propagating the pulse, spectrally broadened by the SLA through 300 m SIF. (b) Bandwidth against input power, normalised to the saturation power, at the output of the SLA for 60 mA and 100 mA, prior to the compression shown in (a)

are not ideal for soliton propagation experiments as they are not time-bandwidth limited and will shed some dispersive wave radiation on propagation. Although the post-SLA pulse shaping was performed using standard fibre this was dispersive compression rather than soliton shaping, so it is likely that some of this additional energy will be absorbed into the pulses on transmission. The pulse shaping by compression of both the chirped DFB and SLA could be slightly optimised. However the 3.5 ps pulse widths obtained will be suitable for propagation at very high data rates through optical time division multiplexing (OTDM). It should also be possible to reduce the pulse widths still further if the input power to the SLA could be increased above +14 dBm driving the SLA further into saturation thus giving further spectral broadening. With re-optimisation of the standard fibre length used for the post-SLA compression it seems likely that pulse widths of ~1 ps or less should be possible, suitable for transmission through OTDM of up to 100 GHz.

6.4 Actively modelocked figure-8 laser

In this section we return once more to a fibre ring laser configuration, this time with an amplitude modulator as the modelocking mechanism. The amplitude modulator chosen here was a fibre device, the two wavelength nonlinear optical loop mirror (NOLM). The second wavelength switching pulses came from a gain switched DFB laser. Whilst the DFB produced long, jittered pulses which were themselves unsuitable for transmission themselves, they were able to provide sufficient cross-phase modulation (XPM, see section 2.7) to switch the NOLM. The remainder of the laser cavity was typical of most erbium-fibre ring lasers.

6.4.1 The nonlinear optical loop mirror

The nonlinear optical loop mirror (NOLM) has received a great deal of interest since first proposed as an ultrafast switching device [183]. The basic operation of the NOLM is that an input signal wavelength is split by a coupler into two components which traverse in opposite directions around a length of fibre before recombining. The phase difference of the recombining waves determines the switching characteristics of the device - if the two components are in phase the wave is transmitted,

out of phase they are reflected. The device relies on the linear phase shift accumulated on propagation of the nonlinear soliton pulses to set the returning phase of the two components. If an unequal coupler ratio is used, the two components will experience a different phase shift due to their different peak powers. For solitons, the π phase shift required for switching means a path length difference of $4Z_0$ for the two components. In practice, the polarisation of the loop mirror plays a role in how the two components of the input pulse recombine and thus the NOLM can be biased by a polarisation controller to either transmit or reflect, if there is a sufficient phase shift, as required [184].

The usefulness of the NOLM was extended when the two-wavelength operation of the device was presented [185]. An equal coupler ratio is used and the phase difference introduced through cross-phase modulation (XPM) of one component of the coupler-split signal by pulses at a second wavelength and propagating in one direction. Again, with the appropriate polarisation setting the NOLM can be biased to transmit or reflect, for a given relative phase shift between the pulse components. This second use of the NOLM is of interest to us here in amplitude modulating an initially c.w. signal into pulses and then maintaining them at a fixed repetition rate.

Many applications of the NOLM in both configurations have been developed. In the self-switching format, they have been used for noise suppression [186, 187], pulse shaping [188], and suggested for maintaining solitons in a highly perturbed transmission line [189]. The two wavelength operation has been used to provide a variable end mirror in linear cavity lasers [190], for OTDM demultiplexing [21, 141, 142, 191], as a optical regenerator and wavelength converter for data streams [192]–[194] and also for RZ to NRZ conversion [195].

6.4.2 Experimental results

The configuration of the laser cavity was as shown in figure 6.16. The main part of the cavity (lower ring of the figure eight) was a typical ring laser with an EDFA protected from backreflections by an isolator before the output coupler and a polarisation controller to set the optimum polarisation state for the main laser cavity. The only significant difference with this configuration was the placement of the 3

nm bandpass filter, which was before rather than after the amplifier. This was to provide additional isolation for the amplifier from 1538 nm leak-through from the NOLM which forms the upper loop of the figure eight cavity. Again, the NOLM was a standard XPM-switched configuration, with a 50:50 coupler splitting the power equally both ways round the NOLM, a polarisation controller to set the correct polarisation for switching and two WDM's to couple in and out the switching 1538 nm signal. In order to achieve sufficient power for switching the gain switched DFB laser was amplified by an erbium-ytterbium amplifier which could provide over 100 mW average optical power. The 100 m of standard fibre was used to provide the medium for XPM to take place.

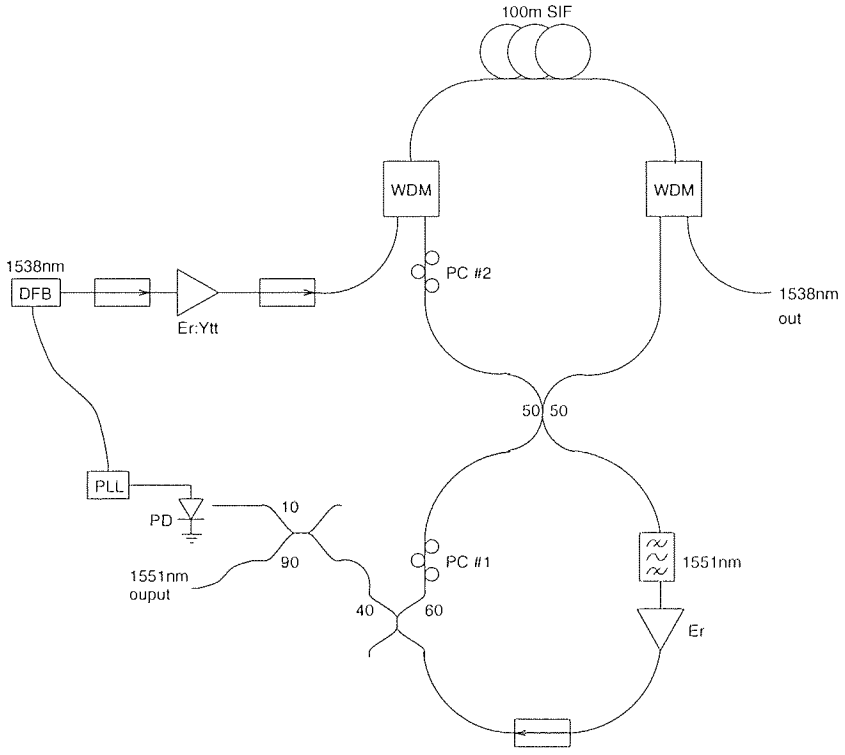

Figure 6.16: Configuration of the ring laser with a NOLM switched by XPM from a gain switched DFB laser as an amplitude modulator. SIF: 100 m step index fibre; PC #1/#2: polarisation controllers; PLL: phase locked loop; PD: 2.5 GHz bandwidth photodiode; Er: erbium fibre amplifier; Er:Ytt; erbium-ytterbium amplifier; WDM; 1538/1555 nm wavelength division multiplexers.

To modelock the laser, the switching pulse frequency must be at a harmonic of the laser cavity. For this laser the fundamental cavity frequency was 1.5 MHz, corresponding to a cavity length of ~138 m. It was desired to modelock the laser at a frequency around 1 GHz, almost the maximum possible with the DFB laser. Ini-

tially this was done by manually tuning the frequency of the DFB using a frequency synthesiser to a harmonic of the laser cavity. Later, once the laser had been shown to work a phase-locked loop (PLL) was introduced to compare the laser output frequency of the laser as given by a photo-diode with the frequency for the DFB, produce an error signal and adjust the driving frequency accordingly by changing the voltage applied to a voltage controller oscillator (VCO). The advantages of this method of modelocking were that it would automatically find the closest harmonic available and lock to it and if there was a change in the cavity frequency due to a temperature induced change in the cavity length, the drive frequency would be adjusted to compensate for it, producing a more stable laser.

Careful adjustment of the NOLM polarisation controller and the DFB power when on a resonance was required in order to initially modelock the laser. The polarisation setting of the main cavity was not critical as there was only one very polarisation dependent element, the filter. It should be possible to remove this dependence by sacrificing the tuning range of the laser by replacing the bulk Fabry-Perot filter used with an in-fibre bandpass Bragg grating which are essentially polarisation independent. The amplified DFB power required to switch the NOLM and give quality modelocking, using the phase-locked loop, was around 40±10 mW, although using manual frequency tuning with the synthesiser this modelocking power could be anywhere in the range 10 – 70 mW, although the pulse widths were 50 % broader at the lowest powers.

The autocorrelation trace for a modelocked pulse train is shown along with the associated spectrum in figure 6.17. The measured pulse width from the autocorrelation trace was 9.9 ps at a spectral width of 3.0±0.5 nm, giving a time-bandwidth product of 0.37±0.6. Whilst this time-bandwidth figure is a little larger than the required soliton transform limited (TL) time-bandwidth product of 0.314, these pulses are sufficiently close to be considered solitons if the device limited error in the spectral width is taken into account. Thus this laser gave short, essentially time-bandwidth limited pulses at 1 GHz.

An important consideration when modelocking this laser using the DFB was whether the DFB jitter would play a significant role in the laser characteristics. The DFB used was measured to have a pulse-to-pulse timing jitter of around 8 ps,

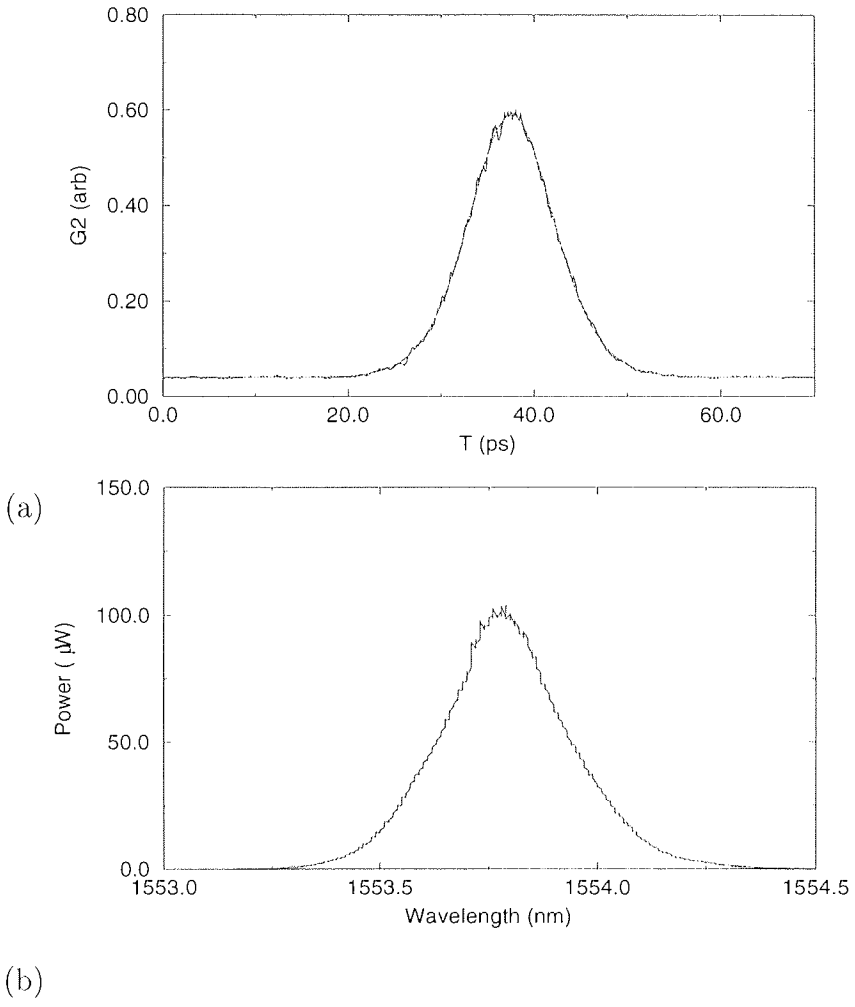

Figure 6.17: Modelocked figure eight laser output (a) 9.9 ps pulse width autocorrelation trace and (b) 0.3 nm spectrum.

far higher than desirable as outlined for the previous laser (section 6.3). However, measuring the jitter of the ring laser showed that it only had a timing jitter of around 2 ps, a factor of 4 improvement and more importantly a more reasonable value for soliton propagation experiments. It is expected that this 2 ps jitter could be further reduced if the DFB jitter was controlled by external feedback as before (section 6.3) should this be necessary.

The above experiments were performed at the maximum pump power available to the EDFA from the Titanium:Saffire pump laser used. In order to check the soliton nature of the laser cavity the intra-cavity power was reduced, by reducing the pump power, and the output pulse width measured. The results of this experiment are shown in figure 6.18 along with theoretical curves of the pulse width – output power relationship expected if soliton shaping were taking place in the 100 m standard fibre of the NOLM only or for the 38 m remainder of the cavity only, ignoring any power variation effects due to the EDFA. We see that as the power was reduced, the pulse width decreased as expected, within the bounds of the theoretical lines. While at low output powers the pulse width was close to that for soliton shaping in the main cavity, the widths were marginally larger at higher powers, suggesting that at higher powers the NOLM standard fibre was providing some pulse shaping though less so at lower powers. It is worth noting that there may be some degree of self-switching in the NOLM, as it was biased very near to this point with the polarisation controller.

A final point that must be addressed is the stability of this laser configuration. Using a phase-locked loop to modelock the laser isolated it from small changes in the cavity length and hence frequency from temperature changes of the optical fibre are essentially removed. The only remaining stability problem was polarisation drift, mainly a problem for the NOLM. When the laser could be kept isolated from polarisation changes (mainly due to air drafts moving the fibre and thus changing the birefringence) the laser would remain modelocked essentially as long as required, i.e. until disturbed. Times between adjustments of over an hour were typical once the environment around the laser had stabilised. This feature would be significantly improved if the laser could be isolated by removing it from the optical bench and encasing it in a box. The short length of the NOLM con-

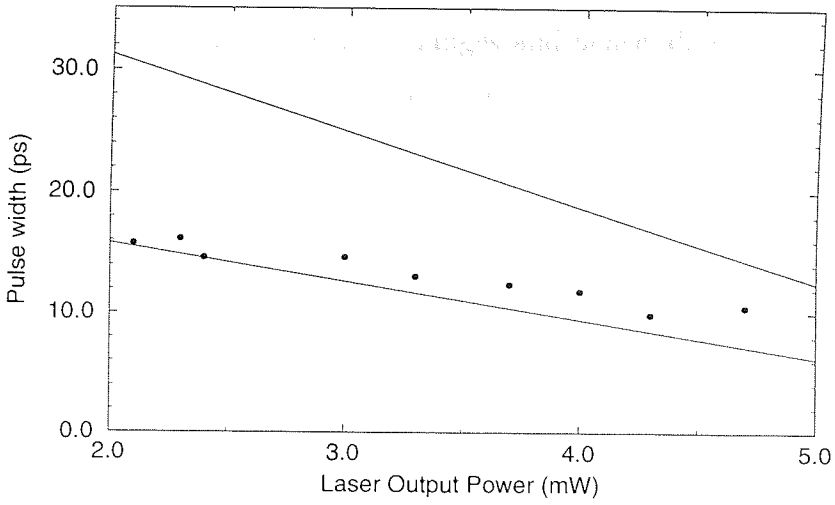

Figure 6.18: Pulse width against laser output power for the figure eight laser. The upper solid line is the theoretical curve fit if only the 100 m SIF of the NOLM provides pulse shaping, the lower solid line for the 38 m remainder of the cavity ignoring the EDFA change in the power.

tributed to the stability of the laser, as even with environmental changes taking place around the laser a reasonable degree of stability was noted. Thus this laser constitutes a good, stable, time-bandwidth limited 10 ps soliton source suitable for propagation experiments.

6.5 Conclusions

Of the three lasers described above, only the last met the strict criteria required of a soliton pulse source at the given repetition rates. However, all three are potentially useful as soliton sources. Whilst the first, phase-modulated ring laser was not able to operate at the required 5 GHz rate, this was due to the characteristic of the phase modulator rather than a fundamental flaw with the laser configuration, as shown by its operation at other modelocking frequencies. It also did not meet the time-bandwidth requirement, but this was due to the laser not being fully optimised in terms of the additional standard fibre length. With a different phase modulator and the correct fibre length, this laser should produce suitable pulses. Regarding size and stability issues, this laser was built within a reasonable sized box, barring the control electronics, and thus was not excessive in size. The use of a box helped

provide insulation from environmental changes and hence allowed several hours of stable operation. A similar laser has been used in soliton transmission experiments [151].

The gain switched DFB laser obviously has a size advantage over the other two. However, in order to achieve the short pulses it was built for the additional amplifiers, fibres, SLA and associated control electronics may be prohibitive. Additionally, although short, the pulses obtained from the combination of devices were not time-bandwidth limited which may lead to unwanted shedding of dispersive wave radiation as the pulse forms to a soliton on propagation. However, the laser itself showed no significant variation due to the environment and if a polarisation insensitive SLA were used this setup should be sufficiently stable.

The final laser, the NOLM modulated ring laser did produce high quality pulses at the required repetition rate. The use of the phase-locked loop allowed modelocking to be maintained despite cavity length changes. While this could also be employed with the phase-modulated ring laser, it is always at the expense of the repetition rate. Any shift in the repetition rate is undesirable for data communications as this leads to a discrepancy in the data rate between sections of the overall communications network. In practice clock recovery, the essence of the phase-locked loop, is required at each network node so this may not be so significant, but any potential problem is undesirable. Complete temperature and draft isolation should reduce this problem to a minimum, should such lasers ever be used. Alternatively, active cavity length control has been shown to allow maintainance of the required repetition rate by either stretching or temperature controlling a section of the fibre ring [196]. Although this laser was not boxed, it did show a high tolerance to environmental changes, which can probably be attributed to the relatively short fibre length within the NOLM.

Thus, all three lasers have their potential uses in soliton communications and are certainly suitable for experimental soliton propagation work. Although at this developmental stage they all still have problems, optimisation could reduce or remove these.

Chapter 7

The recirculating loop

7.1 Introduction

This chapter describes the recirculating loop and its use in modelling the transmission of optical signals over long distances and multiple amplifier spans. Here we only consider an all optical recirculating loop with an erbium-doped amplifier, although the conception of the recirculating loop was in electronically regenerated transmission. In essence both systems are identical bar the difference in the signal amplifier used. The electronic regenerator has the advantage of re-timing and reshaping of the signal, whilst the EDFA is data rate and pulse shape transparent, within limits discussed below. Recirculating loops are useful as a transmission modelling tool as they require only one or a few amplifiers to achieve long distance transmissions, with the distance being instantly reconfigurable, as opposed to straight line transmission experiments where the length is fixed and the full number of amplifiers is required [8, 11, 13, 18, 19, 21, 60, 88, 129, 136, 197]–[202].

The recirculating loop has been used with an EDFA as a transmission model in a variety of experiments and configurations for both RZ [67, 78, 86, 87, 89, 110, 111, 151, 203]–[210] and NRZ [16, 64, 211, 212] transmissions. However it must be kept in mind that the recirculating loop *is* only a model for signal transmission. While a loop experiment may indicate that propagation is possible in a system to some given distance, in practice the in-line achievable distance may be significantly different. This is due to the fact that the recirculating loop configuration assumes that each span of a transmission system is identical and the components of each

span are likewise identical, which is unrealistic due to component tolerances. In addition, certain effects can be enhanced or masked through the use of the recirculating loop, such as polarisation dependencies, which can give very different results in straight-line experiments. These problems are reduced slightly with recirculating loops of a few amplifier spans but do remain. Currently the world's leading recirculating loop researchers are lengthening their loops to such an extent that these problems are essential eliminated, although these systems are fast approaching full length straight line experiments [206]. Certainly they are beginning to exceed the distances required for land based communications of up to around 500 km per exchange node in Europe.

Whilst very long recirculating loops are more useful in testing optical transmissions which are close to system implementation, there remains a use for the fewer amplifier span recirculating loops for proof of principle experiments. With a new transmission line component the first stage of testing is generally done with a single device: if the component is required in each amplifier span a single span recirculating loop is the simplest way to test its effect on long distance transmission. To this end we have built a single amplifier span recirculating loop for such proof of principle experiments. A particular application of this loop in testing a novel long distance signal transmission format is discussed below after a more detailed introduction to the recirculating loop in question.

7.2 The recirculating loop transmission model

The basic configuration for the recirculating loop used in the experiment below is shown in figure 7.1. The control electronics driving the loop have been omitted for clarity but will be included in the discussions. Whilst this diagram includes details of the input and output optics of the loop, the heart of the loop is clearly seen at the top. Essentially all that is required in a recirculating loop is an input/output port (the 50:50 coupler), an amplifier (EDFA #1) and a section of transmission fibre. However, in order to operate the loop two other components are usually included, namely a polarisation controller (PC #1) and a band pass filter.

The polarisation controller is necessary as the recirculating loop will generally have a preferred polarisation state due to the polarisation dependent loss

(PDL) of the components, plus birefringent effects such as PMD can also have a significant effect in propagation experiments. The filter is included to suppress the build-up of amplifier spontaneous emission (ASE) noise which will accumulate as the signal recirculates. This noise generally leads to the recirculating loop lasing at the 1532 nm erbium gain peak, reducing the gain available for the signal if working at a different wavelength. Generally we wish to work at the flatter part of the erbium gain spectrum around 1550 nm as this wavelength is more suitable for wavelength division multiplexing (WDM) transmission. Very short pulse widths would also be limited by spectral filtering of the signal by the relatively narrow spectral width of the 1532 nm gain peak. As the bandwidth of this peak is only around 8 nm the minimum pulse width that could theoretically be propagated at 1532 nm would be 300 fs, in practise such a short pulse would lose so much energy from low gain in the spectral wings that only around the central 2 nm would be supported giving a minimum pulse width around 1 ps or greater. While this is not a significant problem for the 10 ps pulses we shall be using, as the drive to even greater data rates pushes the maximum pulse width down it will become an issue.

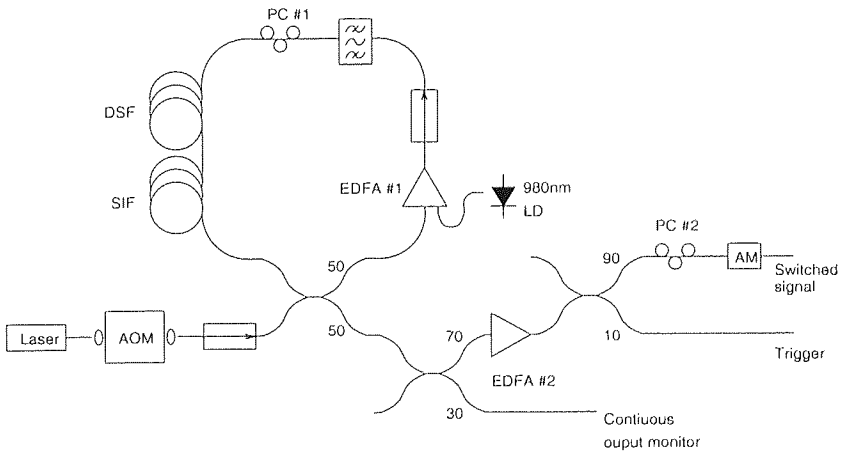

Figure 7.1: The recirculating loop. AOM: bulk acousto-optic modulator; SIF: step index standard fibre; DSF: dispersion shifted fibre; AM: output lithium niobate amplitude modulator; PC: polarisation controller; EDFA #1/#2: erbium-doped fibre amplifiers; 980 nm LD: pump laser diode for EDFA #1.

To operate the recirculating loop, the amplifier must be carefully tailored to provided sufficient gain to compensate for the various losses of the loop components. Too little gain will lead to signal degradation as the power drops. It cannot give

excessive gain however as the loop is generally operated at a round trip gain of unity, otherwise the signal power and hence the pulse energy would increase with each recirculation. It is also vitally important that this gain be given at the appropriate signal output power to support the soliton pulses. With a soliton system if the output power is too high or low this will lead to pulse narrowing or broadening as the solitons settle to the width supported by the amplifier power. To this end, the amplifier must work in saturation, such that if the signal level rises a lower gain will be experienced and a low power signal will experience extra gain bringing the power level back to that required. The characteristics of the amplifier used are shown in figure 7.2 for the 1538 nm wavelength used in the experiment below. Here we required a round trip gain for the loop of $\sim$12 dB and an amplifier output power of around 1 milliwatt (0 dBm), ie. an input power of around 6 μW (-12 dBm). As shown in figure 7.2 this output power was achieved around 5 dB into saturation, with a little too much gain. Fine adjustment of the gain and output power could be made be varying the amplifier pump power. This amplifier was diode pumped, to allow the amplifier to be turned off for a short period to kill the signal in the loop between tests which could be done by turning off the pump diode.

The transmission fibre used was a combination of two sections, one of dispersion shifted fibre (DSF), the other of standard or step index fibre (SIF). This combination was required as the 23.7 km of dispersion shifted fibre had a dispersion zero wavelength of $\lambda_0 = 1556$ nm, in the middle of the region where we wished to operate. For solitons to be supported a small but finite dispersion is required. By adding 2.7 km of standard fibre the net dispersion zero wavelength was reduced to $\lambda_0 = 1537$ nm, giving a dispersion of $\sim$ 1 ps/nm/km at 1550 nm. The measured dispersion of the combination of fibres is given in figure 7.3.

The other components necessary to operate the recirculating loop were the input and output optics and the control electronics. At the input some method of switching signal from the source laser into the recirculating loop must be provided. This signal injection must be of the appropriate length to just fill the loop. This function was performed by the acousto-optic modulator. At the output two different methods of looking at the signal are generally required, continuous and switched. In order to optimise the loop performance a continuous monitor was

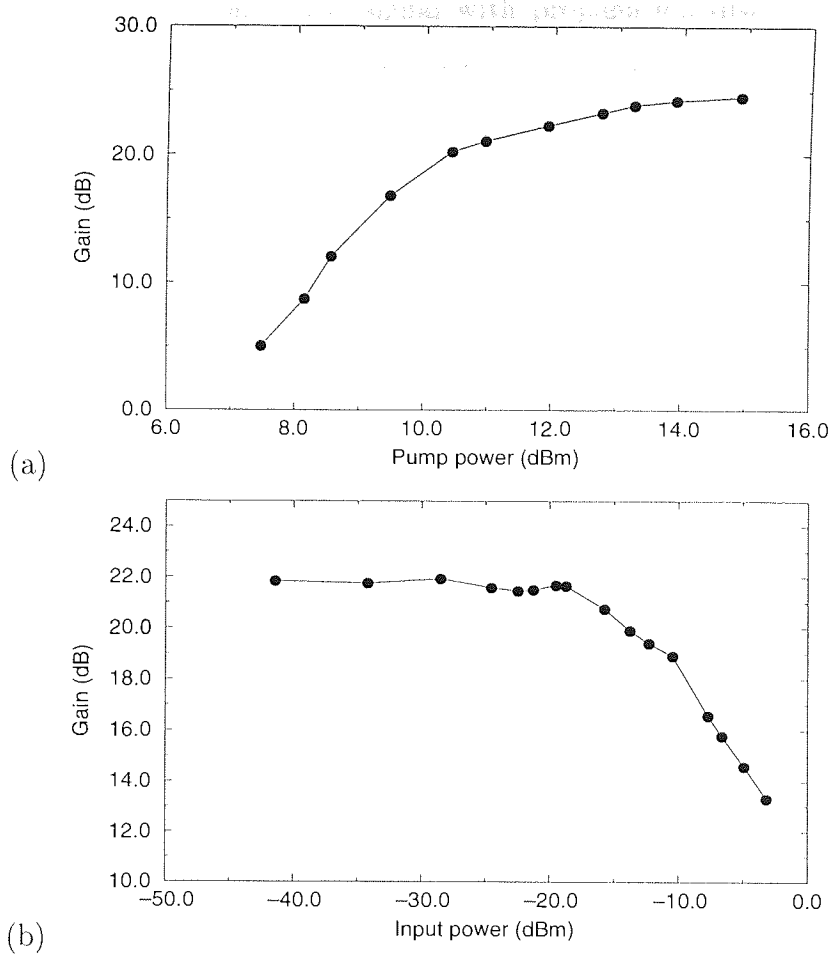

Figure 7.2: Amplifier characteristics for the EDFA, with 8 m of erbium fibre, in the recirculating loop at 1538 nm. (a) Small signal gain for 0.1 μW input power, (b) gain saturation at 16 mW pump power.

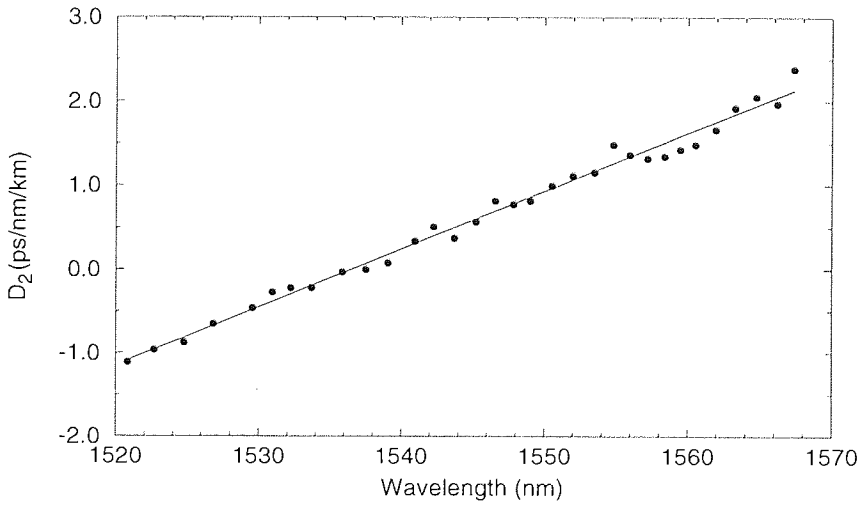

Figure 7.3: Net dispersion of the recirculating loop with the combination of 23.7 km DSF and 2.7 km SIF.

used to study the evolution of the signal with propagation distance. However, if jitter measurements and so forth are to be made after some given distance a switched output is required to gate the signal after it has propagated the appropriate distance. Both methods were possible simultaneously by splitting the output signal through a fused fibre coupler. The continuous output came directly from this coupler. For the switched output a modulator was used, here a lithium-niobate amplitude modulator, although a second acousto-optic switch would give a better extinction ratio. As these modulators generally have fairly high loss (typically 5 – 15 dB) and the output signal powers were low an EDFA precedes the modulator. A second coupler was also used to provide a trigger at the repetition rate for an electronic sampling oscilloscope. Overriding control of the recirculating loop resides with electronic delay generators. These provided electronic control pulses to the various recirculating loop electronic components at the appropriate times for gating in the signal, turning the amplifier off and so forth.

Operation of the loop was as follows. With the recirculating loop amplifier initially on, the delay generators provided a switching pulse to the acousto-optic modulator. This allowed a burst of pulses from the source laser into the recirculating loop, just filling the loop before the acoustic-optic modulator closed. This burst of pulses was then allowed to recirculate to the required distance. As the input-output coupler was a passive device signal leakage occurred during this recirculation period. This leakage could be continuously monitored, allowing fine adjustment of the loop filter, polarisation controller and amplifier gain to optimise performance. After the required propagation distance the output amplitude modulator was opened, again for a period equal to the loop length to gate out a single recirculation for measurement. At this point the delay generators switched off the diode pump for the recirculating loop amplifier, allowing the signal power to decay over a few recirculations. Once the signal was no longer present, the amplifier was turned on again to allow the amplifier to reach inversion before the acousto-optic modulator was once more opened to restart the process.

7.3 RZ pulse transmission utilising nonlinear polarisation rotation

This section presents an experimental investigation of the propagation of 10 ps pulses near the net fibre dispersion zero wavelength for very long distances. Ordinarily, propagation at such a wavelength without some form of control will lead to pulse break-up from effects such as self-phase modulation and four-wave mixing as discussed in chapter 2. Although still nonlinear pulse transmission, the pulse propagation studied here is not what is traditionally called soliton propagation within the context of the average soliton model, as shall be outlined below. Solitons at such low net dispersion as used here have a very low pulse energy, which results in data degradation due to the ASE noise build-up as there is insufficient signal-to-noise ratio. They would however gain the advantage that low dispersion results in low Gordon-Haus timing jitter, even over very long distances [53].

In order to maintain the pulses for any useful distance at low dispersions, a pulse shape control mechanism must be employed to restore the pulse before it becomes too perturbed. Here we study experimentally the use of a fast saturable absorber as this control mechanism. Such control has been studied theoretically for solitons, using such saturable absorbers as quantum well saturable absorbers and the nonlinear optical loop mirror [189, 213]. In these experiments the saturable absorber mechanism used was obtained through the use of nonlinear polarisation rotation (NPR) with a polarisation discriminating element (see section 2.7). Through this mechanism the build-up of ASE noise was essentially eliminated and the pulse shape was maintained for far greater distance than expected at this wavelength and dispersion.

There were two key elements of the recirculating loop for this experiment. The first was the transmission fibre which, through its birefringence, provided the nonlinear polarisation rotation. The second was the 3 nm bandpass Fabry-Perot filter (see figure 7.1). Whereas normally the optical filter provides only the role of wavelength discrimination, here it also provided a second function, that of the polarisation discriminating element. The filter was found to have a reasonably high polarisation dependent loss of 1.5 – 3 dB, depending on wavelength,

which was sufficient to provide the polarisation discrimination required to remove the ASE noise and maintain the pulse shapes. Thus the filter provide temporal discrimination as well as spectral discrimination.

The pulse train source used here was from an F-centre laser operating at 76 MHz, providing ~10 ps time-bandwidth limited $sech^2$ pulses. Initially the loop was nearly filled, with a 2 μs gap left unfilled at the end of the burst of signal in order to provide a method of optimising the polarisation and wavelength of the recirculating signal by minimising the ASE noise floor. This is possible due to the relatively long lifetime ($\sim 10ms$) of the erbium decay from the excited state. As the inversion and hence the ASE output level is only changed by variations in the signal level over time scales on the order of milliseconds, the noise level remains constant through the 2 μs gap in the signal. This allows the noise level to be minimised on the continuous output monitor of the recirculating loop. Through careful adjustment it was found that, after an initial increase in the ASE level over the first several recirculations, the level could be made to reduce and saturate at effectively zero. The initial increase in the ASE was due to the pulse train stabilising to the correct polarisation and wavelength for sufficient polarisation rotation. Figure 7.4(a) shows this initial build-up and saturation over a propagation distance of 8,000 km, as compared with a typical ASE build-up over 10,000 km in figure 7.4(b) for solitons at a higher dispersion and without nonlinear polarisation rotation for noise suppression.

Once the ASE suppression had been optimised, the loop control electronics could be disabled, after injection of a pulse train, such that the amplifier remained on and no new signal was injected giving continuous propagation for times in excess of those possible using the delay generators. Through this it was found that the ASE suppression and signal propagation could be maintained virtually indefinitely, to effectively produce an RZ pulse "storage ring" [103, 105]. Although slightly broadened from 9.5 ps to 11 ps (FWHM), the pulses remained a good approximation to the input $sech^2$ profile as shown in figure 7.5. These pulses could be maintained in shape and power for over half an hour, this only being limited by environmental changes affecting the polarisation setting and hence removing the complete NPR discrimination required to maintain propagation.

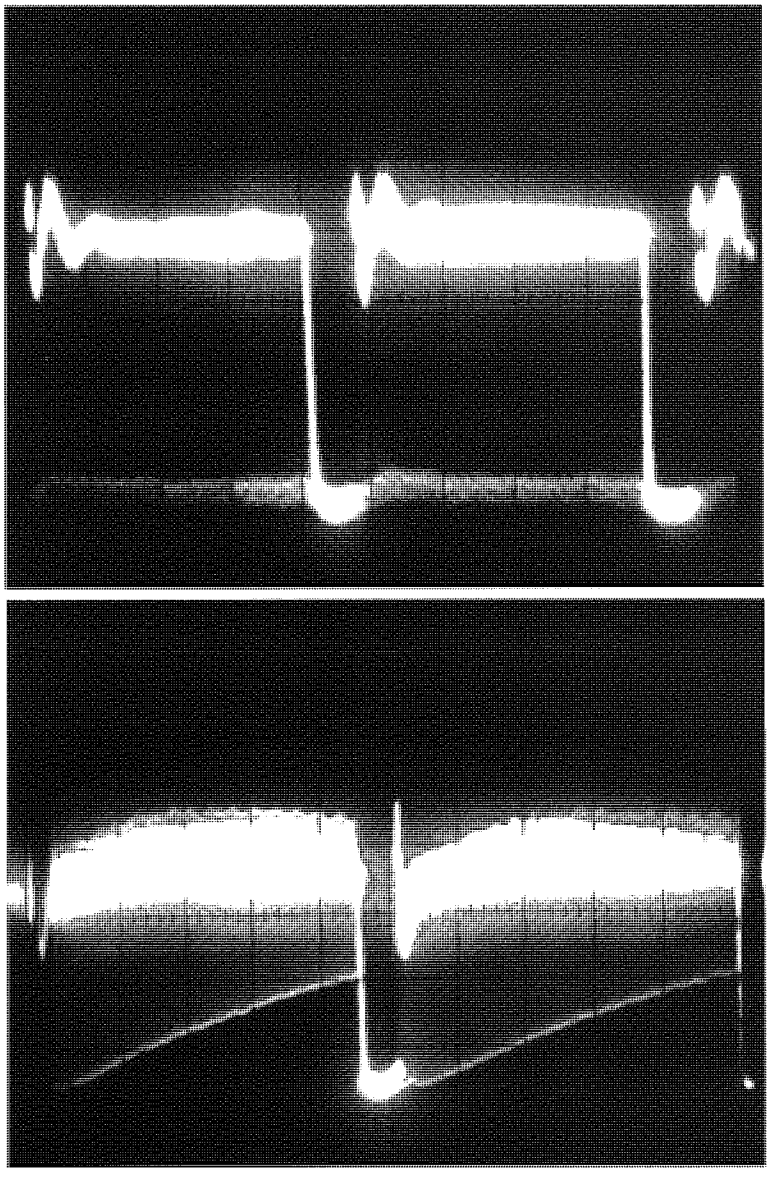

Figure 7.4: Photograph of the ASE floor (lower lines) and the signal (upper lines) for (a) ASE suppression using NPR over 8,000 km and (b) ASE build-up in a 1551 nm soliton transmission to 10,000 km with $D_2 = 1ps/nm/km$ and a low PDL pair of fibre Bragg gratings giving a 6 nm bandpass filter, other parameters as for the NPR setup.

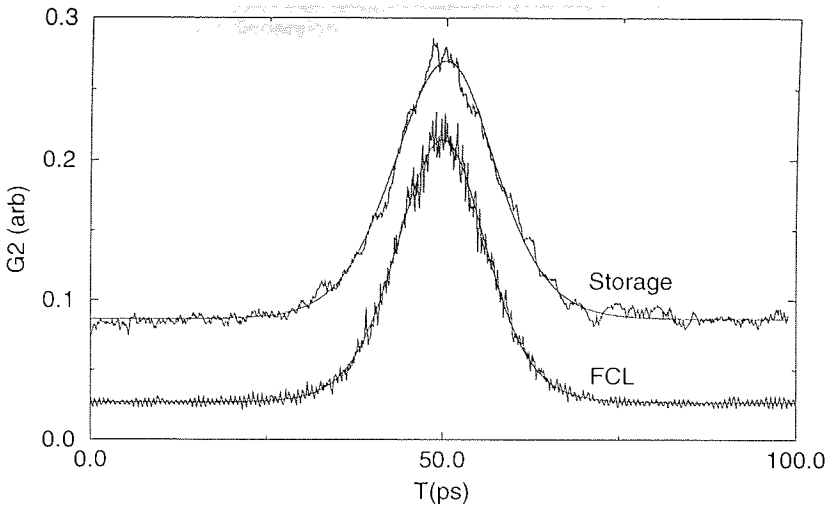

Figure 7.5: Autocorrelation traces of input 9.5 ps and "stored" 11.0 ps pulses, with $sech^2$ curve fits. A y-axis offset has been added to enable comparison.

Figure 7.6 shows the the various spectra of (a) the input FCL pulses, (b) the recirculating loop superfluorescense (amplifier on but with no signal injected) and (c) the loop output when running as a storage ring. Also shown is the appropriate section of the curve fit to the net dispersion curve taken from figure 7.3. The input pulses which were injected at 1537.3 nm spectrally broadened until reaching the stable spectra shown for the storage ring. The two peaks in this spectra (c) correspond to those of the loop superfluorescense (b), and are a result of the polarisation dependence of the filter with wavelength. These stored pulses are heavily chirped, as can be seen by comparing the spectral width with that of the input pulses which are time-bandwidth limited and of similar pulse width. This spectral width was measured as 1.3 nm, giving the time-bandwidth product of $\sim$ 1.8, six times that of fundamental solitons.

The average power level within the loop was also far in excess of that expected for fundamental solitons. The average signal power at the end of the transmission fibre, before the output coupler, was estimated from the power output of the continuous monitor port as 71 μW. Taking the dispersion for the pulse at the centre wavelength to be 0.1 ps/nm/km, the corresponding fundamental average soliton power is only 0.65 μW. Thus, this cannot be purely average soliton propagation, as N$\approx$10 solitons will tend to break up after only a short transmission due to the onset of self-Raman shift [4]. These comparatively high optical powers lead,

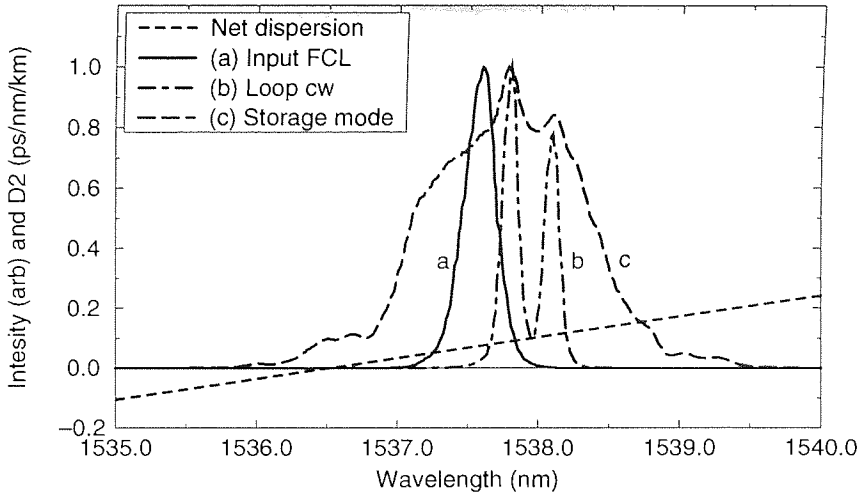

Figure 7.6: Spectra of (a) the input FCL pulses, (b) the recirculating loop superfluorescense and (c) the "stored" pulses (linear scale normalised to the peak intensity of each spectra), along with the measured loop dispersion.

through self phase modulation, to the large spectral broadening shown. We note that there is a slight shift in the central peak of the spectrum, due to the signal stabilising to the wavelength required for the optimum NPR.

Operating in this regime but over measured distances using the delay generators once more, the observed timing jitter did not appear to increase significantly over global distances as shown in figure 7.7, for up to 70 Mm. Indeed, even after 7 seconds (~1450 Mm), the measured standard deviation of the timing jitter σ was only 8 ps. Due to the low repetition rate, the accumulated jitter over the 1000 km following the required propagation distance was measured to reduce the acquisition time. While this meant we were essentially averaging the jitter measurement over the following 1000 km, the low and consistent jitter over such long distances means the errors in this approach were minimal. There was a slight, ~0.5 ps increase in the initial jitter noted before it stabilised (not shown on this scale), which again corresponds to the signal settling to the wavelength for NPR, with individual pulses shifting wavelength at slightly different rates due to amplifier noise in the manner of Gordon-Haus jitter. As the trigger for these jitter measurements was taken optically from a neighbouring pulse and thus also jittered, these values are actually an overestimate by a factor of $\sqrt{2}$. For longer signal wavelengths (higher dispersion) the jitter increased significantly with propagation distance as expected

for solitons.

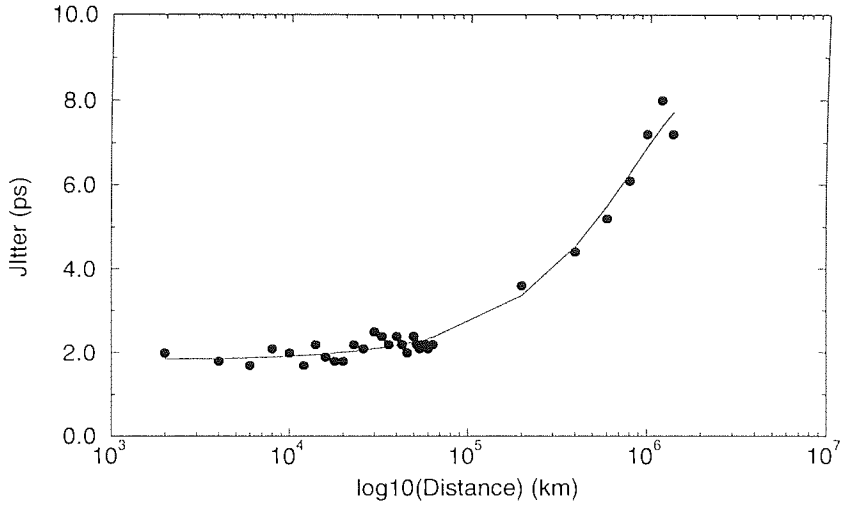

Figure 7.7: Standard deviation σ of timing jitter averaged over 1000km against distance for 2 – 1450 Mm. Note the distance scale is logarithmic.

When operating as a storage ring, the amplifier pump power could be lowered to remove some pulses from the stored train, effectively imposing data on the stored signal [105]. It was noted that these remaining pulses would be supported at these or higher pump powers indicating that data storage is possible with such a setup. However, it must be noted that unlike ref. [105], there was no active temporal control of the pulses and hence the timing jitter build up observed due to the low but finite dispersion will limit the maximum storage time possible.

While the repetition rate for these experiments was far lower than the 10 Gbit/s envisaged for the next generation of high speed communications, the pulse widths used, 10 ps, are suitable for this or higher data rates. This assumes that similar pulse interaction problems as for solitons will exist giving the 1:6 – 1:10 mark-to-space ratio requirement discussed in chapter 2, which may be a rash assumption for these chirped RZ pulses. Also, although no data was imposed on the input signal, in order for the saturable absorber to maintain the pulse shape it must necessarily be fast on the time scale of the pulse width. Hence the saturable absorber will retain no knowledge of previous pulses and thus will not be a source of cross-talk when used with data, a frequent concern when potential propagation method feasibility is shown with continuous pulse streams rather than data streams. This mechanism may well lead therefore to far higher data rate transmission in a

regime of operation forbidden to solitons.

7.4 Conclusions

This chapter has presented the role of the recirculating loop as an experimental transmission model for long distance propagation. The nature, components and operation of such a recirculating loop have been outlined along with some of the loop design considerations. Although the loop considered here is only a single amplifier span design, this is still a useful tool in early experimentation of novel transmission techniques and for initial testing of new transmission line components.

Using the recirculating loop we have demonstrated a novel nonlinear RZ pulse propagation mode with the use of nonlinear polarisation rotation as a saturable absorber mechanism. This permitted operation near the net zero dispersion wavelength, over one amplifier spacing, of the recirculating loop. Stable propagation of ~10 ps pulses over 10's Mm was observed with no significant increase in timing jitter. While NPR may be unattractive for use in long distance transmission systems, other saturable absorbers such as multi-quantum-wells [213] and nonlinear optical loop mirrors [189] should offer a similar propagation regime. Use of a saturable absorber will also allow the use of a narrower filter bandwidth, thereby reducing Gordon-Haus jitter in systems with a higher dispersion. Still shorter pulses may be supported using similar techniques, opening the way to transmission of data rates in excess of 10 Gbit/s.

Finally we note however that NPR may be compatible with wavelength division multiplexed transmissions. If the fibre birefringence and polariser used are wavelength independent, the polarisation rotation and discrimination at each wavelength would be equal. Even if two pulses of different wavelength arrived at the polariser together both would be reshaped. This would not be true for the other two device mentioned above as potential saturable absorbers, the NOLM or the quantum well saturable absorber, as they are threshold dependent thus two pulses arriving together would affect the switching characteristic to resulting in a detrimental effect on the pulses.

Chapter 8

Conclusions

8.1 Thesis conclusions

This thesis has investigated both theoretically and experimentally various possible improvements to the propagation of nonlinear pulses in optical communication systems. The theoretical work concentrated on short system lengths and possible ways to alleviate the problems caused by the average soliton prescription and soliton interactions, whilst the experimental work looked the sources required for optical communications and a novel nonlinear pulse propagation format for long distance systems.

We have shown two methods of improving the fibre profile for soliton propagation. We developed a method of tailoring the fibre profile using steps of readily available dispersion shifted fibres to more closely match the decay in the nonlinearity with a similar decay in the dispersion to improved the GVD–SPM balance and hence improve the soliton propagation. The reduction to the perturbations in the temporal and spectral characteristics showed that this method of fibre tailoring improved the soliton transmission. Pulses which would break up in a system of the same average dispersion and amplifier spacing could be maintained with very little distortion over more than 1000 km if four-fold profiling was employed, allowing soliton propagation in a normally forbidden parameter region.

Our second fibre dispersion profile improvement was involved in improving the transmission of solitons over existing standard fibre. We showed that soliton propagation could be maintained for around 200 km in an existing system if the

regenerators were replaced with EDFAs, and that phase modulation or alternating amplitude transmission formats would not aid propagation in such a highly perturbed systems. However, in order to take this system to longer lengths it was shown that introducing some dispersion compensating fibre just before each EDFA improved the pulse transmission and hence achievable distance. Further improvement in the transmission distance was possible by increasing the input power above that of the average soliton prescription. This unexpected result may be connected with the highly perturbative nature of the fibre profile, through the mixture of anomalous and normal dispersion fibres meaning that the pulse is not experiencing soliton shaping during the latter part of the transmission span, only the first, leading to the propagation of chirped soliton-like pulses. Using this method pulse propagation was possible to over 2000 km of the original system. It was shown that this compensating fibre has to be in the purely dispersive part of the power cycle of the pulse suggesting that the pulses must experience excess nonlinearity during the soliton shaping anomalous fibre to balance out the excess dispersion and lack of GVD–SPM balance through the normal dispersion fibre.

The final piece of theoretical work again returned to improving the propagation of an average soliton in short systems, that of improving the launch condition for solitons in highly perturbed systems. A theoretical model was developed showing that by including a further order of the perturbations in the operator analysis an improved launch position within the energy cycle would reduce the initial perturbations the soliton experienced. This improved launch position, attained by adding a section of fibre prior to the first amplifier in a highly perturbed system, translates into improving the pulse shape coupled into the system by chirping the input perfect $sech^2(t)$ input solitons used through the additional fibre section to that of the stable propagation mode of the system. It was shown that this method reduced the initial excursions of the pulse width and time-bandwidth product. The soliton perturbations and the quantity of dispersive wave radiation shed were hence reduced, leading to improved soliton propagation over the first several amplifiers of the system.

The experimental work concentrated on two main, soliton sources and transmission. The developmental work on soliton sources for transmission systems stud-

ied three different configurations. Two fibre ring lasers were developed to produce reasonably short but more importantly time-bandwidth limited solitons for gigahertz operation. The advantage of this structure is that the main pulse shaping mechanism is soliton shaping in anomalous dispersion fibre thus more likely to produce high quality solitons. The first ring laser used a phase modulator to initially shape the pulses by applying a chirp to the c.w. signal then maintained the pulse position by chirping temporally jittered with the appropriate sign to restore them to the bit centre. Although this laser could not meet the 5GHz operation desired due to a modulator feature, it would produce slightly chirped solitons at other repetition rates. This chirp should be removable with optimisation of the additional fibre length added to the cavity. The second ring laser employed active amplitude modulation to perform pulse shaping and modelocking. Using a NOLM switched with jittered, wide pulses from a DFB laser by cross-phase modulation, short near time-bandwidth limited pulses were obtained. The NOLM fibre length was relatively short, leading to reasonable laser stability, which was further improved through the use of a phase-locked loop to keep the laser locked to a cavity mode.

The final source considered was of a different configuration with the use of the DFB laser for very short pulses useful for very high data rates. The large jitter and long pulse widths of the DFB output were improved by feeding back a proportion of the output signal, with the appropriate phase, to seed the gain-switching of the DFB and essentially modelock the pulses. The resulting pulses were heavily chirped, which was used to reduce the pulse width still further by dispersive compression. In order to attain very short pulses, an SLA was used to spectrally broaden these pulses, which could then be compressed through further fibre to produce 3.5 ps pulses. While these pulses were not time bandwidth limited, they would probably experience soliton shaping if propagated at the appropriate power through further anomalous fibre although some dispersive wave radiation would be shed. Such short pulses could be multiplexed for operation at data rates of up to 30 GHz.

The second part of the experimental work looked at the use of a recirculating loop as a transmission model for long fibre optic communication systems. The

construction and operation of the loop was outlined and a novel propagation regime was investigated. This propagation regime relied on the nonlinear polarisation rotation possible in slightly birefringent fibres to rotate the polarisation of the high power part of a pulse to align with the polarisation discriminating element, here an optical band-pass filter, allowing it to propagate, whilst the low power wings of the pulse and ASE noise did not rotate sufficiently and were attenuated. This allowed the pulse shape to be maintained for more than global distances. It was possible to operate in this regime very near the fibre dispersion zero, nearly eliminating the problem of Gordon-Haus jitter.

The powers required to support these pulse transmissions were far in excess of those for solitons at this dispersion. Here we consider the correlation with the improvements found by increasing the power in the dispersion compensated standard fibre system, where optimum transmission was also found for pulses well above the average soliton power. In the polarisation rotation experiment, as in the improvement to the standard fibre propagation, the fibre used was not a simple section of dispersion shifted fibre but a combination of two fibres, one anomalous, one normal dispersion. Although the fibres were reversed in order of the dispersion sign and had lower dispersion parameters for the NPR experiment, we again found that there was a stable RZ pulse propagation regime in these low average dispersion fibres. In neither case are the pulses solitons in the classic, average soliton sense but stable propagation was possible.

Although we have considered some diverse methods, this thesis has presented a variety of techniques through which the propagation of solitons, or chirped RZ pulses, may be improved. Further work will undoubtedly be required before solitons are accepted sufficiently by the industrial world to be implemented. We have presented results here that may make this possibility more likely.

8.2 The future of optical communications?

It is my belief that with the level of soliton work currently being undertaken worldwide that eventually a soliton system will be installed. This belief was lent further weight recently when field trials were undertaken in Japan at 10 and 20 Gbit/s over 2000 km of an existing fibre system [202, 214]. These successful trials indicate

that solitons are rapidly approaching acceptance by the international telecommunications corporations. This is hardly surprising given the advantages of solitons in very high data rate systems, with their switching and routing capabilities allowing possible all optical networking, their compatibility with wavelength division multiplexing, as well as their negation of dispersive, nonlinear and polarisation effects.

Whilst this thesis has concentrated exclusively on single wavelength channel propagation, wavelength division multiplexed (WDM) systems do present a strong challenge to the soliton advances we propose. In particular, WDM has been used recently to propagate twenty 5 Gbit/s channels over transoceanic distances [215]. However, WDM is generally developed for increasing the data rate once the single channel rate has been maximised. Although an important technique its main drawback is that each channel requires its own transmitter and receiver, adding cost and complexity. By maximising the single channel data rate before considering WDM the number of components required for a given WDM aggregate data rate can be reduced.

Despite this, it is possible that solitons may not reach the wide usage many others now anticipate, as there appears to be another stable propagation regime for chirped RZ pulses in low dispersion fibre-managed systems. The results obtained in chapters 4 and 7 show that pulses of higher powers can be successfully propagated in systems where the instantaneous fibre dispersion is of a reasonable level but the net average dispersion is low from a combination of anomalous and normal dispersions. A similar effect has also been presented elsewhere [216]. Although further theoretical work is required in this area, initial indications are that there is another stable solution of the NLSE when the fibre dispersion is varied for pulses of higher power than that of the average soliton. It is possible that this regime will supersede the use of solitons if it can be shown to have all the advantages of solitons without certain of the drawbacks such as Gordon-Haus jitter.

Thus although approaching commercial viability and acceptance, nonlinear pulse propagation in optical fibre communication systems is still an exciting and developing field. Work looks set to continue in this area for a considerable time to come, within a widening scientific community. I am looking forward with anticipa-

tion to the future results in this field and the installation of the first commercially operated soliton communication system.

Bibliography

[1] J. Thiennot, F. Pirio, and J-B. Thomine. Optical undersea cable system trends. *Proceedings of the IEEE*, 11(1610-1623), 1981.

[2] T. Li. The impact of optical amplifiers on long distance lightwave telecommunications. *Proceedings of the IEEE*, 81(11):1568–1579, 1993.

[3] M. J. O'Mahony. Non-linear optical transmission systems. *European Transactions on Telecommunications and Related Technologies*, 4(6):629–640, 1993.

[4] G. P. Agrawal. *Nonlinear fibre optics.* Academic Press Inc., 1989.

[5] H. Izadpanah, C. Lin, J. L. Gimlett, A. J. Antos, D. W. Hall, and D. K. Smith. Dispersion compensation in 1310 nm–optimised SMFs using optical equaliser fibre, EFDAs and 1310/1550 nm WDM. *Electron. Lett.*, 28(15):1469–1471, 1992.

[6] H. Izadpanah, E. Goldstein, and C. Lin. Broadband multiwavelength simultaneous dispersion compensation near 1550 nm through singlemode fibres optimised for 1310 nm. *Electron. Lett.*, 29(4):364–365, 1993.

[7] M. S. Chaudhry, S. S. Sian, K. Guild, P. R. Morkel, and C. D. Stark. Unrepeatered transmission at 2.5 Gbit/s over 410 km with a single remote amplifier and dispersion compensation. *Electron. Lett.*, 20(24):2061–2063, 1994.

[8] C. D. Chen, J.-M. P. Delavaux, B. W. Hakki, O. Mizuhara, T. V. Nguyen, R. J. Nuyts, K. Ogawa, Y. K. Park, R. E. Tench, L. D. Tzeng, and P. D. Yeates. Field experiment of 10 Gbit/s, 360 km transmission through embedded standard non-DSF fibre cables. *Electron. Lett.*, 30(14):1159–1160, 1994.

[9] D. G. Moodie, A. D. Ellis, and C. W. Ford. Generation of 6.3 ps optical pulses at a 10 GHz repetition rate using a packaged electroabsorption modulator and dispersion compensating fibre. *Electron. Lett.*, 30(20):1700–1701, 1994.

[10] M. Onishi, Y. Koyano, M. Shigematsu, H. Kanamori, and M. Nishimura. Dispersion compensating fibre with a high figure of merit. *Electron. Lett.*, 30(2):161–163, 1994.

[11] C. Das, U. Gaubatz, E. Gottwald, K. Kotten, C. J. Weiske, F. Küppers, and A. Mattheus. Straight line 20 Gbit/s transmission over 617 km standard singlemode fibre with dispersion compensation. *Electron. Lett.*, 31(4):305–307, 1995.

[12] M. Kakui, T. Kato, T. Kashiwada, K. Nakazoto, C. Fukuda, M. Onishi, and M. Nishimura. 2.4 Gbit/s repeaterless transmission over 306 km non-dispersion shifted fibre using directly modulated DFB-LD and dispersion-compensating fibre. *Electron. Lett.*, 31(1):51–52, 1995.

[13] K. Sekine, S. Sasaki, and N. Kikuchi. 10 Gbit/s four-channel wavelength- and polarisation-division multiplexing transmission over 340 km with 0.5 nm channel spacing. *Electron. Lett.*, 31(1):49–50, 1995.

[14] S. G. Evangelides, L. F. Mollenauer, J. P. Gordon, and N. S. Bergano. Polarisation multiplexing with solitons. *IEEE J. Lightwave Technol.*, 10:28–35, 1992.

[15] B. Clesca, J.-P. Thiery, L. Pierre, V. Havard, and F. Bruyère. Bit error rate degradation related to differential group delay and input polarisation for 10 Gbit/s terrestrial systems in presence of chromatic dispersion and polarisation mode dispersion. In *Proc. 21 st Eur. Conf. on Opt. Comm. (ECOC '95 - Brussels), paper We.B.1.6*, pages 581–584, 1995.

[16] T. Widdowson and D. J. Malyon. Error ratio measurements over transoceanic distances using recirculating loop. *Electron. Lett.*, 27(24):2201–2202, 1991.

[17] B. Clesca, C. Cœurjolly, D. Bayart, L. Berthelon, L. Hamon, and J. L. Beylat. Experimental demonstration of the feasibility of 40 Gbit/s transmission through standard fibre. *Electron. Lett.*, 30(10):802–803, 1994.

[18] J. A. J. Fells, M. A. Gibbon, I. H. White, G. H. B. Thompson, R. V. Penty, C. J. Armistead, E. M. Kimber, D. J. Moule, and E. J. Thrush. Transmission beyond the dispersion limit using a negative chirp electroabsorption modulator. *Electron. Lett.*, 30(14):1168–1169, 1994.

[19] A. Sano, Y. Minyamoto, T. Kataoka, H. Kawakami, and K. Hagimoto. 10 Gbit/s, 300 km repeaterles transmission with SBS suppression by the use of the RZ format. *Electron. Lett.*, 30(20):1694–1695, 1994.

[20] T. Widdowson, J. P. Hueting, A. D. Ellis, D. J. Malyon, and P. J. Wilkinson. Global fibre transmission using optically amplified regenerators for maximised repeater spacing. *Electron. Lett.*, 30(24):2056–1057, 1994.

[21] S. Yamamoto, H. Takahira, E. Shibano, M. Tanaka, and Y. C. Chen. BER performance improvement by forward error correcting code in 5 Gbit/s 9000 km EDFA transmission system. *Electron. Lett.*, 30(9):718–719, 1994.

[22] T. Morioka, S. Kawanishi, H. Takara, and O. Kamatani. Penalty-free, 100 Gbit/s optical transmission of < 2 ps supercontinuum transform-limited pulses over 40 km. *Electron. Lett.*, 31(2):124–125, 1995.

[23] A. Hasegawa and Y. Kodama. Guiding–center soliton in optical fibers. *Opt. Lett.*, 15(24):1443–1445, 1990.

[24] K. J. Blow and N. J. Doran. Average soliton dynamics and the operation of soliton systems with lumped amplifiers. *IEEE Photon. Technol. Lett.*, 3:369–371, 1991.

[25] A. Hasegawa and Y. Kodama. Guiding-center soliton. *Phys. Rev. Lett.*, 66:161–164, 1991.

[26] L. F. Mollenauer, S. G. Evangelides, and H. A. Haus. Long-distance soliton propagation using lumped amplifiers and dispersion shifted fiber. *IEEE J. Lightwave Technol.*, 9:194–197, 1991.

[27] L. F. Mollenauer, J. P. Gordon, and M. N. Islam. Soliton propagation in long fibers with periodically compensated loss. *IEEE J. Quantum. Electron.*, 22:157–173, 1986.

[28] P. R. Morkel and R. I. Laming. Theoretical modeling of erbium-doped fiber amplifiers with excited state absorption. *Opt. Lett.*, 14(19):1062–1064, 1989.

[29] E. Desurvire, J. L. Zyskind, and C. R. Giles. Design optimization for efficient erbium–doped fiber amplifiers. *IEEE J. Lightwave Technol.*, 8(11):1730–1741, 1990.

[30] N. Kagi, A. Oyobe, and K. Nakamura. Efficient optical amplifier using a low-concentration erbium-doped fiber. *IEEE Photon. Technol. Lett.*, 2(8):599–561, 1990.

[31] B. Pedersen, K. Dybdal, C. D. Hansen, A. Bjarklev, J. H. Povlsen, H. Vendeltorp-Pommer, and C. C. Larsen. Detailed theoretical and experimetal investigation of high-gain erbium-doped fiber amplifier. *IEEE Photon. Technol. Lett.*, 2(12):863–865, 1990.

[32] A. A. M. Saleh, R. M. Jopson, J. D. Evankow, and J. Aspell. Modeling of gain in erbium-doped fiber amplifiers. *IEEE Photon. Technol. Lett.*, 2(10):714–717, 1990.

[33] M. Shimizu, M. Yadama, M. Horiguchi, T. Takeshita, and M. Okauasu. Erbium-doped fibre amplifiers with extremely high gain coefficient of 11.0 dB/mW. *Electron. Lett.*, 26(20):1641–1642, 1990.

[34] B. Pedersen, A. Bjarklev, O. Lumholt, and J. H. Povlsen. Detailed design analysis of erbium-doped fibre amplifiers. *IEEE Photon. Technol. Lett.*, 3(6):548–550, 1991.

[35] B. Pedersen, A. Bjarklev, J. H. Povlsen, K. Dybdal, and C. C. Larsen. The design of erbium-doped fibre amplifiers. *IEEE J. Lightwave Technol.*, 9(9):1105–1112, 1991.

[36] R. I. Laming, M. N. Zervas, and D. N. Payne. Erbium-doped fiber amplifier with a 54 dB gain and 3.1 dB noise figure. *IEEE Photon. Technol. Lett.*, 4(12):1345–1347, 1992.

[37] F. F. Rühl. Implicit analytical solution for erbium doped fibre amplifier. *Electron. Lett.*, 28(5):465–466, 1992.

[38] M. N. Zervas, R. I. Laming, J. E. Townsend, and D. N. Payne. Design and fabrication of high gain-efficiency erbium-doped fiber amplifiers. *IEEE Photon. Technol. Lett.*, 4(12):1342–1344, 1992.

[39] D. A. Chapman. Erbium–doped fibre amplifiers: the lastest revolution in optical communications. *Electronics & communication engineering jornal*, pages 59–67, April 1994.

[40] I. M. I. Habbab, A. A. M. Saleh, and P. K. Runge. Erbium-doped amplifiers: linear approximations. *IEEE J. Lightwave Technol.*, 13(1):33–36, 1995.

[41] G. R. Walker. Gain and noise characterisation of erbium doped fiber amplifiers. *Electron. Lett.*, 27(9):744–745, 1991.

[42] J. Aspell, J. F. Federici, B. M. Nyman, D. L. Wilson, and D. S. Shenk. Accurate noise figure measurements of erbium–doped fiber amplifiers in saturation conditions. In *Technical Digest, OFC'92, ThA4*, pages 189–190, 1992.

[43] H. Bülow and Th. Pfeiffer. Calculation of the noise figure of erbium–doped fiber amplifiers using small signal attenuations and saturation powers. *IEEE Photon. Technol. Lett.*, 4(12):1351–1354, 1992.

[44] I. M. I. Habbab, A. A. M. Saleh, N. J. Frigo, and G. E. Bodeep. Noise reduction in long–haul lightwave all–amplifier systems. *IEEE J. Lightwave Technol.*, 10(9):1281–1289, 1992.

[45] B. Pedersen, J. Chirravuri, and W. J. Miniscalco. Gain and noise penalty for detuning 980 nm pumping of erbium-doped fiber power amplifier. *IEEE Photon. Technol. Lett.*, 4(4):351–353, 1992.

[46] B. Pedersen, J. Chirravuri, and W. J. Miniscalco. Gain and noise properties of small-signal erbium-doped fiber amplifiers pumped in the 980 nm band. *IEEE Photon. Technol. Lett.*, 4(6):556–558, 1992.

[47] R. G. Smart, J. L. Zyskind, J. W. Sulhoff, and D. J. DiGiovanni. An investigation of the noise figure and conversion efficiency of 0.98 μm pumped erbium-doped amplifiers under saturated conditions. *IEEE Photon. Technol. Lett.*, 4(11):1261–1263, 1992.

[48] Y. Sato, Y. Yamabayashi, and K. Aida. Noise figure monitoring of optical amplifiers via backward amplified spontaneous emission. *IEEE Photon. Technol. Lett.*, 6(2):202–204, 1994.

[49] B. Pedersen, A. Bjarklev, and J. H. Povlsen. Design of erbium doped fibre amplifiers for 980 nm or 1480 nm pumping. *Electron. Lett.*, 27(3):255–257, 1991.

[50] E. Desurvire. Analysis of gain difference between forward– and backward–pumped erbium–doped fiber amplifiers in the saturation regime. *IEEE Photon. Technol. Lett.*, 4(7):711–714, 1992.

[51] B. Pedersen, B. A. Thompson, S. Zemon; W. J. Miniscalco, and T. Wei. Power requirments for erbium-doped fiber amplifiers pumped in the 800, 980 and 1480 nm bands. *IEEE Photon. Technol. Lett.*, 4(1):46–49, 1992.

[52] R. G. Smart, J. L. Zyskind, and D. J. DiGiovanni. Experimental comparison of 980 nm and 1480 nm-pumped saturated in-line erbium-doped fibre amplifiers suitable for long-haul soliton transmission systems. *IEEE Photon. Technol. Lett.*, 5(7):770–772, 1993.

[53] J. P. Gordon and H. A. Haus. Random walk of coherently amplified solitons in optical fiber transmission. *Opt. Lett.*, 11:665–667, 1986.

[54] M. A. Ali, A. F. Elrefaie, R. E. Wagner, F. Mendez, J. Pan, and S. A. Ahmed. Optimised performance of erbium-doped fibre amplifiers in multiwavelength lightwave systems. *IEEE Photon. Technol. Lett.*, 6(8):1039–1042, 1994.

[55] C. S. Gardner, J. M. Green, M. D. Kruskal, and R. M. Miura. *Phys. Rev. Lett.*, 19:1095, 1967.

[56] V. E. Zakarov and A. B. Shabat. *Sov. Phys. JETP*, 34:62, 1972.

[57] C. Desem and P. L. Chu. Effect of chirping on solution propagation in single-mode fibres. *Opt. Lett.*, 11(4):248–251, 1986.

[58] D. Anderson, M. Lisak, and T. Relchel. Asymptotic propagation properties of pulses in a soliton-based optical fibre communication system. *J. Optical Society of America, B*, 5(2):207–210, 1988.

[59] K. J. Blow, N. J. Doran, and D. Wood. Generation and stabalisation of short soliton pulses in the amplifies nonlinear Schrödringer equation. *J. Optical Society of America, B*, 5(2):381–391, 1988.

[60] S. V. Chernikov, J. R. Taylor, and R. Kashap. Experimental demonstration of step-like dispersion profiling in optical fibre for soliton pulse generation and compression. *Electron. Lett.*, 30(5):433–435, 1994.

[61] H. Kubota and M. Nakazawa. Long-distance optical soliton transmission with lumped amplifiers. *IEEE J. Quantum Electron.*, 26:692–700, 1990.

[62] N. J. Smith, K. J. Blow, and I. Andonovic. Sideband generation through perturbations to the average soliton model. *IEEE J. Lightwave Technol.*, 10:1329–1333, 1992.

[63] H. Bülow. Operation of digital optical transmission system with minimal degradation due to polariation mode dispersion. *Electron. Lett.*, 31(3):214–215, 1995.

[64] D. J. Malyon, T. Widdowson, and A. Lord. Assessment of the polarisation loss dependence of transoceanic systems using a recirculating loop. *Electron. Lett.*, 29(2):207–209, 1993.

[65] F. Bruyère and O. Audouin. Penalties in long-haul optical amplifier systems due to polarisation dependent loss and gain. *IEEE Photon. Technol. Lett.*, 6(5):654–656, 1994.

[66] V. J. Mazurczyk and J. L. Zyskind. Polarisation dependent gain in erbium doped fibre amplifiers. *IEEE Photon. Technol. Lett.*, 6(5):616–618, 1994.

[67] T. Widdowson, A. Lord, and D. J. Malyon. Polaristion guiding in ultralong distance soliton transmission. *Electron. Lett.*, 30(11):879–880, 1994.

[68] R. P. Davey, N. Langford, and A. I. Ferguson. Role of polarisation rotation in an Er fibre laser. *Electron. Lett.*, 29(9):758–780, 1993.

[69] E. J. Greer, Y. Kimura, K. Suzuki, E. Yoshida, and M. Nakazawa. Generation of a 1.2 ps, 10 GHz pulse train from all-optically modelocked, erbium fibre ring laser with active nonlinear polarisation rotation. *Electron. Lett.*, 30(21):1764–1765, 1994.

[70] L. F. Mollenauer, K. Smith, J. P. Gordon, and C. R. Menyuk. Resistance of solitons to the effects of polarisation dispersion in optical fibres. *Opt. Lett.*, 14(21):1218–1221, 1989.

[71] L. F. Mollenauer and J. P. Gordon. Birefringence-mediated timing jitter in soliton transmission. *Opt. Lett.*, 19(6):375–377, 1994.

[72] A. F. Mitchell, J. V. Wright, S. F. Carter, A. D. Ellis, A. Lord, J. Lyle, and J. M. Scott. The future of optically amplified submarine systems. In *Techn. Digest of 2-nd Intern. Conf. on Optical Fibre Submarine Telecommun. Systems, Versailles, France*, pages 49–54, 1993.

[73] J. P. Gordon. Interaction forces among solitons in optical fibres. *Opt. Lett.*, 8(11):596–598, 1983.

[74] Y. Kodama and K. Nozaki. Soliton interaction in optical fibres. *Opt. Lett.*, 12(12):1038–140, 1987.

[75] F. M. Mitschke and L. F. Mollenauer. Experimental observation of interaction forces between solitons in optical fibres. *Opt. Lett.*, 12(5):355–357, 1987.

[76] R. P. Davey, N. Langford, and A. I. Ferguson. Interacting solitons in erbium fibre laser. *Electron. Lett.*, 27(14):1257–1259, 1991.

[77] T. Georges and F. Favre. Influence of soliton interaction on amplifier noise–induced jitter: a first–order analytical solution. *Opt. Lett.*, 16(21):1656–1658, 1991.

[78] M. Nakazawa, K. Suzuki, E. Yadama, and H. Kubota. Observation of nonlinear interactions in 20 Gbit/s soliton transmission over 500 km using erbium-doped fibre amplifiers. *Electron. Lett.*, 27(18):1662–1663, 1991.

[79] A. B. Aceves, C. De Angelis, G. Nalesso, and M. Santagiustina. Higher-order effects in bandwidth-limited soliton propagation in optical fibres. *Opt. Lett.*, 19(24):2104–2106, 1994.

[80] W. H. Loh, A. B. Grudinin, V. V. Afansjev, and D. N. Payne. Soliton interaction in the presence of a weak nonsoliton component. *Opt. Lett.*, 19(10):698–700, 1994.

[81] Y. Kodama and S. Wabnitz. Reduction of soliton interaction forces by bandwidth limited amplification. *Electron. Lett.*, 27(21):1931–1932, 1991.

[82] T. Georges and F. Favre. Modulation, filtering and initial phase control of interacting solitons. *J. Optical Society of America, B*, 10(10):1880–1889, 1993.

[83] P.-L. François and T. Georges. Reduction of averaged soliton interaction forces by amplitude modulation. *Opt. Lett.*, 18(8):583–585, 1993.

[84] C. Desem and P. L. Chu. *Optical solitons - theory and experiment*, chapter Soliton-soliton interactions, pages 107–151. Press Syndicate of the University of Cambridge, 1992.

[85] A. Mattheus and S. Turisyn. Pulse interaction in nonlinear communication systems based on standard monomode fibres. In *Proceedings of 19th European conferenceon optical communications, Volume 2, paper MoC2.3*, pages 37–40, 1993.

[86] M. Suzuki, N. Edagawa, H. Taga, H. Tanaka, S. Yamamoto, and S. Akiba. 10 Gb/s, over 12200 km soliton data transmission with alternating-amplitude solitons. *IEEE Photon. Technol. Lett.*, 6(6):7557–7559, 1994.

[87] K. Suzuki, N. Edagawa, H. Taga, M. Takaya, S. Yamamoto, and S. Akiba. Feasibility demonstration of 20 Gbit/s single channel soliton transmission over 11500 km using alternating-amplitude solitons. *Electron. Lett.*, 30(13):1083–1084, 1994.

[88] M. Nakazawa, E. Yoshida, E. Yadama, K. Suzuki, T. Kitoh, and M. Kawachi. 80 Gbit/s soliton data transmission over 500 km with unequal amplitude solitons for timing clock extraction. *Electron. Lett.*, 30(21):1777–1778, 1994.

[89] P. A. Andrekson, N. A. Olsson, J. R. Simpson, T. Tanbun-Ek, A. Logan, and K. W. Wecht. Observation of collision induced termporary soliton carrier frequency shifts in ultra-long fiber transmission systems. *IEEE J. Lightwave Technol.*, 9(9):1132–1135, 1991.

[90] A. Mecozzi and A. Haus, H. Effect of filters on soliton interactions in wavelength-division-multiplexing systems. *Opt. Lett.*, 17(14):988–990, 1992.

[91] S. Chakravarty, M. J. Ablowitz, J. R. Sauer, and R. B. Jenkins. Multisoliton interactions and wavelength-division multiplexing. *Opt. Lett.*, 20(2):136–138, 1995.

[92] D. Marcuse. An alternative derivation of the Gordon-Haus effect. *IEEE J. Lightwave Technol.*, 10:273–278, 1992.

[93] A. Hasegawa and Y. Kodama. *Solitons in optical communications*. Clarendon Press, Oxford, 1995.

[94] A. Mecozzi, J. D. Moores, H. A. Haus, and Y. Lai. Soliton transmission control. *Opt. Lett.*, 16:1841–1843, 1991.

[95] Y. Kodama and A. Hasegawa. Generation of asymptotically stable optical solitons and suppression of the Gordon-Haus effect. *Opt. Lett.*, 17(1):31–33, 1992.

[96] D. Marcuse. Siulations to demonstrate the reduction of the Gordon-Haus effect. *Opt. Lett.*, 17:34–36, 1992.

[97] W. Forysiak, K. J. Blow, and N. J. Doran. Reduction of Gordon-Haus jitter by post-transmission dispersion compensation. *Electron. Lett.*, 29:1225–1226, 1993.

[98] H. Kubota and M. Nakasawa. Soliton transmission control in time and frequency domains. *IEEE J. Quantum Electron.*, 29(7):2189–2197, 1993.

[99] Y. Kodama and S. Wabnitz. Analysis of soliton stability and interactions with sliding filters. *Opt. Lett.*, 19(3):162–164, 1994.

[100] Y. Kodama, M. Romagnoli, and S. Wabnitz. Stabalisation of optical solitons by an acousto-optic modulator and filter. *Electron. Lett.*, 30(3):261–262, 1994.

[101] N. J. Smith, N. J. Doran, K. J. Blow, and W. J. Firth. Gordon-Haus jitter suppression using a single phase modulator. *Electron. Lett.*, 30(12):987–988, 1994.

[102] N. J. Smith, W. J. Firth, K. J. Blow, and K. Smith. Suppression of soliton interactions by periodic phase modulation. *Opt. Lett.*, 19(1):16–18, 1994.

[103] H. A. Haus and A. Mecozzi. Long–term storage of a bit stream of solitons. *Opt. Lett.*, 17(21):1500–1502, 1992.

[104] S. Wabnitz. Suppression of interactions in a phase-locked soliton optical memory. *Opt. Lett.*, 18(8):601–603, 1993.

[105] C. R. Doerr, W. S. Wong, H. A. Haus, and E. P. Ippen. Additive-pulse mode-locking/limiting storage ring. *Opt. Lett.*, 19(21):1747–1749, 1994.

[106] F. X. Kärtner and U. Keller. Stabilisation of soliton-like pulses with a slow saturable absorber. *Opt. Lett.*, 20(1):16–18, 1995.

[107] L. F. Mollenauer, J. P. Gordon, and S. G. Evangelides. The sliding frequency guiding filter: an improved form of soliton jitter control. *Opt. Lett.*, 17:1575–1577, 1992.

[108] P. V. Mamyshev and L. F. Mollenauer. Stability of soliton propagation with sliding-frequency guiding filters. *Opt. Lett.*, 19(24):2083–2085, 1994.

[109] L. F. Mollenauer, P. V. Mamyshev, and M. J. Neubelt. Measurement of timing jitter in filter-guided soliton transmission at 10 Gbit/s and achievement of 375 Gbit/s-Mm, error free, at 12.5 and 15 Gbit/s. *Opt. Lett.*, 19(10):704–706, 1994.

[110] G. Aubin, T. Montalant, J. Moulu, B. Nortier, F. Pirio, and J.-B. Thomine. Demonstration of soliton tranmission at 10 Gbit/s up to 27 Mm using 'signal frequency sliding' technique. *Electron. Lett.*, 31(1):52–54, 1995.

[111] D. LeGuen, F. Farve, R. Boittin, J. Debeau, F. Devaux, M. Henry, C. Thebault, and T. Georges. Demonstration fo sliding-filter-controlled soliton transmission at 20 Gbit/s over 14 Mm. *Electron. Lett.*, 31(4):301–302, 1995.

[112] E. M. Dianov, A. V. Luchinkov, A. N. Pilipetskii, and A. N. Starodumov. Electrostriction mechanism of soliton interaction in optical fibres. *Opt. Lett.*, 15(6):314–316, 1990.

[113] E. M. Dianov, A. V. Luchnikov, A. N. Pilipetski, and A. M. Prokhorov. Long-range interaction of solitnos in ultra-long communication systems. *Sov. Lightwve Commun.*, 1:235–246, 1991.

[114] E. M. Dianov, A. V. Luchnikov, A. N. Pilipetski, and A. M. Prokhorov. Long-range interaction of picosecond solitons through exitation of acoustic waves in optical fibres. *Appl. Phys.*, B 54:175–180, 1992.

[115] E. A. Golovchenko and A. N. Pilipetskii. Acoustic effect and the polarisation of adjacent bits in soliton communication lines. *IEEE J. Lightwave Technol.*, 12(6):1052–1055, 1994.

[116] K. Smith and L. F. Mollenauer. Experimental observation of soliton interaction over long fibre paths: discovery of a long-range interaction. *Opt. Lett.*, 14(22):1284–1286, 1989.

[117] K. Rottwitt, A. Bjarklev, J. H. Povlsen, , O. Lumholt, and T. P. Rasmussen. Fundamental design of a distributed erbium-doped fiber amplifier for long-distance transmission. *IEEE J. Lightwave Technol.*, 10(11):1544–1552, 1992.

[118] K. Rottwitt, J. H. Povlsen, S. Gundersen, and A. Bjarklev. Stability in distributed and lumped gain transmission systems. *Opt. Lett.*, 18:867–869, 1993.

[119] K. Tajima. Compensation of soliton broadening in nonlinear optical fibres with loss. *Opt. Lett.*, 12:54–56, 1987.

[120] H. H. Kuehl. Solitons in an axially nonuniform optical fiber. *J. Opt. Soc. Am.*, B5:709–713, 1988.

[121] P. V. Mamyshev, S. V. Chernikov, and E. M. Dianov. Generation of fundamental soliton trains for high-bit-rate optical fiber communication lines. *IEEE J. Quantum Electron.*, 27(10):2347–2355, 1991.

[122] Q. Ren and H. Hsu. Solitons in dispersion-compensated fiber with loss. *IEEE J. Quantum. Electron.*, 24:2059–2062, 1988.

[123] J. P. Gordon and L. F. Mollenauer. Effects of fiber nonlinearities and amplifier spacing on ultra-long distance transmission. *IEEE J. Lightwave Technol.*, 9(2):170–173, 1991.

[124] S. M. J. Kelly, K. Smith, K. Blow, and N. J. Doran. Average soliton dynamics of a high–gain erbium fiber laser. *Opt. Lett.*, 16(17):1337–1339, 1991.

[125] E. Hummel, P. P. G. Mols, and P. I. Kuindersma. Self phase modulation and dispersion in amplified 10 Gbit/s optical transmission systems in the 1550 nm window. In *Proceedings of European "Cost Workshop 94" Optical Telecommunications, Nice, April 17 - 21*, pages 5–56, 1994.

[126] C. Lin, H. Kogelnik, and L. G. Cohen. Optical–pulse equalisation of low–dispersion transmission in single–mode fibers in the 1.3–1.7 -μm spectral region. *Opt. Lett.*, 5(11):476–478, 1980.

[127] J. M. Dugan, A. J. Price, M. Ramadan, D. L. Wolf, E. F. Murphy, A. J. Antos, D. K. Smith, and D. W. Hall. All–optical fibre–based 1550 nm dispersion compensation in a 10 Gbit/s, 150 km transmission experiment over 1310 nm optimised fibre. In *Dig. OFC'92, Postdeadline Paper PD14*, San Jose, CA, 1992.

[128] A. J. Antos, D. W. Hall, and D. K. Smith. Dispersion-compensating fibre for upgrading existing 1310-nm optimised systems fo 1550-nm operation. In *OFC/IOOC '93 Technical Digest, ThJ3*, pages 204–205, 1993.

[129] A. D. Ellis and D. M. Spirit. Unrepeatered transmission over 80 km standard fibre at 40 Gbit/s. *Electron. Lett.*, 30(1):72–74, 1994.

[130] K. Oda, M. Fukutoku, M. Fukui, T. Kitoh, and H. Toba. 16-channel $\times$ 10 Gbit/s optical FWM transmission ofer a 100 km convertional single-mode fibre employing dispersion-compensating fibre and gain equalisation. In *OFC '95 postdeadline papers, paper PD22*, 1995.

[131] R. A. Fisher, B. R. Suydam, and D. Yevick. Optical phase conjugation for time–domain undoing of dispersive self–phase–modulation effects. *Opt. Lett.*, 8(12):611–613, 1983.

[132] S. Watanabe, T. Naito, and T. Chikama. Compensation of chromatic dispersion in a single-mode fiber by optical phase conjugation. *IEEE Photon. Technol. Lett.*, 5:92–95, 1993.

[133] W. Forysiak and N. J. Doran. Conjugate solitions in amplified optical fibre transmission systems. *Electron. Lett.*, 30(2):154–155, 1994.

[134] S. Wen and S. Chi. Undoing of soliton interaction by optical phase conjugation. *Electron. Lett.*, 30(8):663–663, 1994.

[135] T. Saito, N. Henmi, S. Fujita, M. Yamaguchi, and M. Shikada. Prechirp technique for dispersion compensation for a high–speed long–span transmission. *IEEE Photon. Technol. Lett.*, 3(1):74–79, 1991.

[136] A. D. Ellis, S. J. Pycock, D. A. Cleland, and C. H. F. Sturrock. Dispersion compensation in 450 km transmission system employing standard fibre. *Electron. Lett.*, 29(10):954–955, 1992.

[137] X. Gu, S. J. Pycock, D. M. Spirit, A. D. Ellis, and C. J. Anderson. 10 Gbit/s, 138 km uncompensated duobinary transmission over installed standard fibre. *Electron. Lett.*, 30(23):1953–1954, 1994.

[138] G. May, A. Solheim, and J. Conradi. Extended 10 Gbit/s fibre transmission distance at 1538 nm using a duobinary receiver. *IEEE Photon. Technol. Lett.*, 6(5):648–650, 1994.

[139] P. A. Andrekson, N. A. Olsson, J. R. Simpson, T. Tanbun-Ek, A. Logan, and M. Haner. 16 Gbit/s all–optical demultiplexing using four–wave mixing. *Electron. Lett.*, 27(11):922–924, 1991.

[140] D. M. Patrick and A. D. Ellis. Demultiplexing using cross-phase modulation-induced spectral shifts and Kerr polarisation rotation in optical fibre. *Electron. Lett.*, 29(2):227–228, 1993.

[141] D. M. Patrick, A. D. Ellis, and D. M. Spirit. Bit-rate flexible all-optical demultiplexing using a nonlinear optical loop mirror. *Electron. Lett.*, 29(8):702–703, 1993.

[142] A. D. Ellis, K. Smith, and D. M. Patrick. All optical clock recovery at bit rates up to 40 Gbit/s. *Electron. Lett.*, 29(15):1323–1324, 1993.

[143] N. A. Olsson. Lightwave systems with optical amplifiers. *IEEE J. Lightwave Technol.*, 7(7):1071–1082, July 1989.

[144] D. Marcuse. Calculation of bit-error probability for a lightwave system with optical amplifiers and post-detection Gaussian noise. *IEEE J. Lightwave Technol.*, 9(4):505–513, 1991.

[145] C. J. Anderson and J. A. Lyle. Technique for evaluating system performance using Q in numerical simulations exhibiting intersymbol interference. *Electron. Lett.*, 30(1):71–72, 1994.

[146] N. Akhmediev and A. Ankiewicz. Generation of a train of solitons with arbitrary phase difference between neighbouring solitons. *Opt. Lett.*, 19(8):545–547, 1994.

[147] F. Ouellette. All–fibre filter for efficient dispersion compensation. *Opt. Lett.*, 16(5):303–305, 1991.

[148] J. A. R. Williams, I. Bennion, K. Sugden, and N. J. Doran. Fibre dispersion compensation using a chirped in-fibre Bragg grating. *Electron. Lett.*, 30(12):985–987, 1994.

[149] M. Nakazawa, K. Suzuki, E. Yamada, H. Kubota, Y. Kimora, and M. Takaya. Experimental demonstration of soliton data transmission over unlimited distances with soliton control in time and frequency domains. *Electron. Lett.*, 29:729–730, 1993.

[150] L. F. Mollenauer, E. Lichtman, M. J. Neubelt, and J. T. Harvey. Demonstration, using sliding-frequency guiding filters of error-free soliton transmission over more than 20Mm at 10 Gbit/s, single channel, and over more than 13Mm at 20 Gbit/s in a two channel WDM. *Electron. Lett.*, 29:910–911, 1993.

[151] T. Widdowson, D. J. Malyon, X. Shan, and P. J. Watkinson. Soliton propagation without transmission control using a phase-locked erbium fibre ring laser. *Electron. Lett.*, 30(8):661–663, 1994.

[152] S. M. J. Kelly. Characteristic sideband instability of periodically amplified average soliton. *Electron. Lett.*, 28:806–807, 1992.

[153] J. P. Gordon. Dispersive perturbations of solitons of the nonlinear Schrödinger equation. *J. Optical Society of America, B*, B9:91–97, 1992.

[154] J. N. Elgin and S. M. J. Kelly. Spectral modulation and the growth of resonant modes associated with periodically amplified solitons. *Opt. Lett.*, 18:787–789, 1993.

[155] R. Heidemann, B. Wedding, and G. Veith. 10GB/s transmission and beyond. *Proc. IEEE*, 81:1518–1567, 1993.

[156] F. If, P. Berg, P. L. Christiansen, and O. Skovgaard. Split-step spectral method for nonlinear Schrödinger equation with absorbing boundary conditions. *J. Comput. Phys.*, 72:501–503, 1987.

[157] J. A. Fleck Jr., J. R. Morris, and M. D. Feit. Time-dependent propagation of high energy laser beams through the atmosphere. *Appl. Phys.*, 10:129–160, 1976.

[158] K. Smith, J. R. Armitage, R. Wyatt, N. J. Doran, and S. M. J. Kelly. Erbium fibre soliton laser. *Electron. Lett.*, 26(15):1149–1151, 1990.

[159] R. P. Davey, N. Langford, and A. I. Ferguson. Subpicosecond pulse generation from erbium doped fibre laser. *Electron. Lett.*, 27(9):726–728, 1991.

[160] M. E. Fermann, M. J. Andrejco, Y. Silberberg, and A. M. Weiner. Generation of pulses shorter than 200 fs from a passively mode-locked Er fiber laser. *Opt. Lett.*, 18(1):48–50, 1993.

[161] M. E. Fermann, K. Sugden, and I. Bennion. High-power soliton fibre laser based on pulse width control with chirped fibre Bragg gratings. *Opt. Lett.*, 20(2):172–174, 1995.

[162] J. D. Kafka, T. Baer, and D. W. Hall. Mode-locking erbium-doped fibre laser with soliton shaping. *Opt. Lett.*, 14(22):1269–1291, 1989.

[163] J. B. Schlager, Y. Yamabayashi, D. L. Franzen, and R. I. Juneau. Mode-locked, long-cavity, erbium fiber lasers with subsequent soliton-like compression. *IEEE Photon. Technol. Lett.*, 1(9):264–266, 1989.

[164] A. Takada and H. Miyazawa. 30 GHz picosecond pulse generation from actively mode-locked erbium-doped fibre laser. *Electron. Lett.*, 26(3):216–2217, 1990.

[165] K. Smith, E. J. Greer, R. Wyatt, P. Wheatley, N. J. Doran, and M. Lawrence. Totally integrated erbium fibre soliton laser pumped by laser doide. *Electron. Lett.*, 27(3):244–246, 1991.

[166] C-J. Chen, P. K. A. Wai, and C. R. Menyuk. Soliton fiber ring laser. *Opt. Lett.*, 17(6):417–419, 1992.

[167] R. P. Davey, K. Smith, and A. McGuire. High–speed, mode–locked, tunable, integrated erbium fibre laser. *Electron. Lett.*, 28(5):482–483, 1992.

[168] E. J. Greer and K. Smith. All–optical FM mode–locking of fibre laser. *Electron. Lett.*, 28(18):1741–1742, 1992.

[169] G. T. Harvey and L. F. Mollenauer. Harmonically mode–locked fiber ring laser with an internal Fabry–Perot stabaliser for soliton transmission. *Opt. Lett.*, 18(2):107–109, 1993.

[170] C. R. Doerr, H. A. Haus, and E. P. Ippen. Asynchronous soliton mode locking. *Opt. Lett.*, 19(23):1958–1960, 1994.

[171] M. Romagnoli, S. Wabnitz, P. Franco, M. Midrio, F. Fontana, and G. E. Town. Tunable erbium-ytterbium fibre sliding-frequency soliton laser. *J. Optical Society of America, B*, 12(1):72–76, 1995.

[172] A. D. Ellis and D. M. Patrick. All laser doide compression of 5 GHz picosecond pulses using cross–phase modulation in optical fibre. *Electron. Lett.*, 29(2):149–150, 1993.

[173] S. V. Chernikov, J. R. Taylor, and R. Kashyap. Comblike dispersion-profiled fibre for soliton pulse train generation. *Opt. Lett.*, 19(8):539–541, 1994.

[174] D. M. Patrick and A. E. Ellis. 10 GHz pulse train derived from a CW DFB laser using cross-phase modulation in an optical fibre. *Electron. Lett.*, 29(15):1391–1392, 1993.

[175] N. M. Froberg, G. Raybon, U. Koren, B. I. Miller, M. G. Young, M. Chien, G. T. Harvey, A. Gnauck, and A. M. Johnson. Generation of 12.5 Gbit/s soliton data stream with an integrated laser-modulator transmitter. *Electron. Lett.*, 30(22):1880–1881, 1994.

[176] N.J. Smith, K.J. Blow, W.J. Firth, and K. Smith. Soliton dynamics in the presence of phase modulators. *Optics Communications*, 102:324–328, 1993.

[177] M. J. O'Mahony. Semiconductor laser optical amplifiers for use in future fibre systems. *IEEE J. Lightwave Technol.*, 6:531–544, 1988.

[178] A. E. Siegman. *Lasers*, chapter 10. University Science, Mill Valley, CA, 1986.

[179] I. W. Mashall and D. M. Spirit. Observation of large pulse compression by a saturated travelling wave semiconductor laser amplifier. In *Conf. Dig, CLEO '88*, Washington, DC., 1988. Opt. Soc. Amer.

[180] G. P. Agrawal and N. A. Olsson. Self-phase modulation and spectral broadening of optical pulses in semiconductor laser amplifiers. *IEEE J. Quantum Electron.*, 25(11):2297–2306, 1989.

[181] C. H. Henry. Theory of the linewidth of semiconductor lasers. *IEEE J. Quantum Electron.*, 18:259–264, 1982.

[182] M. Osinski and J. Buus. Linewidth broadening factor in semiconductor lasers - an overview. *IEEE J. Quantum Electron.*, 23:9–29, 1987.

[183] N. J. Doran and D. Wood. Nonlinear-optical loop mirror. *Opt. Lett.*, 13(1):56–58, 1988.

[184] D.B. Mortimore. Fibre loop reflectors. *IEEE J. Lightwave Technol.*, 6:1217–1224, 1988.

[185] K. J. Blow, N. J. Doran, B. K. Nayar, and B. P. Nelson. Two-wavelength operation of the nonlinear fiber loop mirror. *Opt. Lett.*, 15(4):248–250, 1990.

[186] M. Matsumoto, H. Ikeda, and A. Hasegawa. Suppression of noise accumulation in bandwidth-limited soliton transmission by means of nonlinear loop mirrors. *Opt. Lett.*, 19(3):183–185, 1994.

[187] B. Olsson and P. A. Andrekson. Noise filtering with the nonlinear optical loop mirror. *IEEE J. Lightwave Technol.*, 13(2):213–215, 1995.

[188] L. Chusseau and E. Delevaque. 250-fs optical pulse generation by simultaneous soliton compression and shaping in a nonlinear optical loop mirror including a weak attenuation. *Opt. Lett.*, 19(10):734–736, 1994.

[189] N. J. Smith and N. J. Doran. Picosecond soliton propagation using nonlinear optical loop mirrors as intensity filters. *Electron. Lett.*, 30(13):1084–1085, 1994.

[190] B. P. Nelson, K. Smith, and K. J. Blow. Mode-locked erbium fibre laser using all-optical nonlinear loop modulator. *Electron. Lett.*, 28(7):656–657, 1992.

[191] E. Yamada, K. Suzuki, and M. Nawazaka. Subpicosecond optical demultiplexing at 10 GHz with zero-dispersion, dispersion-flattened, nonlinear fibre loop mirror controlled by 500 fs gain-switched laser diode. *Electron. Lett.*, 30(23):1966–1968, 1994.

[192] M. Jinno and M. Abe. All-optical regenerator based on nonlinear fibre Sagnac interferometer. *Electron. Lett.*, 28(14):1350–1352, 1992.

[193] M. Jinno. All optical signal regularizing/regeneration using a nonlinear fibre sagnac interferometer switch with signal-clock walk-off. *IEEE J. Lightwave Technol.*, 12(9):1648–1659, 1994.

[194] K. A. Rauschenback, K. L. Hall, J. C. Livas, and G. Raybon. All-optical pulse width and wavelength conversion at 10 Gb/s using a nonlinear optical loop mirror. *IEEE Photon. Technol. Lett.*, 6(9):1130–1132, 1994.

[195] S. Bigo, E. Desurvire, and B. Desruelle. All-optical RZ–to–NRZ format conversion at 10 Gbit/s with nonlinear optical loop mirror. *Electron. Lett.*, 30(22):1868–1869, 1994.

[196] X. Shan, D. Cleland, and A. Ellis. Stabilising Er fibre soliton laser with pulse phase locking. *Electron. Lett.*, 28(2):182–183, 1992.

[197] D. A. Cleland, X. Y. Gu, J. D. Cox, and A. D. Ellis. Limitations of WDM transmission over 560 km due to degenerate four wave mixing. *Electron. Lett.*, 28(3):307–308, 1992.

[198] A. D. Ellis, T. Widdowson, X. Shan, G. E. Wickens, and D. M. Spirit. Transmission of a true single polarisation 40 Gbit/s soliton data stream over 205 km using a stabilised erbium fibre ring laser and 40 GHz electronic timing recovery. *Electron. Lett.*, 29(11):990–991, 1993.

[199] M. Nakazawa, K. Suzuki, H. Kubota, E. Yadama, and Y. Kimura. Straight-line soliton data transmission at 20 Gbit/s beyond Gordon-Haus limit. *Electron. Lett.*, 30(16):1331–1332, 1994.

[200] A. D. Ellis, T. Widdowson, X. Shan, and D. G. Moodie. Three-node, 40 Gbit/s OTDM network experiment using electro-optic switches. *Electron. Lett.*, 30(16):1333–1334, 1994.

[201] F. Heismann, D. A. Gray, B. H. Lee, and R. W. Smith. Electrooptic polarisation scramblers for optically amplified long-haul transmission systems. *IEEE Photon. Technol. Lett.*, 6(9):1156–1158, 1994.

[202] M. Nakazawa, Y. Kimura, K. Suzuki, H. Kubota, T. Komukai, E. Yamada, T. Sugawa, E. Yoshida, T. Yamamoto, T. Imai, A. Sahara, H. Nakazawa, O. Yamauchi, and M. Umezawa. Field demonstration of soliton transmission at 10 Gbit/s ver 2000 km in Tokyo metropoliton loop network. *Electron. Lett.*, 31(12):992–993, 1995.

[203] L. F. Mollenauer, M. J. Neubelt, S. G. Evangelides, J. P. Gordon, J. R. Simpson, and L. G. Cohen. Experimental study of soliton transmission over more than 10,000 km in dispersion–shifted fiber. *Opt. Lett.*, 15(21):1203–1205, 1990.

[204] H. Taga, M. Suzuki, N. Edagawa, H. Tanaka, Y. Yoshida, S. Yamamoto, S. Akiba, and Wakabayashi. Multi-thousand kilometer optical soliton data transmission experiments at 5 Gb/s using an electroabsorption modulator pulse generator. *IEEE J. Lightwave Technol.*, 12(2):231–235, 1994.

[205] L. F. Mollenauer, B. M. Nyman, M. J. Neubelt, G. Raybon, and S. G. Evangelides. Demonstration of soliton transmission at 2.4 Gbit/s over 12000 km. *Electron. Lett.*, 27(2):178–179, 1991.

[206] M. Nakazawa, E. Yamada, H. Kubota, and K. Suzuki. 10 Gbit/s soliton data transmission over one million kilometers. *Electron. Lett.*, 27(14):1270–1272, 1991.

[207] S. Kawai, K. Iwatsuki, K. Suzuki, S. Nishi, M. Saruwatari, K. Sato, and K. Wakita. 10 Gbit/s optical soliton transmission over 7200 km by using a monolithically integrated MQW-DFB-LD/MQW-EA modulator light source. *Electron. Lett.*, 30(3):251–252, 1994.

[208] T. Widdowson and A. E. Ellis. 20 Gbit/s soliton transmission over 125 Mm. *Electron. Lett.*, 30(22):1866–1868, 1994.

[209] T. Widdowson, D. J. Malyon, A. D. Ellis, K. Smith, and K. J. Blow. Soliton shepherding: All-optical active soliton control over global distances. *Electron. Lett.*, 30(12):990–991, 1994.

[210] G. Aubin, T. Montalant, J. Moulu, B. Nortier, F. Pirio, and J.-B. Thomine. Record amplifier span of 105 km in a soliton transmission experiment at 10 Gbit/s over 1 Mm. *Electron. Lett.*, 31(3):217–219, 1995.

[211] D. J. Malyon, T. Widdowson, E. G. Bryant, S. F. Carter, J. V. Wright, and W. A. Stallard. Demonstration of optical pulse propagation over 10000 km of fibre using recirculating loop. *Electron. Lett.*, 27(2):120–121, 1991.

[212] H. Taga, S. Yamamoto, N. Edagawa, Y. Yoshida, S. Akiba, and H. Wakabayashi. The experimental study of the effect of fibre chromatic dispersion upon IM-DD ultra-long distance optical communication systems with Er-doped fibre amplifiers using a 1000 km fibre loop. *IEEE J. Lightwave Technol.*, 12(8):1455–1461, 1994.

[213] D. Atkinson, W. H. Loh, V. V. Afanajsv, A. B. Grudinin, A. J. Seeds, and D. N. Payne. Increased amplifier spacing in a soliton system with quantum-well saturable absorbers and spectral filtering. *Opt. Lett.*, 19(19):1514–1516, 1994.

[214] M. Nakazawa, Kimura Y., K. Suzuki, T. Kubota, H.and Komukai, E Yamada, T. Sugawa, E Yoshida, T. Yamamoto, T. Imai, A. Sahara, O. Yamauchi, and M. Umezawa. Soliton transmission at 20 Gbit/s over 2000 km in Tokyo metropolitan optical network. *Electron. Lett.*, 31(17):1478–1479, 1995.

[215] N. S. Bergano, C. R. Davidson, A. M. Vengsarkar, B. M. Nyman, S. G. Evangelides, J. M. Darcie, M. Ma, J. D. Evankow, P. C. Corbett, M. A. Mills, G. A. Ferguson, J. R. Pedrazzani, J. A. Nagel, J. L. Zyskind, J. W. Sulhoff, and A. J. Lucero. 100 Gbit/s WDM transsmission if twenty 5 Gbit/s NRZ data channels over transoceanic distances using a gain flattened amplifier chain. In *Proc. 21st Eur. Conf. on Opt. Comm (ECOC'95 - Brussels)*. IMEC, Gent, Belgium, 1995.

[216] M. Suzuki, I. Morita, S. Yamamoto, N. Edagawa, H. Taga, and S. Akiba. Timing jitter reduction by periodic dispersion compensation in soliton transmission. In *Optical Fibre Communications (OFC'95)*, page PD20, Washington, D.C., 1995. Optical Society of America.

Appendix A

Publications

[1] W. Forysiak, F. M. Knox, and N. J. Doran. Average soliton propagation in periodically amplified systems with stepwise dispersion profiled fibre. *Opt. Lett.*, 19(3):174–176, 1994.

[2] W. Forysiak, F. M. Knox, and N. J. Doran. Stepwise dispersion profiling of periodically amplified soliton systems. *IEEE J. Lightwave Technol.*, 12(8):1330–1337, 1994.

[3] F. M. Knox, W. Forysiak, and N. J. Doran. The potential for solitons for 10 Gbit/s communications in standard fibre systems. In *IEE Colloquium on "High capacity optical communications"*, London, May 1994.

[4] F. M. Knox, W. Forysiak, and N. J. Doran. Upgrading standard fibre communication links to 10 Gbit/s using solitons and dispersion compensation. In *Tech. Digest of CLEO Europe '94, paper CWO2*, Amsterdam, Netherlands, August 1994.

[5] N. J. Doran, W. Forysiak, F. M. Knox, and K. J. Blow. Soliton stability in periodic nonlinear Schrödinger equation systems: the advanced average soliton. *Optics Communications*, 117:65–70, 1995.

[6] F. M. Knox for N. J. Doran. Solitons in optical communications. Institute of Physics Annual Congress, Telford, 1995.

[7] F. M. Knox, P. Harper, P. N. Kean, N. J. Doran, and I. Bennion. Low jitter long distance pulse transmission of near net fibre dispersion zero wavelength. *Electron. Lett.*, 31(17):1467–1468, 1995.

[8] F. M. Knox, P. Harper, P. N. Kean, N. J. Doran, and I. Bennion. Stable 10 ps pulse propagation near the average dispersion zero of a fibre loop. In *OSA Annual Meeting & exhibit program, paper ThKK4*, Portland, Oregon, Sept. 10-15 1995. OSA.

[9] F. M. Knox, W. Forysiak, and N. J. Doran. 10 Gbit/s soliton communication systems over standard fibre at 1.55 μm and the use of dispersion compensation. *IEEE J. Lightwave Technol.*, 13(10):1955–1963, 1995.

Appendix B

Acknowledgements

I must acknowledge the help of my co-workers who have been closely involved in a large part of this thesis. Firstly Nick Doran, my supervisor, who has guided me throughout the work. Others are more specific to certain parts of the work. (Unless other wise mentioned, the programs developed were written in Fortran.) As well as those mentioned below I would like to thank Aston Univ. and John Wright at BT Labs, Martlesham Heath for sponsoring my studies.

Chapter 3 was originated by Wladek Forysiak, who originally derived the mathematics. I was involved with some of the maths plus the implementation of the numerical optimisation routine and the simulation work using code added by him to the generalised NLSE propagation code already in place.

Chapter 4 was a development of the stepwise profiling. I wrote several pieces of code, to simulate the random pulse pattern generator with the various initial modulation formats, and for the detector, filter and error rate estimation of the output of the system. Again, Wladek assisted me through the development of the idea.

In chapter 5, the mathematical proof was developed by Keith Blow of BT Labs. The idea was developed by Wladek, who directed the simulation work I was involved with.

Chapter 6 was the product of two sites, BT labs, Martlesham for the first two and Aston Univ. for the final one. Credit for the ideas for both the BT lasers goes to Andrew Ellis, who directed the work there. For the DFB/SLA laser with fibre compression, the simulations were developed first in Mathematica and refined in C++ for this thesis. Liam Pender assisted with the construction of this source. The Aston Univ. figure of eight laser idea came from Peter Kean who helped with the construction and testing, as did Paul Harper.

The recirculating loop in chapter 7 was developed by several people. Peter Kean was closely involved with me on the construction of the original recirculating loop and amplifier and Paul Harper was heavily involved with the NPR experiment.

Finally, but probably most importantly, the others who have made this possible are those that kept me sane by listening to my insane ramblings and shutting me up when necessary. I will probably miss a host of people out, but as far as the thesis is concerned, Katie Allen, Stu Carnochan, Matt Reynolds, Corinne Prior, Allister Pattison, Kate Sugden, Diana Jordan, Scott McDougal, Nick Smith and Alastair, the wee brother, spring to mind right now. Apologies for any damage caused.